

3 GEOCHEMISTRY

3.1 Re-evaluation of Microbial Gas-Generation...

3.1 Re-evaluation of Microbial Gas Generation Rates for Long-Term WIPP Performance Assessment¹

Y. Wang, L. H. Brush, H. Gao, and J. S. Stein
Sandia National Laboratories, MS 1395
4100 National Parks Hwy.
Carlsbad, NM 88220

Abstract

A sensitivity analysis for the U.S. Department of Energy's (DOE's) Waste Isolation Pilot Plant (WIPP) Compliance Certification Application (CCA) has shown that microbial gas generation rates are among the most important parameters for the long-term performance assessment (PA) of the WIPP. Because of this, the DOE decided to continue studies of microbial gas generation at Brookhaven National Laboratory (BNL) and Sandia National Laboratories after submission of the CCA. The objective of these ongoing studies is to reduce the uncertainties associated with microbial gas generation rates used in the CCA and the Performance Assessment Verification Test (PAVT). Based on new data obtained from the long-term experiments at BNL, we have re-evaluated both the inundated and humid microbial gas generation rates. The long-term experimental results demonstrate convincingly that significant reductions in both the inundated and humid rates are warranted. The long-term data support the following rates:

	CCA	Updated rates
Inundated rate for degradation of cellulose, plastics and rubbers (CPR) (mol C/kg/year)	0.01-0.3	0.0029-0.021
Humid rate for CPR degradation (mol C/kg/year)	0.0-0.04	0.0-0.022

The maximum humid rate obtained from an analysis of the experimental data is slightly higher than the maximum inundated rate. Because this is unrealistic, we propose that the maximum humid rate be capped at the inundated rate appropriate for the particular conditions.

The BNL experimental results display two distinct gas-generation rates: a transient, rapid rate during the first 500 days, followed by a much longer phase of significantly slower gas generation. The quantity of gas produced during the initial, transient phase is negligible from the standpoint of the long-term performance of the repository.

Introduction

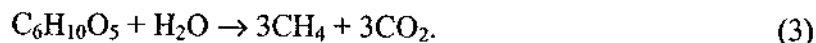
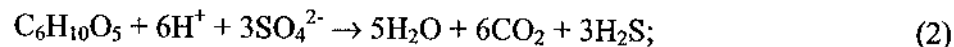
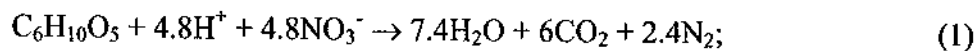
The Waste Isolation Pilot Plant (WIPP) Compliance Certification Application (CCA) performance assessment (PA) calculations were conducted in 1996 as part of the overall

¹This work is covered by WBS #1.3.5.4.1.1.

compliance certification process established by the U.S. Environmental Protection Agency (EPA) in its radiation-protection regulations. A sensitivity analysis has shown that microbial gas generation rates are among the most important parameters for the long-term performance of the repository (Helton et al., 1998). Because of this, the U.S. Department of Energy (DOE) decided to continue the microbial gas-generation studies at Brookhaven National Laboratory (BNL) and Sandia National Laboratories (SNL) after submission of the CCA to reduce uncertainties associated with the gas-generation rates used in the CCA PA. Based on the data obtained from long-term experiments at BNL (Francis and Gillow, 2000; Gillow and Francis, 2001a, 2001b), it is apparent that both the inundated and humid microbial gas-generation rates are significantly less than reported in the CCA. This analysis was conducted in accordance with Francis et al. (2001). All of the calculations were performed using a Microsoft Excel spreadsheet (Gas_Gen_StatisticsWork.xls).

Microbial Gas-Generation in the WIPP

Microorganisms in the repository could degrade cellulose, plastics, and rubbers (CPR) present in transuranic (TRU) waste. Microorganisms would degrade CPR sequentially by the following reaction pathways (Francis et al., 1997, Wang and Brush, 1996a):



Reaction 3 will account for over 95% of the (possible) microbial gas generation in the WIPP (Wang and Brush, 1996a).

Microbial gas generation could have a significant impact on the long-term performance of the repository. The production of CO_2 would acidify the brine in the repository and produce CO_3^{2-} , a potentially significant actinide complexant, thus increasing actinide mobility. In addition, together with steel corrosion, microbial gas generation could pressurize the repository and therefore reduce the rates and extent of brine inflow and room closure, and force direct releases of brine with dissolved and suspended actinides up boreholes from inadvertent human intrusion into the repository. To mitigate the effects of CO_2 generation, the DOE decided to use MgO as an engineered barrier to remove CO_2 and to buffer P_{CO_2} and pH within ranges in which actinide solubilities are minimized. (The experiments discussed here did not simulate the effects of MgO.)

Microbial Gas-Generation Rates for the CCA and the PAVT

To bracket the large uncertainties in microbial activity and the biodegradability of the CPR in TRU waste, it has been assumed in the CCA that any biodegradable material will be totally degradable if it is assumed to degrade; and if plastics and rubbers are degraded, they will

be degraded at the same rates as cellulosics. The biodegradation rates of cellulosics were established at 0.01–0.3 (mol C)/kg cellulose/year under inundated conditions, and 0–0.04 (mol C)/(kg cellulose)/year under humid conditions. The maximum inundated rate was estimated from the transient (approximately 500-day) phase of the CO₂ production curve obtained from NO₃⁻-amended, anaerobic experiments, while the maximum humid rate was calculated from the two data points at 6 days and 415 days, averaged over both nutrient-amended and inoculated-only, anaerobic experiments. The CCA assumed that CO₂ generated by microbial reactions would be removed by MgO carbonation (Wang and Brush, 1996b).

In 1997 the EPA required the DOE to perform a PAVT to evaluate and verify the results of DOE's CCA PA calculations. For the microbial gas-generation rates, EPA concurred that the parameter values used in the CCA were appropriate for long-term WIPP PA.

Analysis for the Brine-Inundated Rate

ROLE OF NITRATE AND RELEVANT DEGRADATION PATHWAY

The results of headspace gas analyses for anaerobic, brine-inundated experiments are shown in Figure 1. The amount of CO₂ accumulated in NO₃⁻-amended experiments was systematically higher than that in runs without excess NO₃⁻ amendment, demonstrating the dependence of cellulose biodegradation on the availability of electron acceptors and nutrients (Francis et al., 1997; Wang and Brush, 1996a). Microbes use NO₃⁻ both as an electron acceptor and as a nutrient for synthesis of biomass. Nutrient-amended experiments initially contained 250 μmol of NO₃⁻/(g cellulose), equivalent to NO₃⁻/C ≈ 0.007, while nutrient-amended samples plus excess NO₃⁻ contained 1240 μmol of NO₃⁻/(g cellulose), equivalent to NO₃⁻/C ≈ 0.033 (Francis and Gillow, 1994, p. 61).

Based on U.S. DOE (1996), the wastes to be emplaced in the WIPP contain 2.85×10^7 kg of total equivalent cellulose materials (or 1.05×10^9 mol of C) and 1.6×10^6 kg (or 2.6×10^7 mol) of NO₃⁻ (Wang and Brush, 1996, p. 14). Therefore, the average molar ratio of NO₃⁻ to organic C in the waste will be 0.025, somewhat less than in the BNL experiments amended with excess NO₃⁻. Therefore, in terms of the enhancement of biodegradation by NO₃⁻, the measurements on NO₃⁻-amended runs provide an upper bound for the microbial-gas-generation rate in actual wastes. On the other hand, also based on the waste inventory estimates, denitrification only accounts for $(1.25 \times 2.6 \times 10^7)/(9.84 \times 10^8) = \sim 3.3\%$ of total organic C degradation in the repository; the rest will proceed in a NO₃⁻-depleted environment. Therefore, for long-term PA, the experiments without excess NO₃⁻ would be more representative of actual repository conditions, and the rates derived from these runs will be much lower. With no further experimental data available, to be conservative, we still use the runs amended with excess NO₃⁻ to constrain the upper limit for brine-inundated rates, as we did for the CCA (Wang and Brush, 1996a).

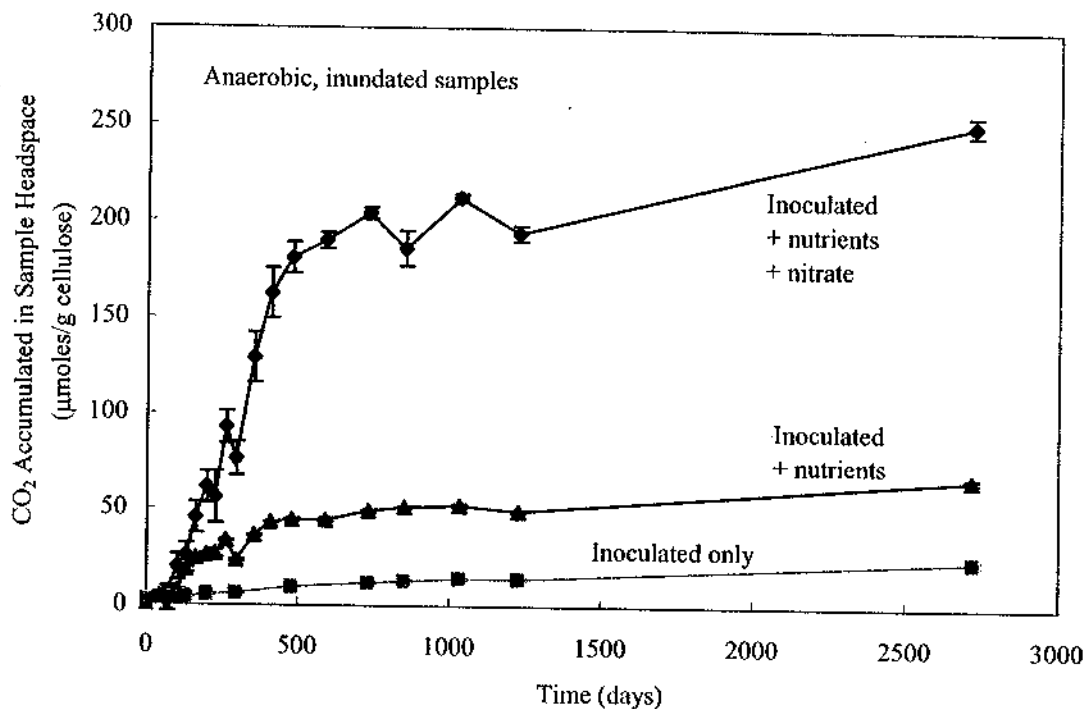


Figure 1. CO₂ production in anaerobic, brine-inundated experiments with cellulose. The data points at 2718 days (7.4 years) were obtained after the CCA. The accumulation of CO₂ in each set of runs displays two distinct gas-generation phases: a rapid increase in the first 500 days, followed by a long period of slow accumulation. All data are from Francis and Gillow (2000, Table 1) and Francis et al. (1997, A-25 to A-27).

TRANSIENT RATE VS. LONG-TERM RATE

The accumulation of CO₂ in each set of experiments displays two distinct gas-generation phases: a rapid transient rate in the first 500 days, followed by a long period of slow accumulation (Figure 1). The transition from the transient to the long-term phase is unlikely to be caused by pH changes or the accumulation of metabolites. In fact, no significant pH changes were detected during incubation (Francis et al., 1997, Table 15). In addition, the occurrence of CH₄ production in amended runs without excess NO₃⁻ (Francis and Gillow, 2000) implies that conditions were not detrimental to microbial activity, since methanogens are generally extremely sensitive to environmental changes (Xing et al., 1997). The continuous production of CO₂ in the long-term phase provides direct evidence that microbial activity in the experiments was not inhibited by metabolite accumulation.

There are two possible reasons for the reduction in CO₂ generation rates in the long-term phase of the BNL experiments: (1) changes in microbial communities and metabolic reaction pathways due to NO₃⁻ depletion, and (2) depletion of labile constituents of the substrate. The solution analyses imply that NO₃⁻ concentrations significantly decreased or became undetectable after 885 days of incubation (Francis et al., 1997, Table 15). The depletion of NO₃⁻ would shift

the biodegradation reaction to less energetic pathways, such as fermentation, SO_4^{2-} reduction, and methanogenesis. Microbes use NO_3^- both as an electron acceptor and as a nutrient for the synthesis of biomass. Many natural biological systems are limited by the availability of N (Schlesinger, 1997), consistent with the observed correlation between NO_3^- depletion and rate reduction in the BNL experiments. However, the depletion of NO_3^- is probably not the only factor responsible for the observed rate decrease during the experiments, because, in the runs amended with excess NO_3^- , a significant level of NO_3^- was still detected at 850 days (Francis et al., 1997, Table 15), much later than the initiation of the slow gas-generation phase. Biodegradability of the labile fraction of the substrate could be another factor causing the decrease in gas-generation rates. Natural cellulotics contain 10 to 40% amorphous materials that are more biodegradable (Leschine, 1995; Xu, 2001). Thus, the transition from the transient to the long-term phase of CO_2 generation could also be partly due to the depletion of a labile fraction of the cellulosic materials in the samples.

Due to the lack of long-term data at the time of the CCA PA calculations, the maximum inundated rate was derived from the transient part of the CO_2 accumulation curve for NO_3^- -amended experiments (Figure 2). However, as more data became available, it became apparent that the rates established for the CCA are overly conservative because they ignore the long-term phase of the CO_2 accumulation curve, which actually accounts for most of long-term biodegradation (see below), and would result in a much lower gas-generation rate. The new rate derived for the long-term data provides a more realistic evaluation.

A simple mass-balance calculation shows that the contribution of the initial gas-generation phase is negligible from the standpoint of long-term WIPP PA. From Figure 2, $\sim 180 \mu\text{mol}$ of CO_2 accumulated during the initial 500 days. With a correction for CO_2 dissolution in the brine (Wang and Brush, 1996a, p. 12), the total C degraded over that time period is $180 \times 1.56 = 281 \mu\text{mol}$, which accounts for only 0.76% of the total organic C initially present in the experiments. In other words, over 99% of organic C would have been degraded over the long-term phase of the runs. Extrapolating this to the entire repository, about $1.05 \times 10^9 \times 0.76\% = 8 \times 10^6$ mol of organic C would be degraded during the transient phase. Since CO_2 in the repository will be removed essentially instantaneously by reactions with periclase (MgO) and/or brucite ($\text{Mg}(\text{OH})_2$), 1 mol of organic C can generate at most 0.5 mol of gas that will remain in the gaseous phase (see Reactions 1–3 above). Therefore, the total gas that can be generated in the repository during the transient phase of degradation is $\sim 4 \times 10^6$ mol. Given an initial pore volume of $370,000 \text{ m}^3$ in the repository and the ideal gas law, the increase in the repository pressure due to transient-phase gas generation is estimated to be 0.26 atm, which is close to the partial pressure of atmospheric O_2 (Richardson and McSween, 1989, p. 88). Of course, corrosion of steel, aerobic microbial activity, and other reductive processes will readily compensate for this very slight increase in the initial pressure by consuming O_2 in the air trapped in the repository at the time of filling and sealing. Therefore, the contribution of the initial gas-generation phase will be negligible, and the appropriate rates for long-term WIPP PA calculations should be derived from the experimental data from the long-term phase of CO_2 accumulation curves.

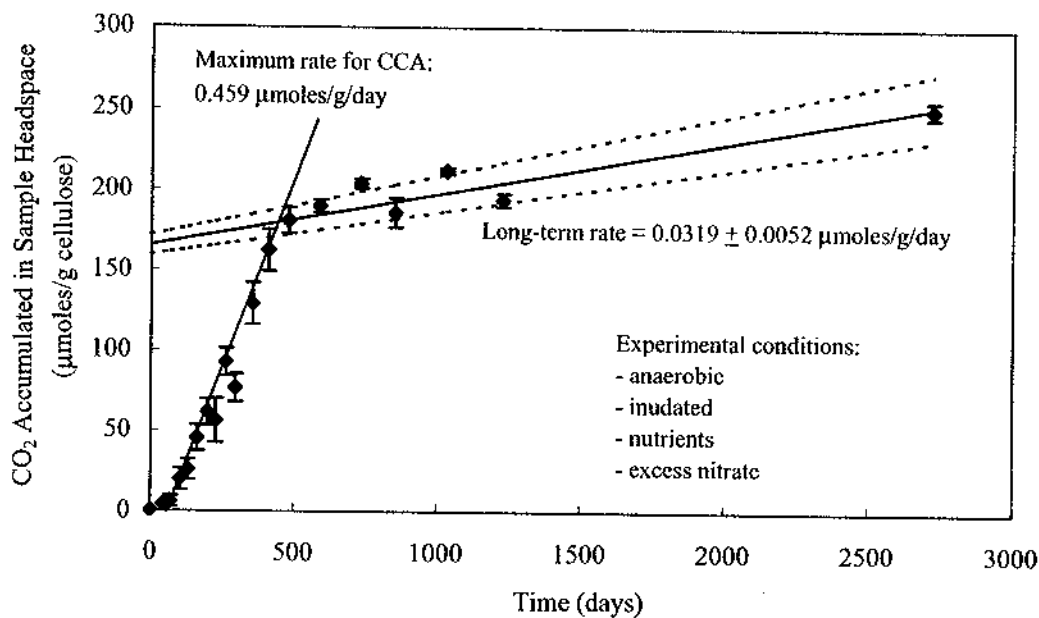


Figure 2. CO₂ production in anaerobic, brine-inundated runs with cellulose and amended with nutrients and excess NO₃⁻. The maximum inundated rate for the CCA was derived from the transient part of CO₂ accumulation curve. The solid red line is a least-squares fit to the data corresponding to the long-term gas-generation phase. The dashed lines define a confidence interval for the fitted line with a confidence level of 95% (i.e., $\pm 2\sigma$). The same confidence level is also applied to the estimated long-term rate. All data are from Francis and Gillow (2000, Table 1) and Francis et al. (1997, A-25 to A-27).

UPDATING INUNDATED MICROBIAL GAS-GENERATION RATES

The upper limit of the inundated rate is constrained by fitting a straight line to the experimental data from the long-term phase of the CO₂ accumulation curve for NO₃⁻-amended experiments (Figure 2). From the slope of the line, the microbial degradation rate is 0.0319 ± 0.0052 $\mu\text{mol/g/day}$ with a confidence level of 95% (Figure 2). Corrected for dissolved CO₂ (Wang and Brush, 1996a, p. 12), the upper limit for the inundated microbial degradation rate is $(0.0319 \pm 0.0052) \times 1.56 = 0.0579$ $\mu\text{mol C/g/day}$, or 0.021 mol C/kg/year.

Similarly, the minimum rate for inundated microbial degradation is established by fitting a straight line to the experimental data from the long-term part of the CO₂ accumulation curve for the samples with no nutrients or excess NO₃⁻ (Figure 3). From the slope of the line, the microbial degradation rate is 0.0062 ± 0.00114 $\mu\text{mol/g/day}$, with a confidence level of 95% (Figure 3). Corrected for dissolved CO₂, the minimum rate for inundated microbial degradation is $(0.0062 - 0.00114) \times 1.56 = 0.00789$ $\mu\text{mol C/g/day}$, or 0.0029 mol C/kg/year.

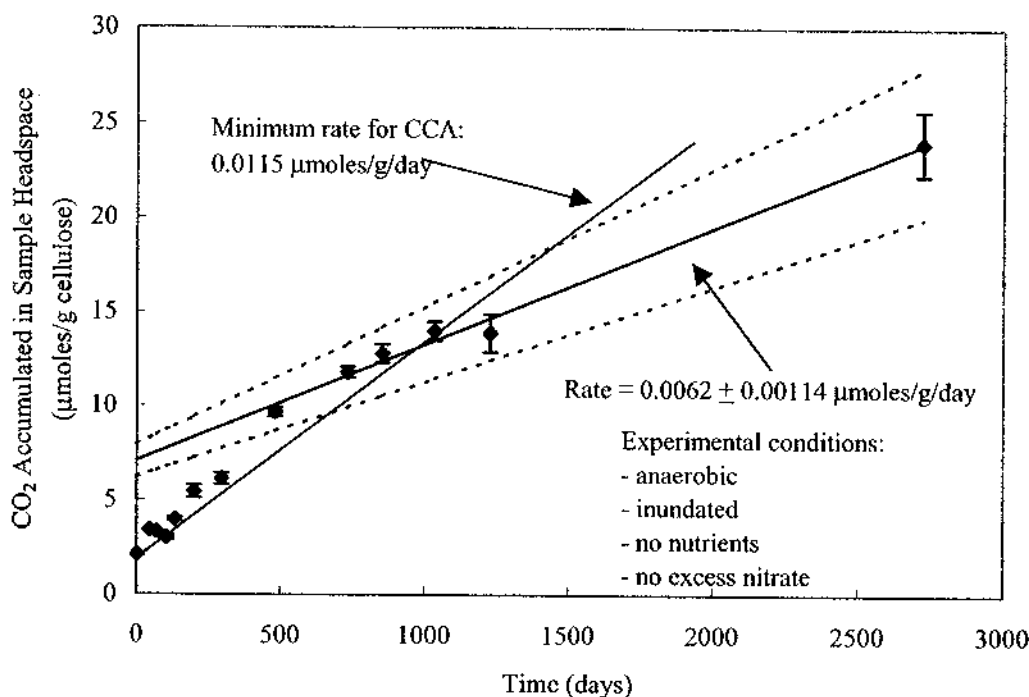


Figure 3. CO₂ production in anaerobic, brine-inundated experiments with cellulose but unamended with nutrients or excess NO₃⁻. The solid red line is a least-squares fit to the data corresponding to the slow gas-generation phase. The dashed lines define a confidence interval for the fitted line with a confidence level of 95% (i.e., $\pm 2\sigma$). The same confidence level is also applied to the estimated long-term rate. All data are from Francis and Gillow (2000, Table 1) and Francis et al. (1997, A-25 to A-27).

Analysis for the Humid Rate

Under humid conditions, the experimental data display no clear correlation between CO₂ production and nutrients (Figure 4). The experimental data also exhibit relatively large uncertainties. The microbial degradation rate is expected to be very low, if not zero, under anticipated WIPP humid conditions, for the following reasons. First, unlike inundated experiments, the amounts of CO₂ accumulated in all humid experiments decreased with time after initial increases (Gillow and Francis, 2001b, Figure 4). This initial increase could be attributed to the introduction of additional liquid in the inoculum added at the start of the runs (see Francis et al., 1997, 17–19, for a description of the experimental setup and procedures). The data thus imply that microbial degradation was not sustainable in humid samples amended with nutrients even with additional moisture added. Furthermore, methanogenesis, the dominant respiratory pathway expected in the WIPP (Wang and Brush, 1996a; Wang, 2000), consumes H₂O (see Reaction 3), and thus the reaction cannot be sustained without a continuous supply of brine, which is inconsistent with humid conditions. It should be noted that the emplacement of MgO in the WIPP will significantly reduce the H₂O vapor pressure in the repository by the hydration reaction:



The H_2O activity ($a_{\text{H}_2\text{O}}$) buffered by this reaction is calculated to be $10^{-6.3}$ atm, based on thermodynamic data from Robie et al. (1978). The actual H_2O activity in the repository, which will ultimately be controlled by the relative rates of both brine inflow *and* MgO hydration, will thus be much lower than that established by WIPP brines, about 0.7 (Brush, 1990). An abundance of laboratory and field data imply that the minimum H_2O activity required by microorganisms in soils is about 0.6, below which microbial activities are significantly inhibited (Kral and Cousin, 1981; Donnelly et al., 1990; Nizovtseva et al., 1995; Barros et al., 1995; Stark and Firestone, 1995; Cattaneo et al., 1997).

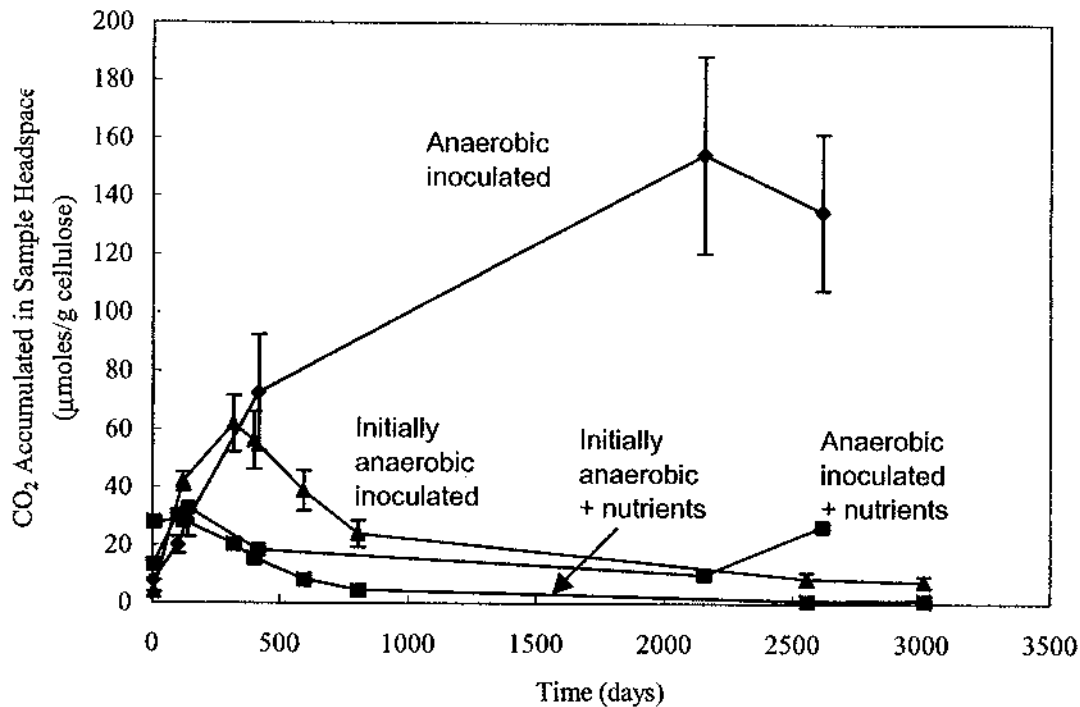


Figure 4. CO_2 production in humid runs with cellulose. The data points for time >415 days were obtained after the CCA. The data show no clear correlation between CO_2 production and nutrients. The amounts of CO_2 accumulated in all humid runs decreased with time after initial increases (although this decrease happened much later in anaerobic, inoculated samples). The initial increases in CO_2 production could be attributed to the introduction of additional liquid during inoculation. For the CCA, the maximum humid rate was calculated from the two data points at 6 days and 415 days, averaged over both nutrient-amended and inoculated-only anaerobic samples. All data are from Gillow and Francis (2001b, Table 12).

Anaerobic, inoculated humid experiments are used to determine the upper limit for the humid rate, because of their relatively high CO_2 production. Using a procedure similar to that used to constrain the inundated rates, the maximum humid microbial degradation rate is

$(0.0335 \pm 0.028) = \mu\text{mol C/g/day}$, or $0.0224 \text{ mol C/kg/year}$ (Figure 5). As in the CCA, the minimum humid rate is set to 0 mol C/kg/year .

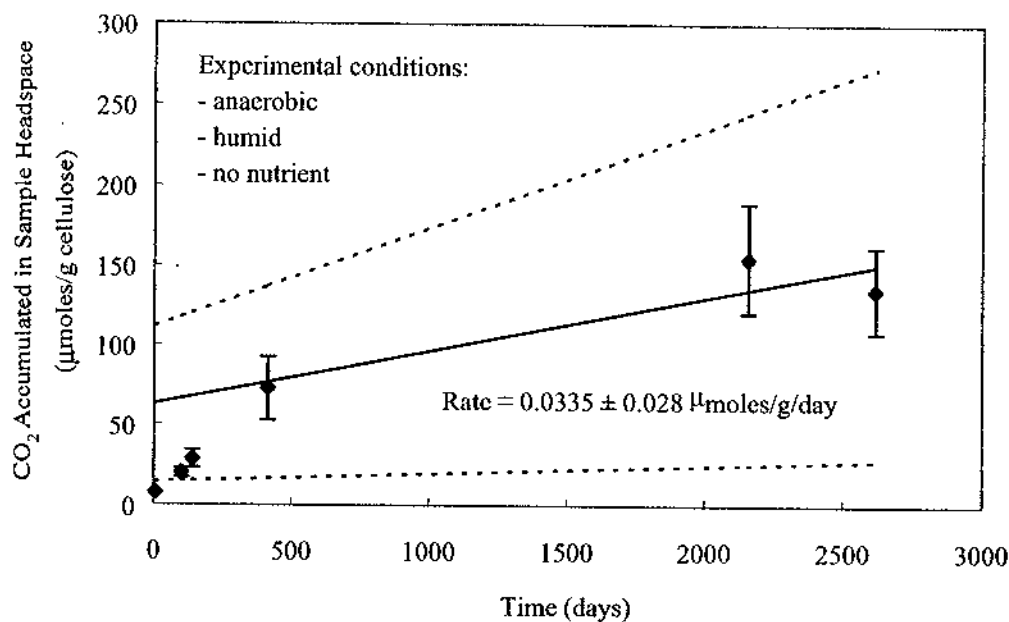


Figure 5. CO₂ production in anaerobic humid, unamended experiments. The solid red line is a least-squares fit to the data corresponding to the slow gas generation phase. The dashed lines define a confidence interval for the fitting line with a confidence level of 95% (i.e., $\pm 2\sigma$). The same confidence level is also applied to the estimated long-term rate. All data are from Gillow and Francis (2001b, Table 12).

Note that the maximum humid rate is slightly higher than the maximum inundated rate. This could be caused by two experimental artifacts in the humid experiments: (1) the introduction of additional liquid to the samples by adding wet inocula; (2) the artificial increase of microbe contact with substrate, all of which are not directly relevant to actual humid conditions in the repository. In any case, for a given environment, the humid rate must be smaller than the inundated (Kral and Cousin, 1981; Donnelly et al., 1990; Nizovtseva et al., 1995; Barros et al., 1995; Stark and Firestone, 1995; Cattaneo et al., 1997). The maximum humid rate obtained from an analysis of the experimental data is slightly higher than the maximum inundated rate. Because this is an unrealistic result, it is proposed that the maximum humid rate be capped at the inundated rate appropriate for the particular conditions.

Conclusion

Based on new data obtained from the long-term experiments at BNL, we have re-evaluated both the inundated and humid microbial gas generation rates. The long-term

experimental results demonstrate convincingly that significant reductions in both the inundated and humid rates are warranted. The long-term data support the following rates:

	CCA	Updated rates
Inundated rate for degradation of CPR (mol C/kg/year)	0.01-0.3	0.0029-0.021
Humid rate for CPR degradation (mol C/kg/year)	0.0-0.04	0.0-0.022

The maximum humid rate obtained from an analysis of the experimental data is slightly higher than the maximum inundated rate. Because this is unrealistic, we propose that the maximum humid rate be capped at the inundated rate appropriate for the particular conditions.

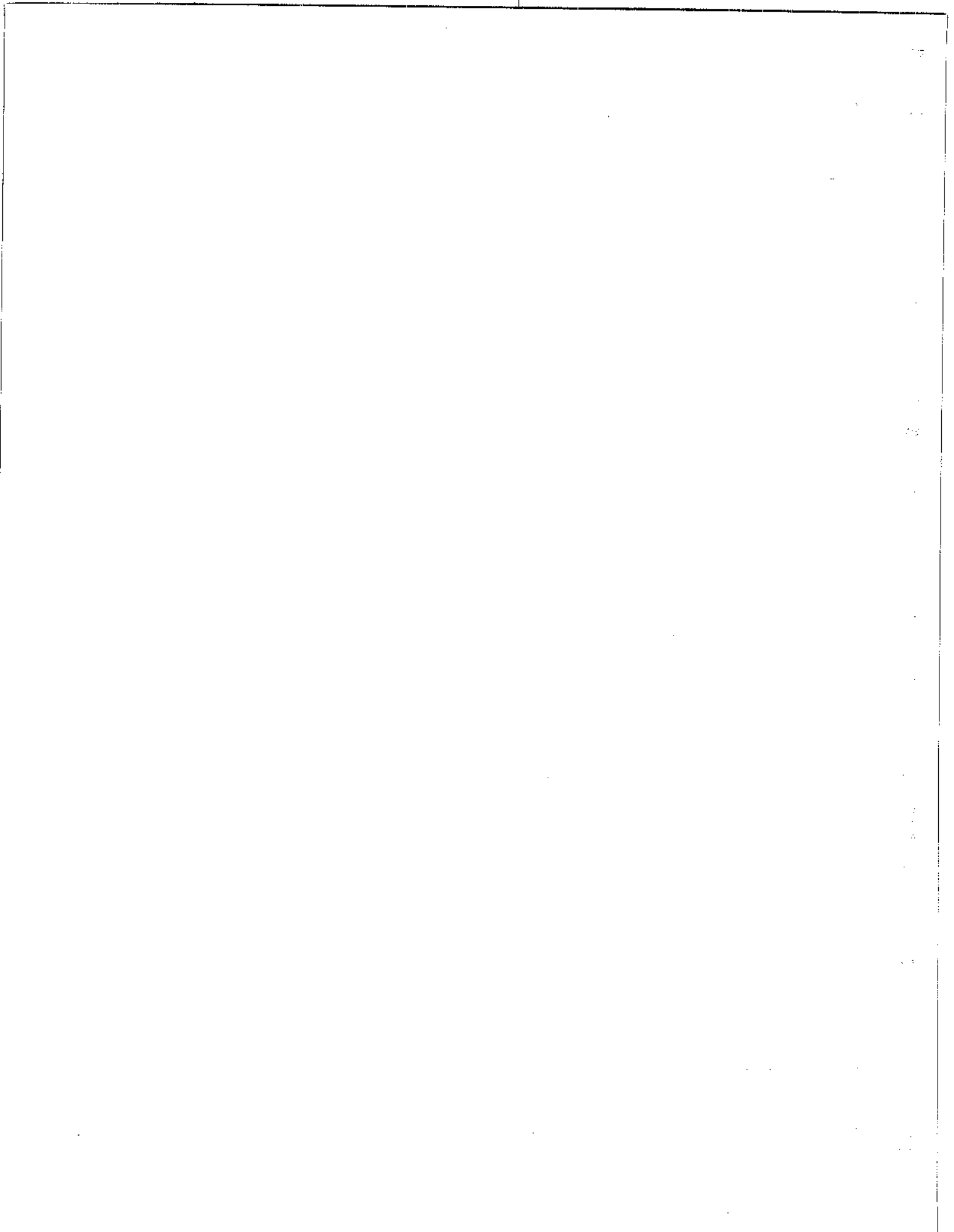
The BNL experimental results display two distinct gas-generation rates: a transient, rapid rate during the first 500 days, followed by a much longer phase of significantly slower gas generation. The quantity of gas produced during the initial, transient phase is negligible from the standpoint of the long-term performance of the repository.

References

- Barros, N., I. Gomez-Orellana, S. Feijoo, and R. Balsa. 1995. "The Effect of Soil Moisture on Soil Microbial Activity Studied by Microcalorimetry," *Thermochimica Acta*. Vol. 249, 161-168.
- Brush, L.H. 1990. *Test Plan for Laboratory and Modeling Studies of Repository and Radionuclide Chemistry for the Waste Isolation Pilot Plant*. SAND90-0266. Albuquerque, NM: Sandia National Laboratories, Albuquerque, NM.
- Cattaneo, M.V., C. Mason, and C.W. Greer. 1997. "The Influence of Moisture on Microbial Transport, Survival and 2,4-D Biodegradation with Generally Marked *Burkholderia cepacia* in Unsaturated Soil Columns," *Biodegradation*. Vol. 8, 87-96.
- Donnelly, P.K., J.A. Entry, D.L. Crawford, and K. Cromack, Jr. 1990. "Cellulose and Lignin Degradation in Forest Soils: Response to Moisture, Temperature, and Acidity," *Microbial Ecology*. Vol. 20, 289-295.
- Francis, A.J. and J.B. Gillow. 1994. *Effect of Microbial Processes on Gas Generation under Expected Waste Isolation Pilot Plant Repository Conditions: Progress Report through 1992*. SAND93-7036. Albuquerque, NM: Sandia National Laboratories.
- Francis, A.J. and J.B. Gillow. 2000. "Progress Report: Microbial Gas Generation Program." Unpublished memorandum to Y. Wang, January 6, 2000. Albuquerque, NM: Sandia National Laboratories.
- Francis, A.J., J.B. Gillow, and M.R. Giles. 1997. *Microbial Gas Generation under Expected Waste Isolation Pilot Plant Repository Conditions*. SAND96-2582. Albuquerque, NM: Sandia National Laboratories.

- Francis, A.J., J.B. Gillow, and Y. Wang. 2001. "Re-evaluation of Microbial Gas Generation under Expected Waste Isolation Pilot Plant Conditions." Unpublished TP 99-01, Rev. 1. Carlsbad, NM: Sandia National Laboratories.
- Gillow, J.B., and A.J. Francis. 2001a. "Re-evaluation of Microbial Gas Generation under Expected Waste Isolation Pilot Plant Conditions: Data Summary Report," "Sandia National Laboratories Technical Baseline Reports, WBS 1.3.5.4, Repository Investigations, Milestone RI010, January 31, 2001." Carlsbad, NM: Sandia National Laboratories. 19-46.
- Gillow, J.B., and A.J. Francis. 2001b. "Re-evaluation of Microbial Gas Generation under Expected Waste Isolation Pilot Plant Conditions: Data Summary and Progress Report, February 1–July 13, 2001," "Sandia National Laboratories Technical Baseline Reports, WBS 1.3.5.4, Repository Investigations, Milestone RI020, July 31, 2001." Carlsbad, NM: Sandia National Laboratories. 3-1 to 3-21.
- Helton, J.S., J.E. Bean, J.W. Berglund, F.J. Davis, K. Economy, J.W. Garner, J.D. Johnson, R.J. MacKinnon, J. Miller, D.G. O'Brien, J.L. Ramsey, J.D. Schreiber, A. Shinta, L.N. Smith, D.M. Stoelzel, C.W. Stockman, and P. Vaughn. 1998. *Uncertainty and Sensitivity Analysis Results Obtained in the 1996 Performance Assessment for the Waste Isolation Pilot Plant*. SAND98-0365. Albuquerque, NM: Sandia National Laboratories.
- Kral, D.M. and M.K. Cousin. 1981. *Water Potential Relations in Soil Microbiology*. SSSA Special Publication No. 9. Madison, WI: Soil Science Society of America.
- Leschine, S.B. 1995. "Cellulose Degradation in Anaerobic Environments," *Annual Reviews of Microbiology*. Vol. 49, 399-426.
- Nizovtseva, D.V., A.M. Semenov, and N.S. Panikov. 1995. "Influence of Humidity on Microbial Cellulose Activity in Peat from a Raised Bog," *Microbiology*. Vol. 64, 701-705.
- Richardson, S.M. and H.Y. McSween, Jr. 1989. *Geochemistry: Pathways and Processes*. Englewood Cliffs, NJ: Prentice Hall.
- Robie, R.A., B.S. Hemingway, and J.R. Fisher. 1978. *Thermodynamic Properties of Minerals and Related Substances at 298.15 K and 1 Bar (10⁵ Pascals) Pressure and at Higher Temperatures*. USGS Bulletin 1452. Reston, VA: U.S. Geological Survey.
- Schlesinger, W.H. 1997. *Biogeochemistry: An Analysis of Global Change*. New York, NY: Academic Press.
- Stark, J.M. and M.K. Firestone. 1995. "Mechanism for Soil Moisture Effects on Activity of Nitrifying Bacteria," *Applied and Environmental Microbiology*. Vol. 61, 218-221.

- U.S. DOE. 1996. *Transuranic Waste Baseline Inventory Report, Rev. 3*. Carlsbad, NM: U.S. Department of Energy Carlsbad Area Office.
- Wang, Y. 2000. "Methanogenesis and Carbon Dioxide Generation in the Waste Isolation Pilot Plant (WIPP)." Unpublished memorandum to B.A. Howard, January 5, 2000. Carlsbad, NM: Sandia National Laboratories.
- Wang, Y. and L.H. Brush. 1996a. "Estimates of Gas-Generation Parameters for the Long-Term WIPP Performance Assessment." Unpublished memorandum to M.S. Tierney, January 26, 1996. WPO #30819. Albuquerque, NM: Sandia National Laboratories.
- Wang, Y. and L.H. Brush. 1996b. "Modify the Stoichiometric Factor y in the BRAGFLO to Include the Effect of MgO Added to WIPP Repository as a Backfill." Unpublished memorandum to M.S. Tierney, February 23, 1996. WPO #30819. Albuquerque, NM: Sandia National Laboratories.
- Xing, J., C. Criddle, and R. Hickey. 1997. "Effects of a Long-Term Periodic Substrate Perturbation on an Anaerobic Community," *Water Resources*. Vol. 31, 2195-2204.
- Xu, H. 2001. "Microstructure Investigation of Cellulose Materials from the Eddy Potash Mine," "Sandia National Laboratories Technical Baseline Reports, WBS 1.3.5.4, Repository Investigations, Milestone RI010, January 31, 2001." Carlsbad, NM: Sandia National Laboratories. 47-54.



IMPORTANT NOTICE: The current, official version of this document is available on the Sandia National Laboratories NWMP Online Documents web site. A printed copy of this document may not be the version currently in effect.

Sandia National Laboratories
Waste Isolation Pilot Plant

Chemical Behavior of Bromine in High Ionic Strength Solutions, Test Plan TP 03-02, Rev. 0

WBS 1.3.5.4.1.1

Effective Date: _____

Donald Wall
Repository Performance and Certification Dept. 6822
Sandia National laboratories
Carlsbad, NM 88220

APPROVAL PAGE

Author:

Donald Wall
Performance Assessment and Decision Analysis Dept. 6821
Sandia National Laboratories
Carlsbad, NM 88220

Date

Technical Reviewer:

Anna Snider
Repository Performance and Certification Dept. 6822
Sandia National Laboratories
Carlsbad, NM 88220

Date

SNL QA:

Martha Mitchell
Quality Assurance
Carlsbad Programs Group 6820
Sandia National Laboratories
Carlsbad, NM 88220

Date

Author:

David Kessel
Performance Assessment and Decision Analysis Dept. 6821
Sandia National Laboratories
Carlsbad, NM 88220

Date

CONTENTS

1 ABBREVIATIONS, ACRONYMS, FORMULAS, AND INITIALISMS	8
2 REVISION HISTORY	10
3 PURPOSE & SCOPE	11
3.1 Objectives	11
3.2 Introduction.....	11
3.3 Production of Hypochlorite.....	13
3.4 Chlorine Species as Oxidants.....	15
3.5 Hydrolysis of Chlorine.....	16
3.6 Bromine Behavior.....	19
3.7 Hydrolysis of Bromine.....	22
3.8 Bromine Absorbance Spectra	23
3.9 Interactions of Oxidized Bromine Species with U, Np, Pu	25
3.10 Reactions of Cl and Br Species.....	27
3.10.1 Conditions Influencing Generation of Oxidized Forms of Bromine.....	27
3.10.2 Determination of the Stability Constant of Br_3^- in Brine	27
3.10.3 Determination of the Partition Coefficient of Br_2	28
3.10.4 Effect of Fe on Production and Concentration of Br Species	28

CONTENTS (cont.)

4 EXPERIMENTAL PROCESS DESCRIPTION.....	28
4.1 Task 1. Determination of Conditions Influencing Generation of Oxidized Br.....	29
4.2 Task 2. Determination of the Stability Constant of Br_3^- in Brine.....	30
4.3 Task 3. Determination of the Partition Coefficient of Br_2 between Phases.....	30
4.4 Task 4. Determination of the Effect of Fe on Oxidized Br Species.....	31
4.5 Measuring and Test Equipment.....	31
4.6 Reagents.....	33
4.7 Experimental Procedures.....	34
4.7.1 General Procedures.....	34
4.7.2 Preparation of Brines.....	34
4.7.3 Determination of Reaction Products and Stoichiometry.....	34
4.7.4 Development of Baseline Spectra of Each Species in Brines.....	34
4.7.5 Determination of Reaction Rate of Br^- with OCl^-	34
4.7.6 Acid Dissociation Constant of Hypobromous Acid.....	35
4.8 Coordination with Organizations Providing Inputs or Using the Results.....	35
4.9 Procedures to Be Used/Developed.....	35
4.10 Known Sources of Error and Uncertainty.....	36
4.11 Data Processing and Mathematical Models.....	37
4.12 Documents to be Maintained as QA Records.....	37
4.13 Sample Handling and Control Requirements.....	37
4.14 Sample Disposal.....	37
4.15 Data Acquisition System.....	38
4.16 Commercial Software, Not Modified.....	38
4.17 Other Software.....	38
4.18 Justification, and Documentation of Deviations from Test Standards.....	39
4.19 Experimental Controls.....	39
4.20 Control and Characterization of Test Media.....	39
4.21 Data Identification and Use.....	39
4.22 Data Transfer and Reduction Controls.....	39
4.23 Identification, Segregation, Disposal of Erroneous Data.....	40
5 TRAINING AND OTHER STANDARD PROCEDURES.....	40
5.1 Training.....	40
5.2 NPs, SOPs, and SPs.....	40
5.3 Procurement Procedures.....	41

CONTENTS (cont.)

6 HEALTH AND SAFETY..... 41

7 PERMITTING AND LICENSING..... 41

8 REFERENCES 42

FIGURES

Figure 1. Generation of hypochlorite as a function of aqueous NaCl concentration.....	15
Figure 2. Plot of $\log \{[\text{HOCl}]/[\text{Cl}_2]\}$ as a function of pH.....	18
Figure 3. Plot of $[\text{HOBr}]/[\text{Br}_2]$ as a function of pH.....	23
Figure 4. Sample spectra of Br species in water.....	24
Figure 5. Molecular orbital diagram for diatomic halogen molecules.....	25
Figure 6. Latimer diagrams for oxidation/reduction behavior of U, Np, and Pu.....	26

TABLES

Table 1. Standard Reduction Potentials for Reactions of HOCl and OCl ⁻ (a).....	16
Table 2. Properties of Cl ₂ and Br ₂	19
Table 3. Aqueous Reactions of Bromine.....	20
Table 4. Thermodynamically Irreversible Reactions of Bromine	21

1 ABBREVIATIONS, ACRONYMS, FORMULAS, AND INITIALISMS

An	actinide
Br	bromine
Br ₂	molecular (or diatomic) bromine
Br ⁻	bromide
Br ₃ ⁻	tribromide anion
BrO ₃ ⁻	bromate
CBFO	(U.S. DOE) Carlsbad Field Office
Cl [•]	atomic chlorine free radical
Cl ₂ ^{•-}	molecular chlorine free radical
D ₂	diatomic deuterium, used as UV light source in UV-vis spectroscopy
DOE	(U.S.) Department of Energy
E ⁰	standard reduction potential
ERDA-6	descriptive label applied to a Castile brine composition
F	the Faraday constant, (96,485 coulombs/mole)
Fe	iron
GWB	Generic Weep Brine (representative of Salado brine composition)
H ⁺	hydronium ion
H [•]	atomic hydrogen free radical
HCl	hydrochloric acid
HOBr	hypobromous acid
HOCl	hypochlorous acid
HOCl ^{•-}	hypochlorous acid, anionic free radical
ICP-OES	inductively coupled plasma-optical emission spectroscopy
NaBr	sodium bromide
NaBrO ₃	sodium bromate
NaOCl	sodium hypochlorite
NaOH	sodium hydroxide
NP	(SNL NWMP) Nuclear Waste Management (QA) Procedure
NWMP	(SNL) Nuclear Waste Management Program
OBr ⁻	hypobromite
OH [•]	hydroxyl free radical
OCl ⁻	hypochlorite
OH ⁻	hydroxide
pcH	negative logarithm of the hydrogen ion concentration of a solution
pH	negative logarithm of the hydrogen ion thermodynamic activity of a solution
pK _a	negative base 10 logarithm of an acid dissociation constant
R	ideal gas constant, 8.314 J/molK
SNL	Sandia National Laboratories
SOP	(SNL) Standard Operating Procedure
SP	(SNL NWMP) Activity/Project-Specific Procedure

1 ABBREVIATIONS, ACRONYMS, FORMULAS, AND INITIALISMS (cont.)

T	temperature, in degrees Celsius or kelvins
U	uranium
UV-vis	ultraviolet-visible (spectroscopy)
WIPP	(U.S. DOE) Waste Isolation Pilot Plant
ΔG	Gibbs free energy of reaction
α particle	high-energy particle expelled from a nucleus during an α -decay process
β_{pqr}	stability constant for a metal/ligand complex
γ	activity coefficient (not related to γ -ray)
μ	ionic strength

2 REVISION HISTORY

This is the first version of this test plan. Subsequent versions will be prepared in accordance with the following Sandia National Laboratories (SNL) Nuclear Waste Management Program (NWMP) Nuclear Waste Management Quality Assurance Procedures (NPs): NP 6-1, NP 6-2, and NP 20-1 (Subsection 5.2).

3 PURPOSE & SCOPE

3.1 Objectives

The high-energy α particles emitted during the course of radioactive decay of many actinide elements intensely interact with the host matrix, whether solid or solution. In aqueous solutions, such as NaCl and MgCl₂ brines, the energy lost by the α particles is transferred to solute and solvent species, leaving them in highly excited states, followed by reactions with each other or with other solution components. The resulting products, referred to collectively as radiolysis products, include hydrogen peroxide (H₂O₂) and hypochlorite (OCl⁻). Radiolysis products, such as OCl⁻, react with bromide (Br⁻), producing oxidized forms of bromine (Br), such as diatomic bromine (Br₂), hypobromite (OBr⁻), or bromate (BrO₃⁻). The products of the oxidation of Br⁻ depend upon solution conditions, such as pH and Br⁻ concentration. The diatomic molecule, Br₂, exhibits greater mobility than the charged OBr⁻ and BrO₃⁻ species, due to partitioning of Br₂ from the aqueous into the gaseous phase. Formation of a complex of Br₂ with Br⁻ to form Br₃⁻ may act to reduce the partitioning of Br₂ into the vapor phase. The oxidized forms of Br are capable of oxidizing U to U(VI), Np to Np(V) and Pu to Pu(VI). However, both metallic and oxidized iron can react with oxidized Br species through oxidation/reduction processes and transition-metal-facilitated catalytic decomposition. Thus, although α -particle induced brine radiolysis may produce oxidized species of Br, the presence of iron may mitigate the attendant oxidizing capacity by reacting with the radiolysis products. In order to assess the potential impact of oxidized forms of Br on actinide (An) solubility and speciation, it is necessary to investigate reactions of Br in brines. The broadly stated goal of the investigation of the chemical behavior of Br in brines is divided into four categories; discussions of the merits of each category are considered individually.

- Task 1. Determination of conditions influencing generation of the oxidized forms of Br: HOBr, OBr⁻, BrO₃⁻, and Br₂.
- Task 2. Determination of the stability constant of Br₃⁻ in brine.
- Task 3. Determination of the partition coefficient of Br₂ between the aqueous and gaseous phases.
- Task 4. Determination of the effect of iron on production and concentration of Br species.

3.2 Introduction

There are two types of brines that naturally occur in the vicinity of the WIPP: Salado-Formation brine, an intragranular brine that includes >1 M Mg²⁺ and is saturated with

respect to NaCl, and Castile-Fm. brine, a predominantly NaCl-saturated brine. Both brine types contain smaller amounts of K^+ , Ca^{2+} , Br^- , SO_4^{2-} , and $B(OH)_4^-$. Synthetic brines have often been used in experimental work to model the behavior of these Salado and Castile brines. Two different brine compositions, referred to as Brine A and GWB, have been used to mimic the Salado brine, whereas work on Castile brine chemistry has utilized a brine type identified as ERDA-6. The compositions of these brines have been described elsewhere (Brush, 1990, Wall, 2002). The brines, which have ionic strengths ranging from 5 to 7, have a small buffering capacity close to $pH = 8$ due to the presence of borate. The high ionic strengths lead to significant departures from ideality of thermodynamic behavior for both solute and solvent species. For example, ionic solutes exhibit thermodynamic activities that depend upon ionic strength as well as the nature of the solution components; there is a decrease in the thermodynamic activity of solvent water and an increase in the activities of other uncharged species. As a result, there are differences in solute behavior, including differing solubilities and stabilities of metal-ligand complex formation due to the differences in characteristics of each of brine type.

Brines that have high chloride contents generate significant amounts of OCI^- when exposed to α irradiation (Kelm, 1999). The present discussion of production of OCI^- is adapted from Wall (2002). This test plan describes production of OCI^- due to α -particle induced radiolysis of brines, and the potential impacts upon aqueous chemistry of WIPP brines. OCI^- may act as a strong oxidant or complexing agent for metal ions, providing two potential routes for mobilization of actinide ions. However, OCI^- may undergo reactions in solution, leading to decomposition, either through reaction with $HOCl$ or OCI^- , or through decomposition reactions catalyzed by redox active metals. Experimental work on OCI^- behavior in brines has been initiated in SNL's Carlsbad laboratory. These studies have focused on the decomposition rates of $HOCl$ and OCI^- in brines. Reaction rates have been studied in 5 m NaCl solutions to determine the influence of pH and other components, such as iron. The behavior of OCI^- in 5 m NaCl is quite different than in GWB or ERDA-6. Representative WIPP brines, including GWB and ERDA-6, contain millimolar quantities of bromide (Br^-), which can be oxidized by $HOCl$, or OCI^- .

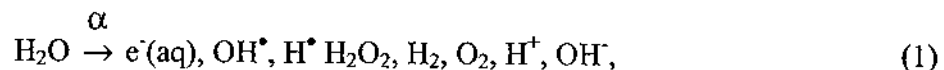
There is immediate oxidation of Br^- upon addition of OCI^- to either GWB or ERDA-6, resulting in a net decrease in OCI^- concentration, accompanied by the formation of oxidized forms of Br. Therefore, from the perspective of $HOCl$ or OCI^- generation, as long as brines contain Br^- , a readily available reaction pathway for the electrochemical reduction of $HOCl$ or OCI^- would exist, effectively limiting the extent to which either $HOCl$ or OCI^- accumulates. However, the issue of the nature of oxidized Br may be of some concern. The products of reaction between OCI^- and Br^- in ERDA-6 and GWB are unknown. Oxidation of Br^- may yield OBr^- , BrO_3^- or Br_2 . The ionic forms, OBr^- and BrO_3^- , although oxidants, would not partition into the gaseous phase, although Br_2 could do so, and would exhibit significantly more mobility than the ionic species. As a result, ionic species produced by α radiolysis would likely be constrained to remain in or near the microenvironments of origin, whereas Br_2 may migrate significantly beyond the region of production.

The amount of oxidized Br that may be produced is limited by the availability of Br⁻ in the pertinent brines. GWB and ERDA-6 respectively contain 11 and 27 mM concentrations of Br⁻. Relatively speaking, these concentrations are sufficiently large to create oxidizing solution conditions if a substantial fraction of Br were to exist in an oxidized state. Br₂, OBr⁻ and BrO₃⁻ are each sufficiently strong oxidants to cause the oxidation of U to U(VI), Np to Np(V) and Pu to Pu(VI). The higher oxidation states of each of the respective actinides, U, Np, and Pu, are more soluble than the lower oxidation states. Actinide solubility influences transport mechanisms with respect to potential releases only in the event of fluid entry into the repository. Clearly, transport of soluble actinides could not be a feature of any release mechanism in the absence of brine. Therefore, production of oxidants and transport of soluble actinides would provide a credible release mechanism only in the event of an inundation. It is not presently possible to make a quantitative determination regarding the potential for accumulation of oxidized forms of Br under inundated conditions. It is the goal of the work proposed in this test plan to measure the chemical behavior of Br in brines in order to assess the potential impact upon chemical conditions within the repository.

3.3 Production of Hypochlorite

In general, α particles travel 30-70 μm in water (Ganguly et al., 1956). The ionization tracks of α particles in aqueous solutions include numerous hydrogen, oxygen, and hydroxyl free radicals. Ordinarily, free radicals have very short lifetimes in solution due to rapid reaction with solute and solvent molecules. Recombination processes are important in the diffusion-limited environment surrounding particle tracks of high-linear-energy-transfer species, which may yield H₂O₂ as a product of the reaction of two hydroxyl radicals. Also significant, but dependent upon the solution composition, are generation of molecular chlorine (Cl₂), hypochlorous acid (HOCl) and OCl⁻.

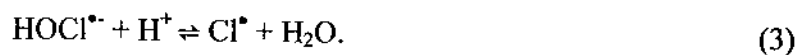
In the following discussion, the symbol "→" denotes a thermodynamically irreversible process, while the symbol "⇌" indicates a thermodynamically reversible process. Water radiolysis in the tracks of α particles leads to generation of numerous species, such as:



In which e⁻(aq) are aquated electrons, OH[•] represents hydroxyl free radicals, and H[•] represents hydrogen free radicals. Aquated electrons (e⁻(aq)) and free radical species are very reactive, rapidly combining with many other dissolved species. Additional reactions take place in the presence of significant concentrations of other solute species, such as Cl⁻. Participation of Cl⁻ in radiolytically initiated reactions leads to generation of additional chemical species due to subsequent oxidation/reduction reactions. For example, the hydroxyl radical can oxidize chloride, yielding the hypochlorous acid anion free radical HOCl^{•-} (Kim et al., 1987)



The hypochlorous-acid free-radical anion equilibrates rapidly with H^+ to give the chlorine free radical:



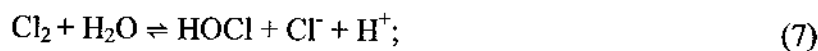
The likelihood of the chlorine radical combining with chloride is greater in solutions with high chloride content:



$Cl_2^{\cdot-}$ reacts rapidly to produce Cl_3^- , which is more stable than $Cl_2^{\cdot-}$,



The Cl_3^- species is in equilibrium with other chlorine species, ultimately producing hypochlorite:



It has been reported that the production of HOCl and OCl^- depends on the Cl^- concentration (Kim et al., 1987). The dependence of OCl^- generation on NaCl concentration is illustrated in Figure 1. Data used to generate this figure were taken from Kelm et al. (1999). Each sample contained 1 Ci/L of ^{238}Pu introduced as finely divided precipitate of Pu(VI) hydroxide. The solutions were adjusted to a pH of ~ 12 . No error bars are included because the literature reference includes insufficient data to estimate or evaluate the uncertainty. The equation for the linear best-fit line is $y = 0.0059x - 0.0105$.

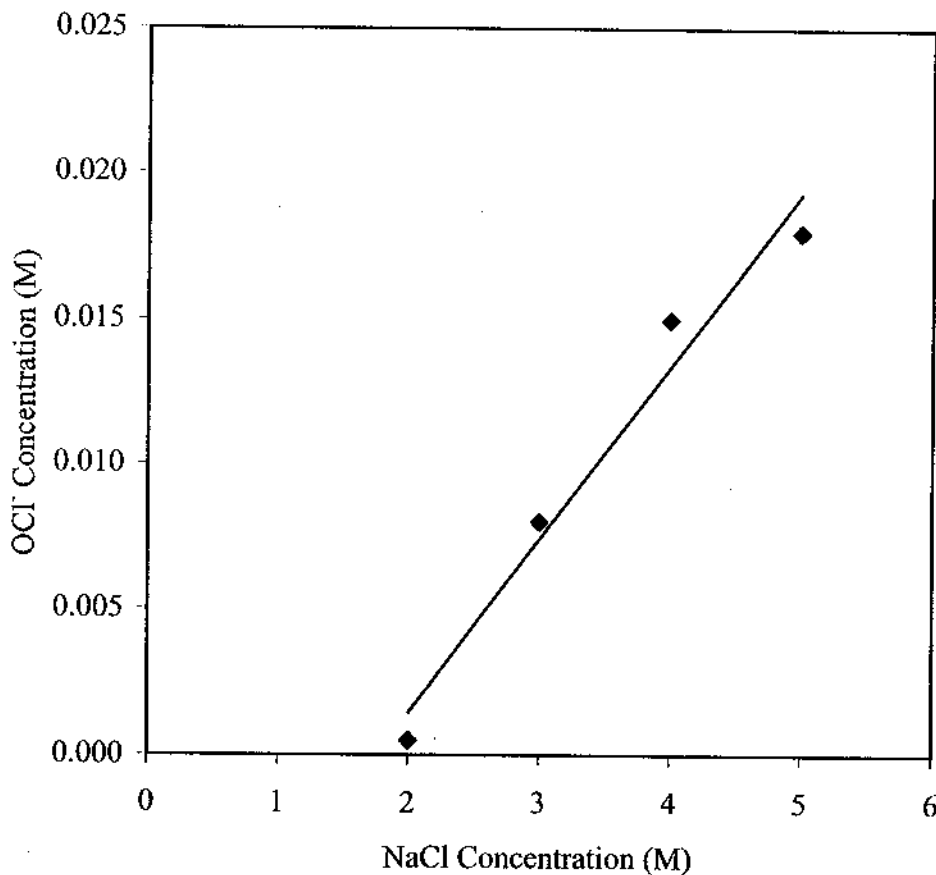


Figure 1. Generation of hypochlorite as a function of aqueous NaCl concentration.

Production of OCl^- is not a significant process for Cl^- concentrations less than ca. 1.8 M at radioactivity levels of 1 Ci/L. The minimum concentration of Cl^- required for OCl^- hypochlorite generation most likely reflects the decreased probability of reactions 4 and 5 taking place. Conversely, the data indicate that the reactions leading to HOCl production in 5 M NaCl solution produce significant quantities of OCl^- , (nearly 20 mM), in the presence of 1Ci/L of α -emitting radionuclides. The pK_a value of HOCl is 7.43 ($\mu = 1.0 \text{ NaClO}_4$, $T = 25 \text{ }^\circ\text{C}$), indicating that at pH relevant to WIPP conditions ($\text{pH} \approx 9\text{-}10$) the conjugate base (OCl^-) will be the predominant form (Martell et al., 1998). The symbol " μ " indicates ionic strength.

3.4 Chlorine Species as Oxidants

HOCl, OCl^- and Cl_2 are all strong oxidants in aqueous solution. Relevant reactions are given in Table 1.

Table 1. Standard Reduction Potentials for Reactions of HOCl and OCl⁻(a)

Reaction Number	Reaction	E° (V)
1.1	$\text{HOCl} + \text{H}^+ + \text{e}^- \rightleftharpoons \frac{1}{2} \text{Cl}_2 + \text{H}_2\text{O}$	1.61
1.2	$\text{HOCl} + \text{H}^+ + 2\text{e}^- \rightleftharpoons \text{Cl}^- + \text{H}_2\text{O}$	1.48
1.3	$\text{OCl}^- + \text{H}_2\text{O} + 2\text{e}^- \rightleftharpoons \text{Cl}^- + 2\text{OH}^-$	0.81
1.4	$\frac{1}{2} \text{Cl}_2 + \text{e}^- \rightleftharpoons \text{Cl}^-$	1.36

(a) Values are taken from Lide (1995)

Reaction 1.1 in Table 1 shows that under acidic conditions HOCl is strongly oxidizing, and may be reduced to elemental chlorine. Reaction 1.1 also shows that the oxidation of molecular chlorine to hypochlorous acid is strongly disfavored in acidic solutions, suggesting that acidic solutions of HOCl will tend to react to produce Cl₂. Reaction 1.2 suggests that HOCl may also be reduced to chloride, depending upon the pH and the identity of the species being oxidized. Reaction 1.3 illustrates that OCl⁻ is a strongly oxidizing anion in basic solutions, lying outside the thermodynamic stability field of water. Cl₂, also a strong oxidant as illustrated by Reaction 1.4, may be present under solution conditions that favor the existence of Cl₂ over HOCl.

3.5 Hydrolysis of Chlorine

The hydrolysis constant of chlorine in water may be calculated by adding reactions 1.1 and 1.4 from Table 1:

$\frac{1}{2} \text{Cl}_2 + \text{H}_2\text{O} \rightleftharpoons \text{HOCl} + \text{H}^+ + \text{e}^-$	<u>E° (V)</u>
	- 1.61
$\frac{1}{2} \text{Cl}_2 + \text{e}^- \rightleftharpoons \text{Cl}^-$	1.36
<hr/>	
$\text{Cl}_2 + \text{H}_2\text{O} \rightleftharpoons \text{HOCl} + \text{H}^+ + \text{Cl}^-$	- 0.25

The thermodynamic equilibrium constant (or hydrolysis constant) for reaction of Cl_2 with water is defined as

$$K = \frac{a_{\text{HOCl}} a_{\text{H}^+} a_{\text{Cl}^-}}{a_{\text{H}_2\text{O}} a_{\text{Cl}_2}} \quad (9)$$

The subscripted terms in Equation 9 indicate the thermodynamic activities for the respective species. The activities of each species may be expressed as products of the concentrations and the respective activity coefficients:

$$K = \frac{[\text{HOCl}] \gamma_{\text{HOCl}} [\text{H}^+] \gamma_{\text{H}^+} [\text{Cl}^-] \gamma_{\text{Cl}^-}}{a_{\text{H}_2\text{O}} [\text{Cl}_2] \gamma_{\text{Cl}_2}} \quad (10)$$

The activity of water is ≈ 0.7 in NaCl brines, which, as a first approximation, is the value used in this example. The equilibrium constant can be calculated by combining the thermodynamic relationships

$$\Delta G = -nFE \quad (11)$$

and

$$\Delta G = -RT \ln K \quad (12)$$

ΔG is the Gibbs free energy of reaction, n is the number of electrons exchanged, F is the Faraday constant, E is the cell potential, in volts, for the reaction, R is the ideal gas constant, T is the temperature in kelvins, and $\ln K$ is the Naperian logarithm of the equilibrium constant. Combining equations 10 and 11, and solving for $\ln K$ gives

$$\ln K = \frac{EF}{RT} \quad (13)$$

Solving for the hydrolysis of chlorine in water at $T = 298$ yields

$$\ln K = \frac{(-0.25\text{V})(96500\text{coulombs/mol})}{(8.314\text{J/molK})(298\text{K})} = -9.737 \quad (14)$$

Raising e to the power -9.737 yields the equilibrium constant K :

$$e^{-9.737} = 5.91 \times 10^{-5} \quad (15)$$

The hydrolysis constant may be used to calculate the approximate ratio of HOCl to Cl₂ as a function of pH by rearranging equation 9 and using a Cl⁻ concentration of 5 m NaCl:

$$\frac{K_{a_{H_2O}} \gamma_{Cl_2}}{[H^+] \gamma_{H^+} [Cl^-] \gamma_{Cl^-} \gamma_{HOCl}} = \frac{[HOCl]}{[Cl_2]} \quad (16)$$

The values of the activity coefficients for each species depend upon ionic strength and solution composition. The activity coefficients for HOCl and OCl⁻ in brines are unavailable; therefore, for the sake of this example, are assumed to be unity, along with the corresponding values for Cl₂, H⁺, Cl⁻ and H₂O. The plot in Figure 2 illustrates the relative concentrations of HOCl and Cl₂, as a function of pH. The equation for the straight line is $y = x - 4.93$, which suggests that Cl₂ is the predominant species at pH values less than 4.93, while HOCl becomes the dominant species at $4.93 < \text{pH} < \approx 8$; above $\text{pH} \approx 8$ hypochlorous acid deprotonates to form OCl⁻. Hypochlorite solutions that are acidified to pH values less than ca. 4.9 should react in the presence of Cl⁻, releasing chlorine gas.

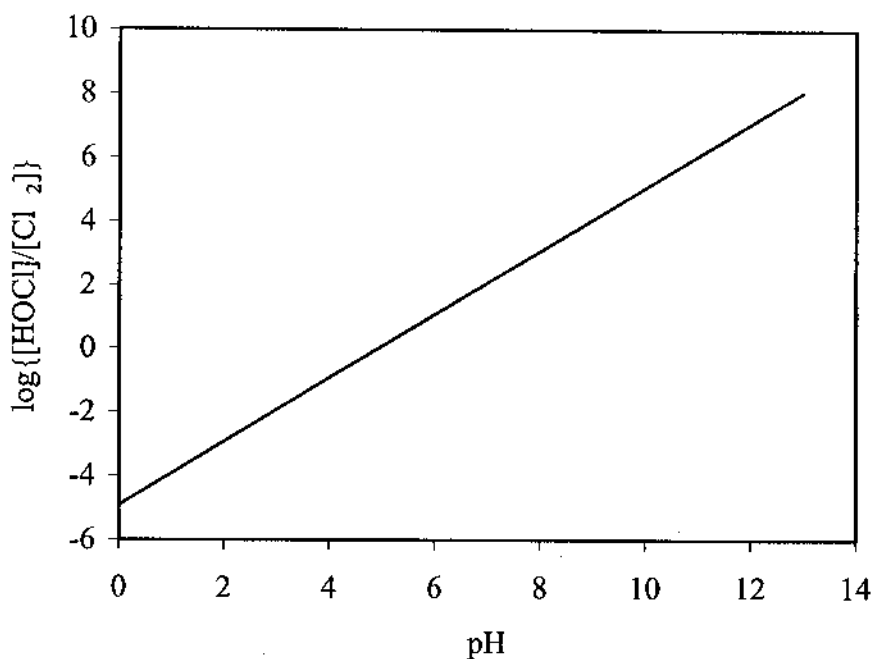


Figure 2. Plot of $\log \{[HOCl]/[Cl_2]\}$ as a function of pH.

3.6 Bromine Behavior

Bromine, (Greek *bromos*, stench) a dark brown mobile liquid, was first isolated by A.J. Balard in 1826. Commercial recovery of Br₂ in the United States is carried out on brines found in Arkansas and Michigan which respectively contain 4000-5000 ppm and ca. 2000 ppm Br⁻. The Br⁻ anion is oxidized to Br₂ by contact with Cl₂, and subsequently separated by partitioning of Br₂ into a stream of air or steam, from which it may be condensed as liquid Br₂. Some properties of Cl and Br are summarized in Table 2.

Table 2. Properties of Cl₂ and Br₂

Property	Cl ₂	Br ₂
Melting point (°C)	-101	-7.25
Boiling point (°C)	-34.0	59.5
Density (liquid, g/ml)	1.66 (-70 °C)	3.187 (0 °C)
Density (gas, g/l at 20 °C)	3.214	7.59

It should be noted that while Cl₂ is a gas at room temperature, Br₂ is a liquid, but has a substantial vapor pressure, resulting in partitioning into the vapor phase. Br₂ is a vigorous oxidant, and may react with many substances. Some reactions featuring Br are presented in Table 3.

Table 3. Aqueous Reactions of Bromine

Reaction Number	Reaction	E° (V)
3.1	$\text{OBr}^- + \text{H}_2\text{O} + 2\text{e}^- \rightleftharpoons \text{Br}^- + 2\text{OH}^-$	0.76
3.2	$\text{H}^+ + \text{HOBr} + \text{e}^- \rightleftharpoons \frac{1}{2} \text{Br}_2 + \text{H}_2\text{O}$	1.59
3.3	$\text{BrO}_3^- + 3\text{H}_2\text{O} + 6\text{e}^- \rightleftharpoons \text{Br}^- + 6\text{OH}^-$	0.61
3.4	$\text{BrO}_3^- + 6\text{H}^+ + 5\text{e}^- \rightleftharpoons \frac{1}{2} \text{Br}_2 + 3\text{H}_2\text{O}$	1.52
3.5	$\frac{1}{2} \text{Br}_2(\text{g}) + \text{e}^- \rightleftharpoons \text{Br}^-$	1.07

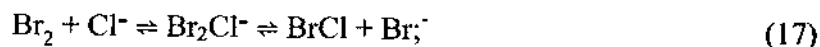
Reaction 3.1 shows that OBr^- is a strong oxidant in basic solution; comparison with Reaction 1.3 in Table 1 indicates that Br^- may be oxidized to OBr^- by OCl^- . Reaction 3.2 demonstrates that HOBr is strongly oxidizing in acidic solutions, and may yield diatomic bromine upon reduction of HOBr . Reactions 3.3 and 3.4 show that BrO_3^- is a strong oxidant under acidic and basic conditions. Reaction 3.5 illustrates that Br_2 is a strong oxidant in solution, and that the standard reduction potential for this reaction does not depend upon the pH of the solution. As ionic solutes, both OBr^- and BrO_3^- could exhibit mobility by diffusion through the solution, but its presence would be limited to the liquid phase. Conversely, Br_2 , which possesses a substantial vapor pressure at room temperature, could readily partition into the gaseous phase, in which it would have the means to migrate more rapidly and over greater distances than is possible for liquid phase components.

Both OBr^- and HOBr form metastable solutions in water, and may undergo thermodynamically irreversible decomposition reactions. HOBr can disproportionate into BrO_3^- and Br^- , whereas OBr^- can decompose to yield oxygen and Br^- . Two examples of thermodynamically irreversible reactions are illustrated in Table 4.

Table 4. Thermodynamically Irreversible Reactions of Bromine

Reaction Number	Reaction
4.1	$3\text{HOBr} \rightarrow \text{BrO}_3^- + 2\text{Br}^- + 3\text{H}^+$
4.2	$2\text{OBr}^- \rightarrow \text{O}_2 + 2\text{Br}^-$

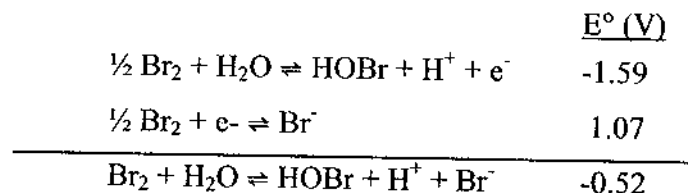
Br_2 can also react with chloride to form a bromine-dichloride anion, which may release bromide to give bromine chloride (Wang et al. 1994). BrCl , a red-brown gas at room temperature, dissociates to give Br_2 and Cl_2 . The formation of Br_3^- is well documented, with a formation constant of $\sim 10^2$ although it is unlikely that Br_3^- can form to a significant extent in ERDA-6 or GWB due to the relatively low concentration of Br^- (Pink, 1970). Hypobromous acid is a weak acid, with a pKa of 8.7 to 9.2, which suggests that it may either appear as the acid HOBr or conjugate base OBr^- in WIPP brines. Reactions of Br with Cl, and the dissociation reaction of HOBr are illustrated in equations 17 through 19. The equilibrium constant for reaction 18 is $\log K \approx 2$.



The reaction pathways that will dominate within the repository are unknown at this time. For example, Br^- may be oxidized to OBr^- , which may become protonated to HOBr, depending upon solution pH.

3.7 Hydrolysis of Bromine

The hydrolysis of Br in aqueous solutions can be expressed by adding equations 3.2 and 3.5 from Table 3:



The equilibrium constant for the hydrolysis reaction may be calculated applying the formats of equations 12 and 14:

$$\ln K = \frac{(-0.52\text{V})(96500\text{coulombs/mol})}{(8.314\text{J/molK})(298\text{K})} = -20.25; \quad (20)$$

$$K = e^{-20.25} = 1.6 \times 10^{-9}. \quad (21)$$

The hydrolysis constant may be used to calculate the ratio of HOBr to Br₂ as a function of pH:

$$\frac{K\gamma_{\text{Br}_2}}{[\text{H}^+]\gamma_{\text{H}^+}[\text{Br}^-]\gamma_{\text{Br}^-}\gamma_{\text{HOBr}}} = \frac{[\text{HOBr}]}{[\text{Br}_2]} \quad (22)$$

A plot of the ratio of HOBr to Br₂ in ERDA-6 is illustrated in Figure 3. The function was calculated using a Br⁻ concentration of 0.011 m and a hydrolysis constant of 9.6×10^{-9} at zero ionic strength (Pink, 1970). The values for the activity coefficients of WIPP brines are not known, so were not taken into account in the calculation of the relationship illustrated in Figure 3, therefore the ratio must be regarded as an approximation. The equation that describes the line in Figure 3 is $y = x - 6.26$, which indicates that at pH values less than ca. 6.26 HOBr tends to react to form Br₂. Conditions that favor formation of Br₂ include the higher ionic activity coefficient of the H⁺ ion in brines, which is not taken into account in Equation 21, and the partitioning of Br₂ out of the aqueous phase into the vapor phase.

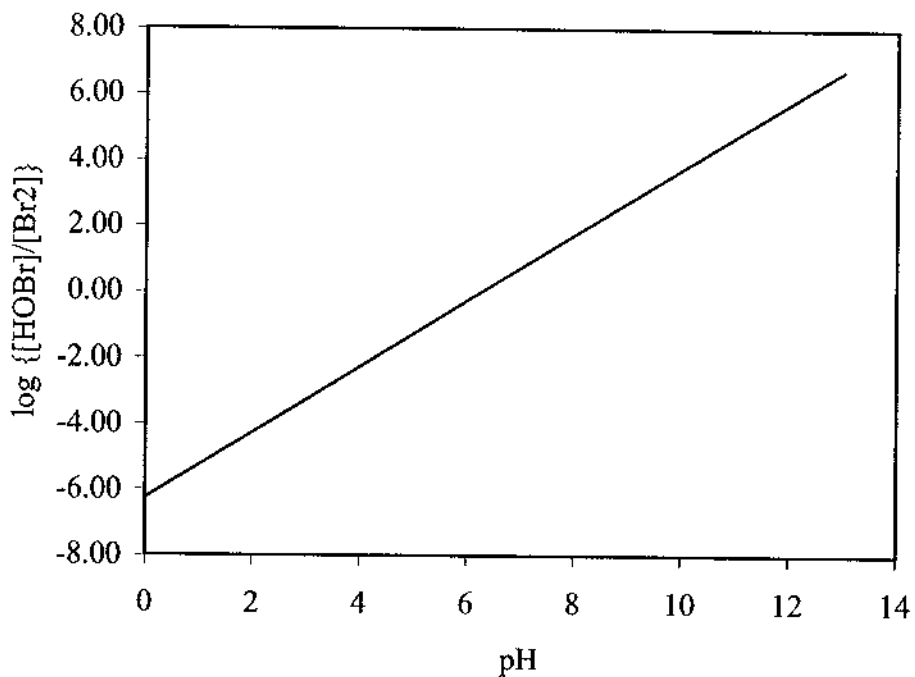


Figure 3. Plot of $[\text{HOBr}]/[\text{Br}_2]$ as a function of pH.

3.8 Bromine Absorbance Spectra

Some reference spectra of Br species are illustrated in Figure 4 (Betts and MacKenzie 1951, Pink 1970).

The spectra of Br_2 , Br_3^- , HOBr and BrO_3^- allow the absorption bands to be used as a means of both identification and quantification. HOCl and OCl^- have absorbance maxima at 242 nm and 292 nm, respectively. The concentration of a chromophore (light-absorbing species) in solution is related to the spectral absorbance by the Beer-Lambert Law:

$$A = \epsilon_n c l. \quad (23)$$

A is the absorbance, ϵ_n is the molar absorptivity (sometimes called molar extinction coefficient) at wavelength n , c is the concentration of the absorbing species, and l is the path length of the sample. As a result, when the sample size and molar absorptivities are known the UV-vis spectra may be used to monitor the concentrations of the species in solution.

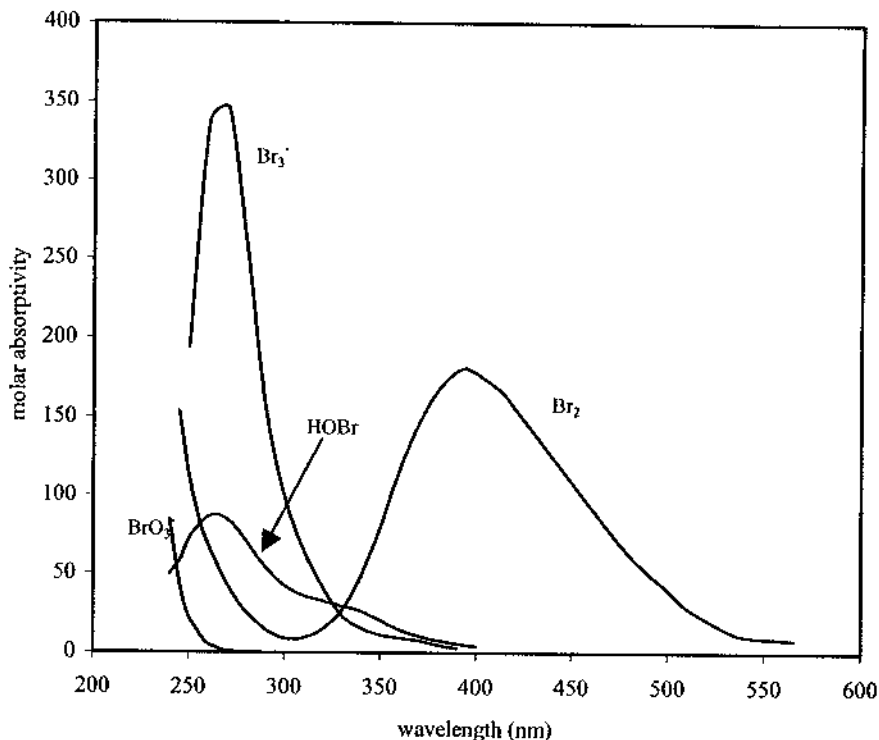


Figure 4. Sample spectra of Br species in water.

The UV absorbance maximum of Br_2 at ~ 390 nm, is due to excitation of an electron from the highest occupied molecular orbital (π_g) to the lowest unoccupied molecular orbital (σ_u). The symbols π_g and σ_u refer to the symmetry of the orbitals; both are antibonding orbitals. An interaction between a halogen molecule and another solution component, either solute or solvent, that tends to lower the energy of the π_g orbital or raise the energy of the σ_u orbital causes an increase in the difference in energy between the orbitals, with a concomitant increase in the energy required to promote an electron from the lower energy to the higher energy orbital, which would cause the absorbance peak to shift toward the higher energy blue region of the electromagnetic spectrum. Conversely, an interaction tending to increase the energy of the π_g orbital or decrease the energy of the σ_u orbital leads to lesser separation in the orbital energies, thus demanding less energy input to cause an electronic transition between the respective levels, resulting in a shift toward the lower energy red region of the electromagnetic spectrum. The possible transitions are illustrated in Figure 5, which shows the relative molecular orbital energies for diatomic halogens.

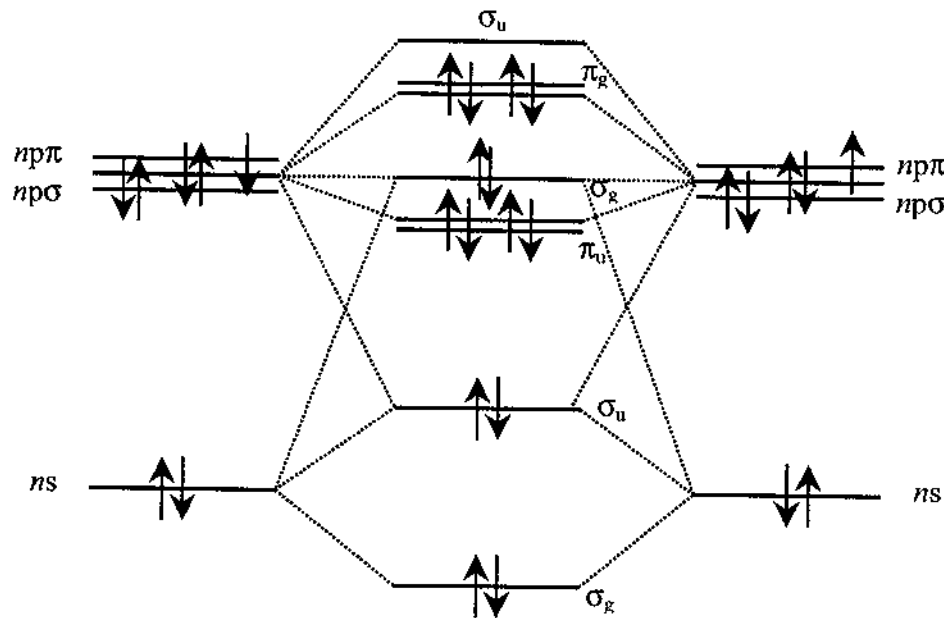


Figure 5. Molecular orbital diagram for diatomic halogen molecules

The ns and np levels correspond to the principle quantum number of the contributions by the linear combination of atomic orbitals, which are $n = 3$ and $n = 4$ for Cl and Br, respectively. It is unknown what type of interactions may occur between Br_2 species and other brine components; as a result, it will be necessary to experimentally determine the spectra of Br_2 , OBr^- , $HOBr$, BrO_3^- and Br_3^- to establish a spectral reference library.

3.9 Interactions of Oxidized Bromine Species with U, Np, Pu

Br_2 , OBr^- , and BrO_3^- will oxidize Pu to Pu(VI), U to U(VI), and Np to Np(V). Figure 6 illustrates the Latimer diagrams for redox reactions of U, Np, and Pu.

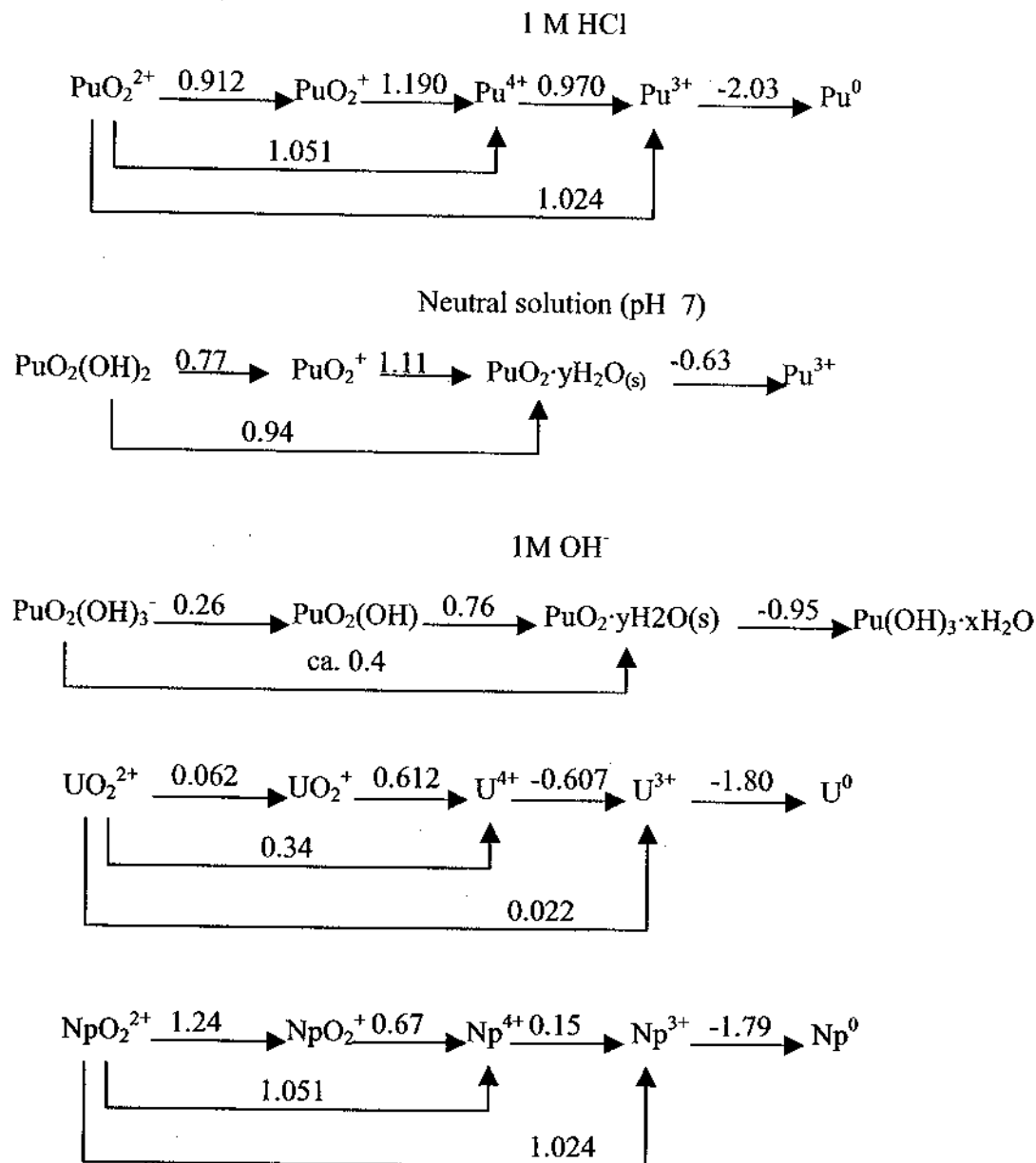


Figure 6. Latimer diagrams for oxidation/reduction behavior of U, Np, and Pu.

Pu data in Figure 6 are adapted from Cleveland (1979); U and Np data are adapted from Katz et al. (1986).

Comparison of the standard reduction potentials of Br species in Table 3 with the potentials for Pu suggests that Br_2 , HOBr , OBr^- and BrO_3^- may all oxidize Pu to Pu(VI) under a wide range of pH. Br_2 is even capable of oxidizing Pu to Pu(VI) under acidic conditions, at which Pu(III) is the most stable. Use of BrO_3^- as a holding oxidant to prepare and store Pu(VI) solutions is also a widely practiced procedure. Diatomic bromine can oxidize Pu to Pu(VI), and U to U(VI), but does not oxidize Np beyond Np(V). In fact, it is the capability to oxidize U and Pu to their VI oxidation states that makes Br_2 a useful oxidant to separate either U or Pu from Np. For example, addition of Br_2 to a slightly acidic ($\text{pH} \approx 2$) solution of Np and Pu will result in the Pu being oxidized to Pu(VI), leaving the Np as Np(V). The two may be easily separated by extraction of PuO_2^{2+} with a solution of di-2-ethylhexylphosphoric acid in heptane.

3.10 Reactions of Cl and Br Species

Solutions of HOCl and OCl^- are sufficiently reactive that they will oxidize Br^- to HOBr , OBr^- or BrO_3^- when added to a solution containing Br^- . The identity and concentrations of the products, i.e., the preferred reaction pathway, depend upon conditions such as reactant concentrations. The significantly different mobility of the ionic (OBr^- and BrO_3^-) vs. molecular (Br_2) species makes it quite important to determine the identity of the products of Br^- oxidation in WIPP brines, based upon quantitative, experimental data. The objectives outlined in subsections 3.10.1 through 3.10.4 are described in terms of the previous discussion on the behavior of chlorine and bromine, and how the behaviors may influence other materials such as iron or the actinide elements.

3.10.1 Conditions Influencing Generation of Oxidized Forms of Bromine

It is unknown what form the oxidized species of Br may take in WIPP brines. For example, the reaction of HOBr with Br^- and H^+ may give Br_2 as a product at neutral to basic pH conditions, depending upon activity coefficients of the reactants and products. The impact of high ionic strength on the hydrolysis equilibrium of Br_2 is unknown. It is necessary to experimentally determine which species predominate under conditions similar to those expected to persist in the repository environment.

3.10.2 Determination of the Stability Constant of Br_3^- in Brine

Br_2 in aqueous solution combines with Br^- to form Br_3^- . The Br_3^- anion would tend to reduce the partitioning of Br_2 from the aqueous phase into the vapor phase due to the nonvolatility of the charged species. A sufficiently stable Br_3^- anion may serve to reduce the mobility of Br_2 by formation of the ionic species. It is not known whether the presence of Br^- in WIPP brines will lead to the formation of Br_3^- , with concomitant reduction of transfer of Br_2 to the vapor phase; therefore, it is necessary to determine whether formation of complexes of Br_2 can cause retention of Br_2 in the aqueous phase.

3.10.3 Determination of the Partition Coefficient of Br₂

Br₂ exhibits a solubility of 33.6 g/l in water at 25 °C. Increases in ionic strength usually cause increased activity coefficients of uncharged atomic and molecular species, which generally leads to decreases in solubility in aqueous solutions, often described as the "salting-out effect." The effect of WIPP brine compositions on aqueous Br₂ solubility is not known. Increased solubility would have a demobilizing influence on Br₂, while decreased solubility would cause the movement of greater amounts of Br₂ into the gaseous phase. Therefore, it is necessary to investigate the dependence on solution composition of the partitioning of diatomic bromine between the aqueous and gaseous phases.

3.10.4 Effect of Fe on Production and Concentration of Br Species

The presence of Fe may have a significant impact upon the steady-state aqueous-phase concentrations of oxidized Br species. Metallic Fe, and Fe(II) will be available as reductants in the repository, and may react with oxidized Br species, yielding Br⁻. The goal of this task is to examine the effect of the presence of Fe on the stability and concentration of the oxidized Br species: Br₂, HOBr, OBr⁻, and BrO₃⁻.

4 EXPERIMENTAL PROCESS DESCRIPTION

The experimental process description includes further definition and explanation of the tasks to be performed, which will serve as a narrative depiction of a proposed experimental matrix. The objectives of this study will be addressed by defining and carrying out a series of tasks that will provide the data to assess issues of bromine behavior in brines. Descriptions of measuring and test equipment, experimental procedures and materials follow the descriptions of the tasks.

This test plan is not intended to provide a complete description of the details of proposed experiments or in the manner of their implementation. Procedures that will be used during the course of this experimental program are standard laboratory analytical procedures, such as titration and UV-vis spectrophotometry. It is not anticipated that it will be necessary to develop new or unusual experimental methods to carry out the work described within this test plan. All procedures that are employed during the course of this work will be described in detail in the laboratory notebooks in such a way that an independent reader may understand and duplicate the work. It will be necessary to evaluate the results of experiments in order to assess appropriate methods for further experimental procedures; therefore, it is impracticable to attempt to define or employ standardized procedures for much of the work.

Sources of experimental error and evaluation of the impact of error are discussed in Subsection 4.10, Known Sources of Error and Uncertainty.

4.1 Task 1. Determination of Conditions Influencing Generation of Oxidized Br

There are several factors that may affect the identities and concentrations of the reaction products, including:

- ionic strength and chloride concentration,
- temperature, and
- pH.

Sets of standard UV-vis spectra for each chromophore will be obtained by dissolving known amounts of each analyte in each solution matrix and measuring the spectra. The absorbance at each wavelength for a series of samples of known composition will be plotted as a function of concentration to obtain the molar absorption coefficients.

The products of reaction between HOCl/OCl⁻ and Br⁻ will be investigated by adding each component to salt solutions of different compositions. The solution matrices will include various concentrations of NaCl from 0.1 to 5 m. Other samples will be prepared in representative WIPP brines, such as ERDA-6 and GWB, and at various dilutions of the WIPP brines. The reaction of oxychlorine species and oxidation of Br⁻ will be followed by monitoring the change in the UV-vis absorbance spectra of each species. Some reactions may be slow enough to follow the change in concentrations over time by measuring the changing intensity of the UV-vis absorbance. For example, OCl⁻ decomposes slowly in aqueous solutions, and the rate may be easily measured by monitoring the change over time of the intensity of the UV absorbance at 292 nm. HOBr and OBr⁻ are also thermodynamically unstable in water, and will decompose over time, although the reaction rates in brine of oxidized Br species are not currently known. If the formation and decomposition of HOBr and OBr⁻ are sufficiently slow, i.e., on a time scale of minutes to days, the reaction will be monitored and the rate constants determined. For the purposes of this work, reactions will be considered to take place instantaneously if the rates are too rapid to be followed by UV-vis spectroscopy.

The temperature of the solutions will be monitored and controlled. A set of experiments will be initially performed to determine the magnitude of temperature dependence of the bromine hydrolysis reaction and the deprotonation reaction of hypobromous acid. These reactions will be carried out in a titration vessel of a Mettler DL 25 automatic titrator. The vessel will be immersed in a thermostatted water bath to maintain a controlled-temperature environment. Subsequent experiments will be carried out under controlled-temperature conditions (e.g., in a constant-temperature water bath) if it is determined that temperature is a critical variable that must be controlled.

Variations in pH affect the redox potentials for the oxidation and reduction of Cl and Br species, possibly exerting an influence on the reaction pathway and products. Therefore, a series of solutions of OCl⁻ and Br⁻ with pH values between 5 and 10 will be examined. The experiment

will be repeated at each of the ionic strengths used in the set of variable-ionic-strength experiments described above.

Each of the activities described in this section involves combining the appropriate reagents under a variety of conditions, with ensuing analysis of the reaction products. Each test will be carried out at least in triplicate in order to evaluate experimental reproducibility and uncertainty. It is anticipated that, in order to adequately capture an acceptable range of parameter possibilities, it will be necessary to prepare and analyze more than 100 samples, varying in size from 5 to 250 mL. The appropriate number and compositions of the samples will be determined on an ongoing basis according to the judgment of the principal investigator; sample preparation, analysis and justification will be documented in the laboratory scientific notebooks.

4.2 Task 2. Determination of the Stability Constant of Br_3^- in Brine

The stability constant of Br_3^- may be determined by simultaneously measuring the concentrations of Br_2 and Br_3^- in a solution containing a known amount of Br^- . The concentrations of Br_2 and Br_3^- may be determined by measuring the intensity of the UV-vis absorbance peaks of the two species. The Br_2 will be introduced to the solution by dissolution of Br_2 vapor, obtained from a stock sample of $\text{Br}_2(\text{l})$.

This task will be carried out with a series of sample batches to study the dependence of partition coefficients on various independent variables. The impact of each variable (solution composition, pH, temperature, etc.) will be examined through analysis of triplicate samples for a particular set of parameter values, each of which will be systematically varied while holding the values of the remaining parameters constant. Thus, it is likely that this activity will involve the generation of at least dozens, and possibly as many as several hundred samples. The sample sizes are expected to be on the order of 5 to 10 mL per sample, which makes labeling, storage, handling and testing a routine and simple matter.

4.3 Task 3. Determination of the Partition Coefficient of Br_2 between Phases

Br_2 , which exhibits considerable solubility in water, may be less soluble in brines due to the salting-out effect. The partition coefficient between the aqueous and gaseous phase will be determined by preparing aqueous samples of Br_2 in sealed containers, allowing the sample to come to equilibrium, then withdrawing aliquots of each phase for analysis. The aqueous samples will be analyzed by UV-vis spectroscopy for Br_2 concentration, as well as for the presence and concentrations of other hydrolysis products and oxidized Br species. Samples of the gas phase will be analyzed either by passing the gaseous aliquot through a solution of sodium hydroxide (NaOH), in order to form OBr^- , followed by UV-vis determination of the OBr^- concentration or by GC/MS analysis of the gas sample.

Analogous to Task 2 described in Section 4.2, this task requires generation of numerous batches of small samples.

4.4 Task 4. Determination of the Effect of Fe on Oxidized Br Species

Redox active transition metals, such as Fe and Cu are also likely to react with OBr^- . The change in concentration of the reacting Br species will be determined by following the change in the UV-vis absorbance spectra of the reactants and products. The experiments will be performed in brine solutions with different amounts of Br_2 , HOBr/OBr^- or BrO_3^- . The experiments will be repeated at a variety of pH values from 5 to 10 to ascertain the hydrogen-ion-concentration effects.

Aliquots of oxidized Br species (Br_2 , HOBr , OBr^- and BrO_3^-) will be added to brine solutions (5m NaCl, ERDA-6, GWB) along with metallic iron or ferrous chloride salts. A multi-variable test matrix in no less than four-dimensional space will be established to specifically include as independent variables the following parameters:

- identity and concentration of oxidized Br species;
- solution composition (i.e., brine type, including salt composition and concentration);
- additional solution components, such as Fe; and
- pH.

Additional independent variables may be added if it is determined during the course of the experimental work that parameterization of additional independent variables is a necessary factor to adequately characterize the system behavior.

It has been previously determined that the decomposition rates of OCl^- may be measured over the course of 3 to 4 weeks. It is likely that decomposition reactions of OBr^- would proceed at a more rapid pace than OCl^- due to the greater reactivity of OBr^- relative to OCl^- . Oxidation/reduction reactions between Fe and oxidized Br species are likely to proceed at a rapid rate, reaching completion within seconds to minutes. Consequently, an experimental matrix may be devised to elucidate the effect of variation of parameter values, such as solution composition and pH, and execution of such a matrix would entail generation of at least several dozen samples.

4.5 Measuring and Test Equipment

Measuring and test equipment, include the following instruments and types of apparatus:

- Perkin Elmer Optima 3300DV inductively coupled plasma optical emission spectrometer,
- Mettler DL 25 automatic titrator with Mettler Toledo DG111-SC pH electrode,
- Cary 300 Conc UV-vis spectrophotometer,
- Mettler Toledo Delta Range AT261 analytical balance,

- Sartorius Basic balance,
- RC6 Lauda temperature controller,
- Ertco-Eutechnics digital thermometer model 4400,
- Varian 3900 gas chromatograph and Varian 2100T mass spectrometer, and
- JEOL JSM 5900LV scanning electron microscope.

All measuring and test equipment will be used in accordance with NP 12-1 (Subsection 5.2).

The ICP-OES is an inductively coupled plasma atomic-emission spectrometer. Liquid samples are introduced into the instrument through an auto sampler. The samples are aspirated into a plasma ionization chamber, which destroys the sample matrix, atomizes, and ionizes the component atoms. Photons of discrete energies are emitted upon transition from the quantized excited to ground electronic states for each component element, which allows quantification by wavelength-dispersive analysis of the intensities of the light given off during the de-excitation process. External-standard calibration is done by measuring instrument response as a function of analyte concentration for a series of samples containing standardized amounts of the analyte of interest. Under ordinary circumstances the instrument has a dynamic range of several orders of magnitude, and features linear response to sample concentration. Second (parabolic) or higher order response in analytical instruments often indicates detector saturation, matrix interference, or other concentration-dependent instrumental responses. Evaluation and documentation of calibration, and calibration data will be recorded in the scientific notebook. Use of internal standards, surrogate standards, blank spikes, matrix spikes, or other methods of batch control will be documented in the scientific notebook.

The Mettler DL 25 automatic titrator is equipped with a combination glass electrode for potentiometric measurement of hydrogen-ion activity. The titrator can be programmed to measure the pH and to make controlled additions of a titrant from an automatic buret to a sample vessel. The temperature of the titration vessel is controlled by immersion in a thermostatted water bath. N₂ gas is introduced to the interior of the vessel to maintain an inert atmosphere. Data output from the instrument is fed directly to a laser printer, which provides tables of raw data. The data may be transferred to Microsoft Excel (or a comparable spreadsheet program) for further analysis.

Analytical balances will be calibrated before use on a daily basis, at a minimum. Certified, traceable calibration-standard weights will be used as calibration standards, continuing calibration-check standards, or both.

Solution volumes will be measured either with Class A glass pipettes, or autopipettes equipped with disposable tips. Calibration of all pipettes will be confirmed before use by

measuring the volume of water dispensed, which will be determined by mass, as indicated by a calibrated analytical balance.

Instrument response of the pH-measurement system will be checked by calibration against traceable, standard buffer solutions, or by titration of standardized acid and base solutions. Identity of the calibration solutions will be recorded in the scientific notebook. Constant-temperature and constant-atmosphere conditions will be maintained during titrations, if necessary, by immersion of the titration vessel in a thermostatted water bath, the temperature of which will be monitored with a thermometer that will be calibrated against a certified, traceable standard thermometer. If necessary, inert atmosphere will be maintained by purging the titration vessel with N_2 . Temperature and atmosphere control and conditions will be recorded in the scientific notebook.

The UV-vis spectrophotometer is a Cary 300, equipped with D_2 and tungsten-filament lamps. The instrument performs an internal wavelength calibration upon start up, using emission lines generated by the D_2 lamp. The 100%-transmittance calibration is performed by placing a cuvette containing the solvent without the chromophore, and scanning the instrument through the analytical wavelengths. The 0%-transmittance calibration is performed by blocking the sample path with an opaque object, such as black painted sheet metal, and scanning the instrument through the same wavelength region as used in the 100%-transmittance measurement. The instrument responses are assigned to the respective 0- and 100%-transmittance measurements at each wavelength.

4.6 Reagents

Deionized water will be used to prepare all aqueous solutions. All solutions will be filtered to remove insoluble matter.

$NaOCl$ will be obtained from documented commercial sources such as Fisher Chemical Co. The concentration of OCl^- may be determined spectrophotometrically or by potentiometric titration (Vogel, 1989; Adam and Gordon, 1999).

Br_2 will be obtained from documented commercial sources such as Fisher Chemical Co. or prepared by oxidation of Br^- by OCl^- . Oxidation of Br^- may be done as follows: A cold, saturated solution of $NaBr$ in water, acidified to $pH = 1$, will be transferred to a separatory funnel, which is cooled in an ice bath. A second separatory funnel will be used to slowly add a cold solution of $NaOCl$ to the $NaBr$ solution. The OCl^- oxidizes Br^- to Br_2 under acidic conditions. In a cold solution, the Br_2 condenses in the bottom of the funnel, from which it may be removed as the liquid Br_2 . The liquid Br_2 may be conveniently stored in a sealed glass bottle. Supplies of Br_2 will be generated as needed. Aqueous solutions of Br_2 will be prepared by transferring aliquots of gaseous Br_2 from the stock storage container to a syringe and bubbling the Br_2 gas through water or brine. The concentration of Br_2 and other Br species will be determined by UV-vis spectrophotometry.

All other reagents, such as salts used to prepare brine solutions, will be obtained from commercial sources. The quality of the reagents will be appropriate for the intended use. The name of the commercial vendor and lot number for the material will be recorded in the scientific notebook.

4.7 Experimental Procedures

4.7.1 General Procedures

Sample preparation and analysis procedures, (weighing, pipetting, etc.) are standard laboratory analytical procedures. Instrumental analyses, such as UV-vis spectroscopy, will be performed in accordance with written procedures supplied by the instrument manufacturer. Any deviations will be described and justified in the scientific notebook.

Calibration of pH measurement instrumentation will be performed under inert (N_2) atmosphere with temperature control. Design of experimental apparatus and method of control of parameters (temperature, atmosphere, etc.) will be fully described in the laboratory notebooks. Temperatures of samples will be monitored and recorded.

4.7.2 Preparation of Brines

Brine solutions will be prepared according the method given in the SNL NWMP Technical Operating Procedure (TOP)-544 (Subsection 5.2).

4.7.3 Determination of Reaction Products and Stoichiometry

Solutions containing known amounts of NaOCl and will be combined with standardized Br^- solutions. Product identities and yields will be monitored by measuring the change in the UV-vis absorbance spectra.

4.7.4 Development of Baseline Spectra of Each Species in Brines

Known quantities of $NaBrO_3$ will be dissolved in water, ERDA-6, GWB, and Brine A. The UV spectra will be obtained, and used to determine molar absorptivity coefficients for use in quantitative analysis of samples that contain unknown amounts of BrO_3^- .

4.7.5 Determination of Reaction Rate of Br^- with OCl^-

The rate of change in the amounts of products resulting from the oxidation of Br^- by OCl^- will be monitored by measuring the rate of change of the concentrations of the products over time, using UV-vis spectroscopy. The kinetics of the oxidation reactions in brine are not known,

so it is not possible to state whether this analytical method is suitable to follow the progress of the reaction. If the reaction is too fast to follow by this method, no further work will be done to determine the rate constants.

4.7.6 Acid Dissociation Constant of Hypobromous Acid

The acid dissociation constant of hypobromous acid will be determined by spectrophotometric titration and/or potentiometric titration.

In a spectrophotometric titration, a series of samples containing the same total Br concentration will be adjusted to different pH values, and the UV-vis spectra obtained. The values of the molar absorptivities can be used to calculate the concentrations of HOBr and OBr⁻ at each step in the titration. The concentration values may be entered into the Henderson-Hasselbalch equation, and used along with the pH values to determine the acid dissociation constant.

4.8 Coordination with Organizations Providing Inputs or Using the Results

There are no other organizations providing inputs in terms of data, experimental design, sample analysis, data compilation or interpretation of results. No coordination activities for inputs are planned at the time of the writing of this test plan.

The outcome of the experimental work described herein is unknown at the time of the writing of this test plan, although it may be anticipated that the data will be used to further evaluate the long-term effects of radiolytic generation of oxidants. The results of the experimental work will be provided to the DOE CBFO for further evaluation.

4.9 Procedures to Be Used/Developed

The procedures that will be used are part of commonly practiced standard laboratory techniques such as titrations and spectrophotometry. The procedures that will be employed are generally described in the section describing reagents and procedures, although specific procedures as applied to a particular experiment will be completely documented in the scientific notebook.

No prerequisites or special controls are specified at the time of the writing of this test plan. No unusual procedures to control specific environmental conditions, such as storage under controlled atmospheres, are necessary. Controls over other relevant conditions will be recorded in the laboratory notebooks. No unusual processes are anticipated to be employed. The skills developed during the course of work in an analytical or inorganic chemistry laboratory are anticipated to be sufficient to successfully perform the work.

4.10 Known Sources of Error and Uncertainty

Sources of error include:

- pH measurement,
- volume measurement,
- weighing error,
- impure reagents, and
- temperature.

Errors of pH measurement will be minimized by calibration of measuring equipment with standard buffer solutions and by titration with standardized acid and base solutions. Standard procedures for instrumental pH measurement are widely practiced and published in peer-reviewed literature. Procedures will be described in the laboratory notebook and relevant procedural references provided. Typical magnitudes of uncertainties in pH measurements are 0.01 to 0.02 log units. Uncertainties in pH are generally introduced by the inherent uncertainty in the pH of calibration standards, instrumental drift, and variations in electrode response due to variations in solution composition. These sources of error can be very difficult to control, therefore assessments must be made on an ongoing basis with respect to balancing the efforts required to minimize sources of uncertainty with the cost in terms of time required to implement extraordinary measures to minimize uncertainties. Uncertainties of 0.01 to 0.02 log units on the pH scale are considered acceptable, and will have minimal impact upon the quality of the results.

Errors in volume and mass measurements have the potential to exert considerable impact upon the quality of the results. Uncertainties in volume measurements will be controlled by use of Class A volumetric glassware that will be calibrated by measuring a standard volume of water with a calibrated laboratory balance. Volumetric glassware must exhibit less than 0.5% error in order to be considered acceptable for use. Mass measurements will be made with standard laboratory analytical balances that have been calibrated and checked against traceable standard weights. Calibration of all volumetric and weighing equipment will be documented in the appropriate scientific notebooks.

All reagents will be certified ACS reagent grade or better. If necessary, reagents will be purified by standard, documented procedures. The reagent grade, source, and if applicable, purification methods will be documented in the laboratory notebooks.

Temperature as a variable may have a significant impact upon the results of kinetics experiments, and a smaller but measurable effect on pH measurements. Kinetics trials will be conducted at a variety of temperatures to assess the importance of this variable. If necessary, the samples will be stored under controlled-temperature conditions, such as within a thermostatted oven or water bath. Assessment of temperature as a variable, and temperature monitoring and

control procedures will be fully documented within the laboratory notebooks. A thermometer that will have been subjected to a calibration check against a traceable standard thermometer will be employed to monitor the titration apparatus during the course of pH measurements. The temperature of the titration apparatus will be controlled with a thermostatted circulator that is capable of temperature control to within 0.1 °C.

4.11 Data Processing and Mathematical Models

Data processing may be done by hand calculation with the aid of an electronic calculator, or with a standard spreadsheet program, such as Microsoft Excel. Data processing more complicated than simple algebraic manipulations are not anticipated at the time of the writing of this test plan. Requirements for documentation of routine calculations are described in the NP 9-1 (Subsection 5.2). Routine calculations will be verified and documented in the laboratory notebooks, in accordance with the procedural requirements described in NP 9-1.

4.12 Documents to be Maintained as QA Records

Scientific notebooks and hardcopies of instrumental output will be maintained as QA records. Instrument output in electronic format will be preserved on a computer disk or other suitable media, and will be submitted to the SNL Records Center along with other QA records.

4.13 Sample Handling and Control Requirements

Standard procedures for sample identification, handling, storage, shipping, archiving and disposition have been described in NP 13-1. Sample handling will be performed in accordance NP 13-1.

Samples will be labeled with unique identification numbers, the date, and will be referenced in the laboratory notebook. Solutions, such as standardized stock metal solutions, will be handled and stored in accordance with documented procedures.

Samples will be stored within the working area of the chemistry and geochemistry research area at SNL's Carlsbad laboratory. No special precautions are planned to secure the samples.

4.14 Sample Disposal

Aqueous solutions of HOCl and OCl⁻ in brines are non-hazardous, and may be disposed of directly into the sewer, without any special precautions. Organic solutions will be disposed of in accordance with standard operating procedures in place at SNL's Carlsbad laboratory. Hazardous waste generation is not anticipated at the time of this writing.

4.15 Data Acquisition System

Calibrations and calibration checks will be performed on instruments in the manner described in Subsection 4.5. Analytical instruments and laboratory equipment will be considered to be exhibiting acceptable performance when the following criteria are met:

- Calibrations for the ICP-OES instrument will be considered successful if the initial calibration data exhibit linearity within tolerances established by the instrument manufacturer.
- Initial or continuing calibration of analytical balances will be considered as indicating fitness for use when the instrument indicates that all standard calibration check weights conform within 0.1% of the nominal value.
- Volumetric equipment must exhibit less than 1% relative standard deviation error in order to be considered acceptable for use.
- Calibration of pH-measuring apparatus will be considered acceptable if the data exhibit linearity, and the instrument response is greater than 90% efficient (i.e., >53.1 mV/pH unit).
- Wavelength and percent-transmittance calibration of the Cary-300 UV-vis spectrophotometer will be performed upon instrument start up, at least one time per day that the instrument is used.

4.16 Commercial Software, Not Modified

The commercial, off-the-shelf software that will be used in the work described in this test plan includes the software that is used to operate the analytical instruments, and Microsoft Excel for performing routine calculations. The software will be used in accordance with NP 19-1 (Subsection 5.2). The commercial, off-the-shelf software will be used as originally written by the software supplier, without changes to the original source code.

Routine spreadsheet calculations will be performed with Microsoft® Excel 2000 run on a Dell Precision 620 desktop PC, or equivalent. Use of any other spreadsheet programs will be described and documented in the scientific notebook.

4.17 Other Software

No software other than commercial, off-the-shelf software, not modified, will be used in this work.

4.18 Justification, and Documentation of Deviations from Test Standards

Significant departures from procedures documented in the open scientific literature will require revision of this test plan.

4.19 Experimental Controls

Each experimental determination of decomposition rate constants, acid dissociation constants, and any other experiment yielding thermodynamic or kinetic values, will be repeated in order to reduce likelihood of inadvertent introduction of indeterminate errors. In order to evaluate reproducibility and develop statistical estimates of uncertainty, each experiment will be replicated with a minimum of duplicate samples and duplicate analyses as is normally expected within the scientific community as a part of sound experimental practice. If it is deemed necessary to use blank spikes, matrix spikes, internal or surrogate standards, the relevant procedures will be documented in the scientific laboratory notebook.

4.20 Control and Characterization of Test Media

Test media and samples will be characterized by the analytical methods described elsewhere in this test plan.

4.21 Data Identification and Use

Data amenable to written recording will be inscribed by hand in appropriate laboratory notebooks. Such information includes, but is not limited to:

- reagent and solution preparation and purification procedures and results;
- sample preparation procedures;
- sample composition and conditions (e.g., pH, reagent volume, reagent concentration, temperature);
- sample handling; and
- sample-analysis procedures and results.

Instrumental data output, such as tabulated values and parameters, will be stored in a data binder, and appropriate reference to the data location will be made in the laboratory notebook.

4.22 Data Transfer and Reduction Controls

Typical data transfer is from instrumental output to laboratory notebook and from

laboratory notebook to a spreadsheet program. Printed copies of spreadsheets with full explanations of spreadsheet calculations will be permanently attached to the laboratory notebook or in a data binder specifically designated for the purpose. Data stored separately from the laboratory notebook, e.g., in a designated three-ring binder, will be appropriately referenced in the laboratory notebook.

4.23 Identification, Segregation, Disposal of Erroneous Data

Data suspected of being erroneous will be tested by comparison to replicate samples or replicate experiments. Statistical justification for rejection of erroneous data will be provided within the laboratory notebook.

5 TRAINING AND OTHER STANDARD PROCEDURES

5.1 Training

All personnel participating in the work described in this test plan will be trained and qualified for the assigned tasks. This requirement will be implemented in accordance with NP 2-1 (Subsection 5.2).

5.2 NPs, SOPs, and SPs

The following NPs, SNL Standard Operating Procedures (SOP), and SNL NWMP Activity/Project-Specific Procedures (SPs), and TOPs are applicable. Note that the versions listed below may not be the current versions. Always check the SNL NWMP web site (www.nwmp.sandia.gov/onlinedocuments/) to find the current version of these or other NPs, SOPs, or SPs.)

- NP 2-1, "Qualification and Training;"
- NP 4-1, "Procurement;"
- NP 6-1, "Document Review Process;"
- NP 6-2, "Document Control Process;"
- NP 9-1, "Analyses;"
- NP 12-1, "Control of Measuring and Test Equipment;"
- NP 13-1, "Sample Control;"
- NP 17-1, "Records;"

- NP 19-1, "Software Requirements;"
- NP 20-1, "Test Plans;"
- SOP-C001, "Standard Operating Procedure for Activities in the SNL/Carlsbad Laboratory Facility;"
- SP 1-1, "QA Grading;" and
- SP 13-1, "Chain of Custody;"
- TOP 544, "Preparing Synthetic Brines for Chemical Retardation and Transport Experiments."

5.3 Procurement Procedures

Procurement of materials or services will be done in accordance with NP 4-1 (Subsection 5.2). Procurement of capital equipment is not expected.

6 HEALTH AND SAFETY

Elemental bromine exhibits considerable volatility and due to its activity as an oxidant, exhibits corrosivity and reactivity that make it hazardous if inhaled. Accordingly, work that has the potential to release significant amounts of gaseous bromine will be performed in a fume hood with adequate ventilation in order to preclude inhalation of hazardous vapors. The principal investigator of this project has considerable experience working with hazardous materials, including experience in experimental work in glove boxes and fume hoods. All experimental work will be performed in a manner that minimizes risk and does not adversely affect worker health or safety. Working within a fume hood is not at all unusual in a laboratory environment and is generally considered to be a part of routine good laboratory practice when handling materials that may generate hazardous vapors. There are no unusual health and safety requirements for the work described in this test plan. The health and safety requirements relevant to the tasks for work in this test plan are described in SOP-C001 (Subsection 5.2).

7 PERMITTING AND LICENSING

There are no special licenses or permitting requirements for the work described in this test plan.

8 REFERENCES

- Adam, L.C., and G. Gordon. 1999. "Hypochlorite Ion Decomposition: Effects of Temperature, Ionic Strength, and Chloride Ion," *Inorganic Chemistry*. Vol. 38, 1299-1304.
- Betts, R.H., and A.N. MacKenzie. 1951. "Formation and Stability of Hypobromous Acid in Perchloric Acid Solutions of Bromine and Bromate Ions," *Canadian Journal of Chemistry*. Vol. 29, 666-677.
- Brush, L.H. 1990. *Test Plan for Laboratory and Modeling Studies of Repository and Radionuclide Chemistry for the Waste Isolation Pilot Plant*. SAND90-0266. Albuquerque, NM: Sandia National Laboratories
- Cleveland, J.M. 1979. *The Chemistry of Plutonium*. La Grange Park, IL: American Nuclear Society.
- Ganguly, A.K., and J.L. Magee. 1956. "Theory of Radiation Chemistry. III. Radical Reaction Mechanism in the Tracks of Ionizing Radiations," *Journal of Chemical Physics*. Vol. 25, no.1, 129-134.
- Katz, J.J., G.T. Seaborg, and L.R. Morss, eds. 1986. *The Chemistry of the Actinide Elements*. New York, NY: Chapman and Hall.
- Kelm, M., I. Pashalidis, and J.I. Kim. 1999. "Spectroscopic Investigation on the Formation of Hypochlorite by Alpha-Radiolysis in Concentrated NaCl Solutions," *Applied Radiation and Isotopes*. Vol. 51, 637-642.
- Kim, J.I., C. Lierse, K. Bueppelmann, and S. Magirius. 1987. "Radiolytically Induced Oxidation Reactions of Actinide Ions in Concentrated Salt Solutions," *Proceedings: Scientific Basis for Nuclear Waste Management: Materials Research Society Symposia Proceedings, Boston, Massachusetts, December 1-4, 1986*. Eds. J.K. Bates and W.B. Seefeldt. Pittsburgh, PA: Materials Research Society. 603-612.
- Lide, D., ed. 1995. *Handbook of Chemistry and Physics, 76th Edition*. Boca Raton, FL: CRC Press.
- Martell, A.E., R.M. Smith, and R.J. Motekaitis. 1998. *Critically Selected Stability Constants of Metal Complexes Database, Version 5.0*. College Station, TX: Texas A&M University Press.
- Pink, J.M., 1970. "Spectrophotometric Determination of the Hydrolysis Constant of Bromine at 25 °C," *Canadian Journal of Chemistry*. Vol. 48, 1169-1171.

- Vogel, A.I., 1989. *Vogel's Textbook of Quantitative Chemical Analysis, 5th ed.* New York, NY: John Wiley and Sons.
- Wang, T.X., M.D. Kelley, J.N. Cooper, R.C. Beckwith, and D.W. Margerum 1994. "Equilibrium, Kinetic, and UV-Spectral Characteristics of Aqueous Bromine Chloride, Bromine, and Chlorine Species," *Inorganic Chemistry*. Vol. 33, 5872-5878.
- Wall, D.E. 2002. "Chemical Behavior of Hypochlorite in High-Ionic-Strength Solutions." Unpublished test plan, TP 02-01, Rev. 1. Carlsbad, NM: Sandia National Laboratories.

NOTICE: This document was prepared as an account of work sponsored by an agency of the United States Government. Neither the United States Government nor any agency thereof, nor any of their employees, nor any of their contractors, subcontractors, or their employees, makes any warranty, express or implied, or assumes any legal liability or responsibility for the accuracy, completeness, or usefulness or any information, apparatus, product or process disclosed, or represents that its use would not infringe privately owned rights. Reference herein to any specific commercial product, process or service by trade name, trademark, manufacturer, or otherwise, does not necessarily constitute or imply its endorsement, recommendation, or favoring by the United States Government, any agency thereof or any of their contractors or subcontractors. The views and opinions expressed herein do not necessarily state or reflect those of the United States Government, any agency thereof or any of their contractors.

This document was authored by Sandia Corporation under Contract No. DE-AC04-94AL85000 with the United States Department of Energy. Parties are allowed to download copies at no cost for internal use within your organization only provided that any copies made are true and accurate. Copies must include a statement acknowledging Sandia Corporation's authorship of the subject matter.

3 GEOCHEMISTRY

3.3 Effects of the MgO Engineered Barrier...

100
101
102
103
104
105
106
107
108
109
110
111
112
113
114
115
116
117
118
119
120
121
122
123
124
125
126
127
128
129
130
131
132
133
134
135
136
137
138
139
140
141
142
143
144
145
146
147
148
149
150
151
152
153
154
155
156
157
158
159
160
161
162
163
164
165
166
167
168
169
170
171
172
173
174
175
176
177
178
179
180
181
182
183
184
185
186
187
188
189
190
191
192
193
194
195
196
197
198
199
200

IMPORTANT NOTICE: The current official version of this document is available via the Sandia National Laboratories NWMP On-line Documents web site. A printed copy of this document may not be the version currently in effect.

Sandia National Laboratories
Waste Isolation Pilot Plant (WIPP)
Test Plan, TP 02-02

Effects of the MgO Engineered Barrier on the Possible Presence of Mg-Bearing Colloids and Humic Acids in WIPP

Revision 1

Task 1.3.5.4.1.2

Effective Date: 11/07/02

Prepared by:

Nathalie A. Wall (6822)

Sandia National Laboratories
Carlsbad, NM

WIPP:1.3.5.4.1.2:TD:QA:DPRP1:NF;Test plan for Colloids in WIPP, TP02-02

1. Approval Page

Author:	<u>Original signed by Nathalie A. Wall</u> Nathalie A. Wall (6822)	<u>11/6/02</u> Date
Technical Reviewer:	<u>Original signed by R.A. Jepsen</u> by F.D.H. R.A. Jepsen (6822)	<u>11/6/02</u> Date
Management Reviewer:	<u>Original signed by F.D. Hansen</u> F.D. Hansen (6822)	<u>11/6/02</u> Date
QA Reviewer:	<u>Original signed by M.J. Mitchell</u> M.J. Mitchell (6820)	<u>6 Nov 02</u> Date

2. Table of Contents

1. Approval Page.....	2
2. Table of Contents.....	3
3. List of Acronyms.....	4
4. Revision History.....	5
5. Purpose and Scope.....	5
6. Background.....	5
6.1. Generalities about Colloids.....	5
6.2. Colloidal Coagulation/Stability.....	6
6.2.1. Generalities (Hunter 1993).....	6
6.2.2. The particular case of WIPP.....	8
7. Experiments.....	11
7.1. Task 1: Colloids generated from WIPP backfill.....	11
7.1.1. Materials.....	11
7.1.2. Agitation, Time.....	12
7.1.3. Atmospheric Control.....	12
7.1.4. Colloid concentration determination.....	12
7.1.5. pH Control.....	14
7.2. Task 2: HA in WIPP.....	14
7.2.1. Materials.....	14
7.2.2. Agitation, Time, Light Exposure.....	15
7.2.3. Atmospheric Controls.....	15
7.2.4. TOC Measurements.....	16
7.2.5. pH Control.....	16
7.3. Sample Handling, Storage, and Disposal.....	16
7.4. Equipment Testing.....	17
8. Data Handling.....	17
8.1. Data Processing and Mathematical Models.....	17
8.2. Data Identification and Use.....	17
8.3. Data Transfer and Reduction Controls.....	18
8.4. Identification, Segregation, Disposal of Erroneous Data.....	18
9. Training and Other Standard Procedures.....	18
10. Health & Safety.....	18
11. Permitting/Licensing.....	19
12. References.....	19

3. List of Acronyms

ξ	zeta potential
κ	Debye-Hückel parameter
γ	solution activity coefficient
AFM	atomic force microscope
a_{H^+}	proton H^+ activity
CO_2	carbon dioxide
DI water	deionized water
DLVO theory	theory named after Deryaguin, Landau, Verwey and Overbeek
HA	humic acids
HEPES	N-(2-hydroxyethyl)piperazine-N'-(-2-ethanesulfonic acid)
I	ionic strength
ICP-OES	induced coupled plasma optical emission spectrometer
IEP	isoelectric point
kD	kilo Dalton (1 kD = 1 NMWL (i.e. nominal molecular weight limit))
KHP	potassium hydrogen phthalate
MES	2-(N-morpholino)ethanesulfonic acid
$MgCO_3$	magnesite
MgO	magnesium oxide
MgOH	brucite
μm	micrometer
nm	nanometer
NMWL	nominal molecular weight limit
PA	Performance assessment
pCH	$-\log[H^+]$
pHr	pH meter reading
P_{CO_2}	CO_2 partial pressure
PZC	point of zero charge
Rev	revision
SEM	scanning electron microscope
SNL	Sandia National Laboratories
T	temperature
TOC	total organic carbon
TRU	transuranic
UF	ultrafiltration
US DOE	United States Department of Energy
US EPA	United States Environmental Protection Agency
UV-vis	ultraviolet-visible
V_T	total potential energy of interaction
WIPP	Waste Isolation Pilot Plant

4. Revision History

This is the first revision of this test plan. The original title of TP 02-02, Rev. 0, was "Generation of Colloids from the WIPP Backfill". The former title has been changed in this revision to capture the nature of the work more accurately. Two tasks are included in TP 02-02, Rev 1: Task 1 (on colloids issued from WIPP backfill) was part of TP 02-02, Rev 0 and Task 2 (on the behavior of humic acids, HA, in the WIPP environment) was part of TP 00-07, Rev 1, "Experimental Study of WIPP MgO backfill at Sandia National Laboratories Carlsbad Facility". Subsequent revisions of the test plan TP02-02 will be made in accordance with the Sandia National Laboratories Nuclear Waste Management Program Procedures: NP 20-1 Test Plans, NP 6-1 Document Review Process and NP 6-2 Document Control Process.

5. Purpose and Scope

This document describes experiments to study the generation and persistence of colloids under expected WIPP conditions. Colloids may be important to WIPP performance assessment (PA) because of their very large surface areas, mobility, and their ability to bind cations.

- We will evaluate whether MgO, which is being used as an engineered barrier in the WIPP to mitigate the effect of microbial CO₂ generation on actinide mobility in the post-closure repository environment, will generate colloids and whether these colloids will be stable under WIPP conditions.
- HA are products of the biodegradation of animals and vegetal materials; in the case of WIPP, HA may be generated from the degradation of organic materials present in the TRU wastes (cellulosics, plastics, and rubbers). In this task, we will determine the solubility of HA in the presence of MgO in brines representative of the WIPP environment.

6. Background

6.1. Generalities about Colloids

A colloidal phase is an intermediate state between a solution containing dissolved entities of ionic or molecular dimensions, and a solution containing suspended particles sufficiently large to settle by gravity. The size range of colloids is from 1 nm to 1 μ m (Figure 1).

Colloids can be generated by dispersion or condensation. In case of dispersion, material breaks down to colloidal dimensions by some mechanical process (e.g., grinding), or very

high frequency sound waves (ultrasonication) in a liquid-liquid dispersion. Condensation includes dissolution and reprecipitation, condensation from vapor through formation of a mist or fog from a supersaturated vapor, or chemical reactions, including reduction, oxidation or decomposition.

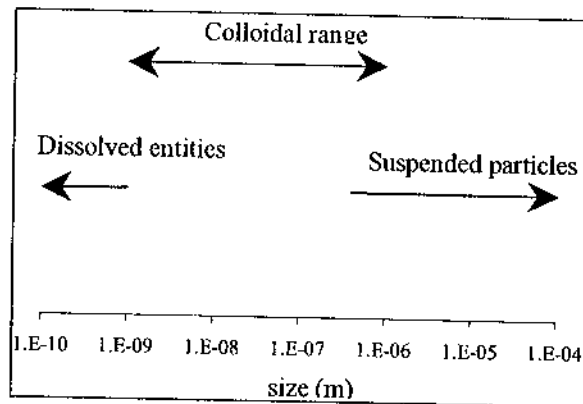


Figure 1. Size ranges of aqueous particles. (Adapted from Gaffney et al., 1996).

Colloids may be important to WIPP PA because they have very large surface areas and may be mobile in aqueous solutions. Additionally, some colloids can retain cations. For example, magnesite (MgCO_3) retains cations such as Co^{2+} , Zn^{2+} , Cs^+ , Ba^{2+} (Shahwan et al., 1998; Erten and Gokmenoglu, 1994); HA form complexes with metals, such as Cr, Cu, Zn, Sr, Cd, Pb (Benes and Mizera, 1996; Esteves Da Silva et al., 1997; Fukushima et al., 1995; Hamilton-Taylor et al., 1997; Samadfam et al., 1996) and in particular with actinides such as Th, U, Np, Am, Cm (Choppin, 1988; Nash and Choppin, 1980; Labonne-Wall et al., 1999; Seibert et al., 2001; Wall et al., 2002; Kim et al., 1991). Consequently, colloids from the WIPP backfill and HA could increase the solubilities of actinides.

6.2. Colloidal Coagulation/Stability

6.2.1. Generalities (Hunter 1993)

Colloids would affect actinide mobility only if they remain as stable suspended entities; coagulated colloids are not mobile. Therefore, it is important to understand the processes leading to stable colloids versus coagulated entities.

The DLVO theory (named after the four scientists Deryaguin, Landau, Verwey and Overbeek) explains the colloidal stability in terms of forces: a repulsive one due to formation of a double layer and an attractive one due to van der Waals interactions. Colloids can possess high negative charges at their surface. As a result, dissolved ions present are retained in a compact layer adjacent to the colloid (i.e., the Stern layer) and a diffuse double layer adjacent to this compact layer. The diffuse double layer contains a

gradually decreasing ionic concentration with increased distance from the colloid surface. When double layered systems interact with each other due to random Brownian motion, the sum of the interactions taking place in the immediate vicinity of the colloid creates a total potential energy of interaction V_T , which defines an energy barrier. V_T is the sum of interactions and repulsions. The stability of a system depends on the height and thickness of the energy barrier. If the potential energy barrier is higher than the thermal energy of the colloidal particles, coagulation is hindered. As the potential energy barrier approaches the thermal energy level, coagulation is increasingly favored. Although the DLVO theory is incomplete (Manciu and Ruckensein, 2001), it has the advantage of simplicity and offers a reasonable approach for obtaining quantitative results.

V_T depends on many parameters that will eventually affect the stability and coagulation of the colloidal population: the temperature T , the charge z of the ion present in the double layer, the double layer thickness $1/\kappa$, in which κ is the Debye-Hückel parameter and is directly proportional to the square root of the ionic strength I . For example, coagulation can result from increasing the ionic strength of the system or increasing the charge density of the neighboring ions.

The colloidal stability will also depend on the degree of ionization of the colloidal surface, which itself is a function of pH. The electrical potential between the bulk solution and the colloid is called zeta potential (ξ); this potential indicates the stability of the colloidal system: the greater ξ (positive or negative), the greater the colloidal stability, as illustrated on Figure 2.

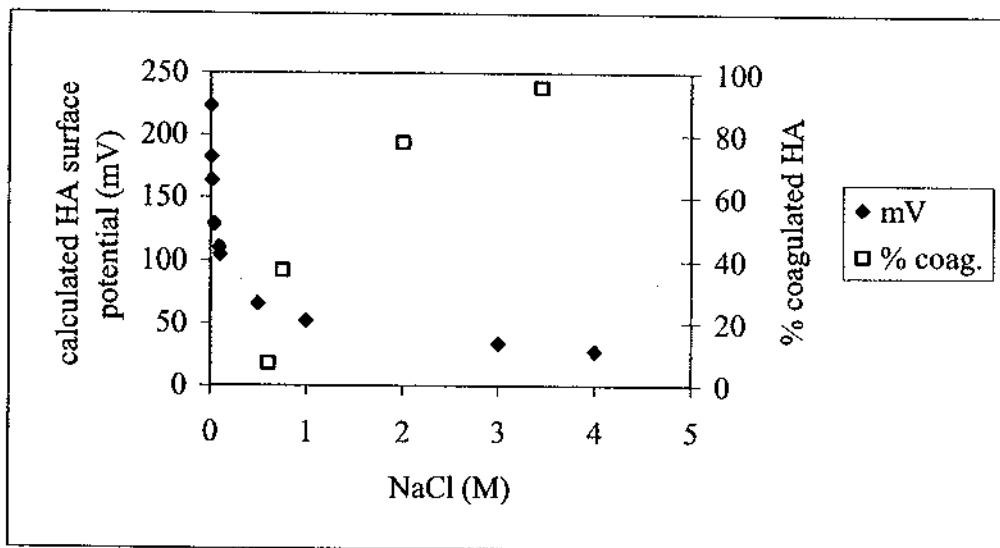


Figure 2. Surface potential and coagulation of humic acids in NaCl solutions, pH 7.5 (adapted from Tombacz and Meleg, 1990).

The isoelectric point (IEP) or point of zero charge (PZC) represents the value of pH at which the colloid has a zero net charge ($\xi = 0$), i.e., the least colloidal stability. For hydroxo complexes $M^{z+}(OH)_n^{z-n}$, the PZC is the pH resulting in an electrically equivalent concentrations of positive and negative complexes. Examples of PZC values for MgO and $Mg(OH)_2$, and HA are presented in Table 1.

Table 1. Examples of PZC values.

Material	PZC	Ref.
MgO	12.4 ± 0.3	Parks, 1965
$Mg(OH)_2$	≈ 12	Parks, 1965
HA in 10^{-3} M NaCl	< 2	Tombacz and Meleg, 1990
HA in 0.1 M NaCl	< 2.5	Tombacz and Meleg, 1990
HA in 0.5 M to 3 M NaCl	< 3	Tombacz and Meleg, 1990

6.2.2. The particular case of WIPP

The pcH values (i.e., $-\log[H^+]$) of WIPP brines after equilibration with MgO were calculated (US EPA 1998) for the different magnesium carbonate phases expected in the repository; these pcH values are presented in Table 2. Comparison between Tables 1 and 2 show that the estimated WIPP brine pcH values are within the region of colloidal stability for MgO, $Mg(OH)_2$, and HA colloids; unfortunately no PZC values were found in the literature for hydromagnesite, magnesite or nesquehonite.

Table 2. Effects of different magnesium carbonate equilibria with brucite on solution conditions predicted by the FMT model (version 2.2 of FMT, updated version created by SNL in April, 1997, after the CCA).

Salado Brine				
	Hydromagnesite ^a	Hydromagnesite ^b	Nesquehonite ^c	Magnesite ^d
pcH	9.13	9.37	9.36	9.31
Log[CO _{2(g)}]	-5.31	-5.39	-3.84	-6.89
Castile Brine				
	Hydromagnesite ^a	Hydromagnesite ^b		
pcH	9.9	9.89		
Log[CO _{2(g)}]	-5.5	-5.39		

Hydromagnesite^a - Mg₅(CO₃)₄(OH)₂·4H₂O
Hydromagnesite^b - Mg₄(CO₃)₃(OH)₂·3H₂O
Nesquehonite^c - MgCO₃·3H₂O
Magnesite^d - MgCO₃

Dr. Bernhard Kienzler, from Forschungszentrum Karlsruhe in Germany, has communicated to the author of this document unpublished results regarding the finding of stable colloids originating from brucite. Dr. Kienzler stated: "Literature concerning existence, stability and mobility of colloids in highly concentrated salt solutions is rarely available. In our institute we did some work, however, it is not yet published. In German salt domes Mg bearing salts are available to a large extent, resulting in highly concentrated brines (Q-brine: ~4 m MgCl₂). The brines have a high buffer capacity with respect to pH. In the presence of cement, pH is buffered by precipitation of brucite (Mg(OH)₂) or various magnesium oxychloride hydrates. These phases are not crystalline and show a slow flocculation. We consider the possibility that colloidal phases may be formed even in highly concentrated solutions" (Kienzler, 2001). Moreover, Kienzler has also mentioned that the colloids observed were slow to form (months) and very small at first, consequently difficult to observe.

The experiments planned in this test plan will help determine the concentration of stable colloids generated from MgO under expected WIPP conditions.

It would be difficult to predict the concentration of colloidal HA present in WIPP brines, because HA formation is a slow process; the rate of dissolved HA accumulation reaches an equilibrium in periods of time that vary from 110 years in fine-grained soils to 1500 years in sandy soils (Stevenson, 1994, p. 8). HA coagulation is an easier process to

study. Some studies of HA coagulation under WIPP conditions have been performed at Florida State University (Wall and Choppin, 2000).

Solutions of known ionic strength, pH, Mg, and Ca concentrations were prepared with HA and filtered to obtain the fraction smaller than 100 kD. Over a 50-day period, samples of these solutions were filtered again through 100 kD membranes and the total organic carbon (TOC) of the filtered solutions measured (HA is c.a. 50 wt % TOC). Coagulation occurs in both the absence and presence of light. HA coagulation increases with NaCl concentration. Coagulation also increases in the presence of divalent cations such as Ca^{2+} and Mg^{2+} , but in high ionic strength solutions, neither the Ca^{2+} nor the Mg^{2+} concentrations representative of WIPP brines are sufficient to fully coagulate HA (see Figure 3 and Table 3).

Table 3. Ca^{2+} and Mg^{2+} concentrations in WIPP brines. (Brush, 1990)

	G Seep	Brine A	ERDA 6
Ca^{2+}	$7.68 \cdot 10^{-3}$ M	$20 \cdot 10^{-3}$ M	$12 \cdot 10^{-3}$ M
Mg^{2+}	0.630 M	1.44 M	$19 \cdot 10^{-3}$ M

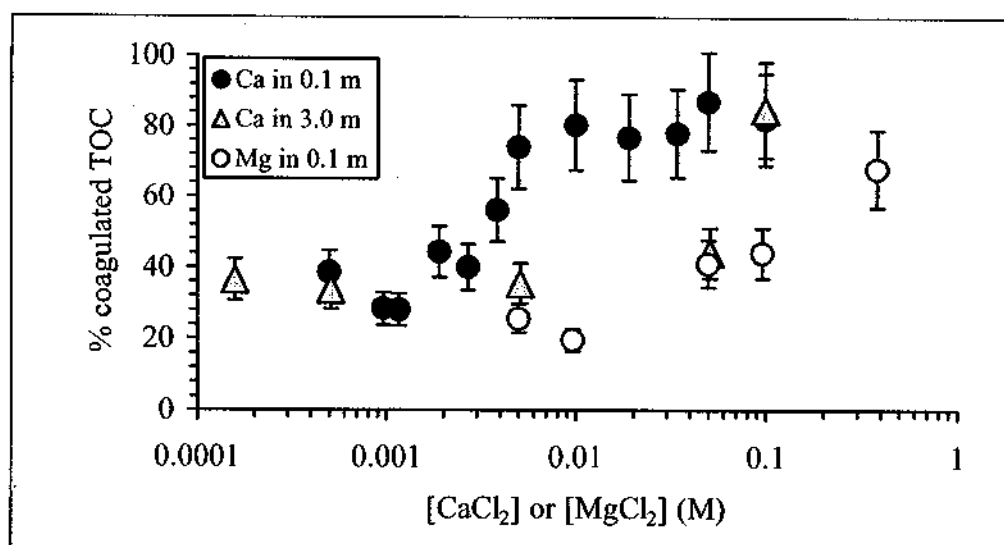


Figure 3. HA (initial TOC = 40 ppm, i.e. HA c.a. 80 ppm) coagulation in NaCl media in presence of varying concentration of CaCl_2 or MgCl_2 , at pH 8.3, after 50 days of equilibration.

No experiments were performed to study HA coagulation in the presence of MgO and at very high ionic strength (5 m). This document is a plan for such experiments.

7. Experiments

7.1. Taks1: Colloids generated from WIPP backfill

7.1.1. Materials

Experiments will be conducted on two MgO samples: pure MgO (Fisher chemicals) and Premier Chemicals MgO. The latter is used as the WIPP engineered barrier. The Premier Chemicals MgO contains impurities such as forsterite [Mg_2SiO_4], monticellite [$MgCaSiO_4$], and portlandite [$Ca(OH)_2$].

MgO suspensions will be prepared in different solutions:

- de-ionized water
- NaCl of different ionic strengths (10^{-3} m to 5 m)
- synthetic WIPP brines prepared in our laboratory:
 - Generic Weep Brine (GWB), which simulates intergranular fluids from the Salado Formation,
 - ERDA-6, which simulate fluids from brine reservoirs in the Castile Formation.

The compositions of GWB and ERDA-6 are presented in Table 4.

Table 4. WIPP Brine Compositions (Brush, 1990)

	GWB (Salado)	ERDA-6 (Castile)
B (mM)	78	63
Br (mM)	27	11
Ca (mM)	14	12
Cl (M)	5.609	4.8
K (mM)	467	97
Mg (M)	1.018	0.019
Na (M)	3.536	4.87
SO ₄ (mM)	178	170
pH	NA	6.17

Different liquid:solid ratios will be applied: 1 g:g – 100 g:g. A variation of the liquid:solid ratio will allow the extrapolation of the results to conditions representative of WIPP. A realistic liquid:solid ratio for WIPP is 0.72 g:g, but the solution analysis of such a sample would be difficult due to the small liquid sample size.

7.1.2. Agitation, Time

Some of the samples will be vigorously shaken while others will be left undisturbed. The shaking motion should accelerate the colloidal process of formation and/or coagulation. The kinetics of the system will be studied by sampling at regular time intervals.

7.1.3. Atmospheric Control

It was estimated in the PAVT (PA Verification Test; Novak, 1997) that the CO_2 fugacity in WIPP would equilibrate at $10^{-5.5}$ (Novak, 1997), while the total gas pressure would range from 30 to 150 MPa (Helton et al., 2000). In WIPP, MgO is expected to convert to hydromagnesite (US EPA, 1998), but experiments presently performed (Wang et al., 2002) show that carbonation of brucite is very slow, even under atmospheric conditions of $\text{CO}_{2(g)}$ (fugacity ca. $10^{-3.5}$). To accelerate the conversion process, experiments are also performed in a glovebox containing 5% CO_2 (fugacity ca. $10^{-1.3}$) (Snider and Xiong, 2002).

The first set of colloid experiments will be performed under atmospheric conditions of $\text{CO}_{2(g)}$. Then, the experiments will be conducted in a glovebox, under 5% CO_2 , in which conditions the conversion product of MgO and the rate of conversion will be known from the experiments of Snider and Xiong, (2002).

A gas cylinder will provide CO_2 to an airtight glovebox and P_{CO_2} will be monitored with a Bacharach CO_2 analyzer; this instrument monitors CO_2 concentration up to 60%. Additional supply of CO_2 may sometimes be needed to avoid drastic changes of CO_2 pressure in the glovebox after opening the glovebox for sampling. Reaction of sodium bicarbonate with sulfuric acid will provide the needed infusion of CO_2 in the glovebox.

7.1.4. Colloid concentration determination

The supernatant of the solutions will be filtered through filtration membranes, which retains particles larger than 1 μm , the largest colloidal size (e.g. Whatman Nuclepore Track-Etch Membranes). The Mg colloids that would be present in the filtered solutions will be dissolved by adding nitric acid and the Mg concentration (from colloids and soluble species) will be determined with a Perkin-Elmer induced coupled plasma optical emission spectrometer (ICP-OES). Before each daily analysis, the instrument will be calibrated using Mg standards solutions, containing a matrix identical to that of the samples to be analyzed. To correct for drift, an internal standard (e.g., Sc) will be added to the samples and the calibration standard solutions.

A preliminary study was performed to verify the validity of the technique. Variable amounts of MgO (Fisher and Fisher that was previously ground) were stirred in water and nitric acid was added to the samples to obtain a final concentration of 3% HNO₃. The Mg concentration of the samples was measured with the ICP-OES. Figure 4 shows the results of this test.

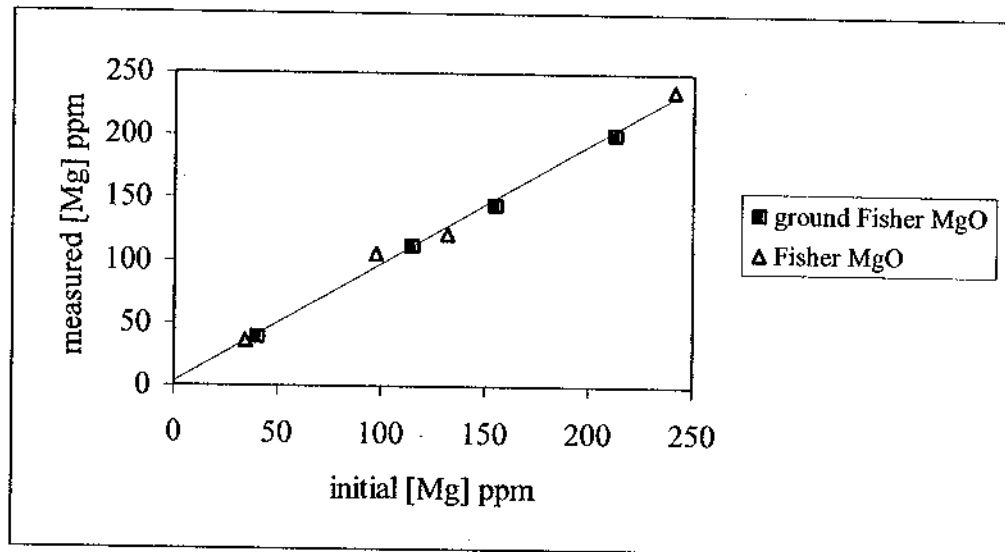


Figure 4. Method development for MgO colloid detection.
 $[Mg]_{\text{measured}} = 0.950 (\pm 0.024) \times [Mg]_{\text{initial}} + 2.9 (\pm 3.3)$, $R^2 = 0.996$

Aliquots of the μm fraction (i.e., fraction of size larger than $1 \mu\text{m}$) will be filtered on Millipore/Amicon UF (i.e. ultra-filtration) membrane 1kD, using a pressurized AMICON ultra-filtration cell. 1 kD (kilo Dalton) is equivalent to 1000 NMWL (nominal molecular weight limit). Although there is not a one-to-one relationship of NMWL or cut-off rating of UF membranes to their pore size, an estimation of the membrane pore size was given by Millipore technical assistance to the author of this document: a 1 kD UF membrane presents a pore size of c.a. 1.3 nm, which is the limit between colloids and soluble species. The 1 kD-filtered sample will be acidified with nitric acid and the Mg concentration (representing the soluble Mg species present in the original sample) will be measured by ICP OES. The difference between the Mg concentrations of the 1- μm -filtered samples and the 1-kD-filtered samples will provide the Mg concentration due to Mg colloids.

If colloids are detected, we will study their stability by measuring their zeta potential ξ for the different systems considered, using a Coulter Delsa 440 zeta potential sizer. We will follow the specific procedure for the calibration, use, and maintenance of this instrument (SP 12-3, Rev 0).

7.1.5. pH Control

We will not study the influence of pcH (i.e., $-\log[H^+]$) on the stability of MgO colloids. Biological buffers, such as MES (2-(N-morpholino)ethanesulfonic acid, pKa 6.1) or HEPES (N-(2-hydroxyethyl)piperazine-N'-(-2-ethanesulfonic acid), pKa 7.5) can be used to avoid cation complexation, but they will not buffer MgO suspensions with liquid:solid ratios less than 10^4 g:g. The hydrogen-ion concentration, $[H^+]$, will be measured and expressed as the negative log of the concentration, pcH, rather than using the pH meter reading pH_r, i.e. $-\log a_{H^+}$, in which a_{H^+} is the proton activity; the product of the proton concentration $[H^+]$ and the solution activity coefficient γ . Although pH reference solutions (e.g., Fisher certified color-coded pH buffers, pH 4, 7 or 10) are used for glass electrode calibration in dilute solutions, their use for concentrated solutions is limited because of the significant difference of activity coefficients and liquid-junction potentials between the reference solutions and the solutions to be tested (Chen et al., 1996). To determine the pcH of solutions of high ionic strength, the pH electrode is calibrated daily by titration at fixed ionic strength (NaCl, 0 to 5 *m*). The solutions used for the titration are 0.1 M NaOH, which is prepared weekly from a saturated NaOH solution and standardized with potassium hydrogen phthalate (KHP) and a 0.1 M HCl solution, which is standardized with KHP and the standardized NaOH solutions. At each ionic strength, the equation relating pcH (calculated $-\log[H^+]$) and the solution potential (in mV) is established. The measured potential of a solution can then be converted to pcH. For example, the equation relating pcH, pH_r and the ionic strength of NaCl solutions is: $pcH - pH_r = 0.2212 \times I_{NaCl} + 0.0881$, in which I_{NaCl} is the concentration of NaCl (*m*) (Wall and Choppin, 2002).

WIPP brines contain a variety of constituents (see Table 4). A specific pcH calibration procedure will be determined for these brines, as sulfates and borates would buffer the pH of the solutions.

7.2. Task 2: HA in WIPP

7.2.1. Materials

Two types of MgO will be studied: pure Fisher MgO and Premier Chemicals MgO. HA will be purchased from Aldrich, but the ash content, an indication of impurities, was found to be 50–60 %, after heating a sample at 500 °C for 5 hours (Wall and Choppin, 2002). Most purification techniques described in the literature (Bertha and Choppin, 1978; Nash and Choppin, 1980; Kim et al., 1989) produce very pure organic matter but are very time consuming; such procedures are used when very small amounts of pure HA are needed. Although our experiments require a reasonably pure product, they will also require large amounts (grams) of HA. Aldrich HA will be successively dissolved in base (1 g HA/L in 10^{-2} M NaOH), precipitated in concentrated HCl, and centrifuged. The isolated precipitate will be freeze-dried using a Labconco FreeZone Freeze Dry System

and the ash content of the dried product measured. Such a process has been reported to give less than 5% ash (Wall and Choppin, 2002).

We will study the influence of different media:

- de-ionized water
- NaCl of different ionic strengths (10^{-3} m to 6 m)
- synthetic WIPP brines prepared in our laboratory:
 - GWB
 - ERDA-6

Stock solutions of purified HA will be prepared by dissolving dry organic matter in NaOH solutions in de-ionized water, NaCl or WIPP brine. The stock solution will be filtered through a 1- μ m-pore membrane. The TOC of the stock solutions will be determined (see below). The filtered stock solution will be refrigerated when not in use, because the HA size does not change at low temperature (Wall and Choppin, 2002). Aliquots of the stock solution will be diluted in the solution of interest and MgO will be added. The initial TOC will vary from few ppm to few hundred ppm HA.

The liquid:solid ratios will vary from 1 g:g to 100 g:g, for the reasons explained in paragraph 7.1.1. The slurry will be filtered through a 1 μ m membrane and the TOC of the filtered solution measured.

7.2.2. Agitation, Time, Light Exposure

The purpose of this task is to study the coagulation/precipitation of humic acids. The samples will be shaken for 1 day to allow homogenization and then they will be left undisturbed throughout the rest of the experiments. The kinetics of the system will be studied by sampling at multiple time intervals. Previous results had shown that the coagulation process is accelerated by light exposure (Wall and Choppin, 2002); therefore, a set of experiments will be permanently exposed to light and another set will be kept dark.

7.2.3. Atmospheric Controls

The first set of experiments will be performed under atmospheric conditions of CO₂. The chemistry of elements such as Ca and Mg, and of HA depend on the CO₂ concentration, so a set of experiments will be conducted in a CO₂-free glovebox, purged with N₂ and monitored with a Bacharach CO₂ analyzer.

7.2.4. TOC Measurements

HA concentrations are traditionally determined by UV-visible spectroscopy or total organic carbon content (i.e. TOC) measurement. UV-vis spectroscopy is inadequate for quantitative analysis of HA of small (nm range) variable sizes (Wall and Choppin, 2002). Problems may arise from analyzing TOC in WIPP brines; for example, material containing Na^+ or K^+ will attack the quartz combustion tube. As a result, TOC measurement is time consuming; HA must be extracted from the matrix, and re-dissolved in very low ionic strength medium.

We will study whether the concentration of large (μm) size HA can be determined accurately using UV-vis spectroscopy. The HA concentration of μm -fractionated HA solutions prepared in DI water will be estimated by UV-vis spectrophotometry and compared to the TOC of these solutions. If spectrophotometry provides accurate results, this technique will be adopted for the analysis of the HA coagulation experiment samples.

The absorbance at 465 nm of the μm -fractionated HA samples will be compared to a calibration curve established by recording the absorbance at 465 nm of unfractionated HA solutions of known concentration; the calibration solutions must be of same pH and medium as the fractionated samples. It is also useful to record the absorbances at 665 nm, as the ratio of the absorbances at 465 nm and 665 nm, referred to as the "E4/E6 ratio," gives useful information as to the size fluctuation of the humic molecules. Such measurements will be performed in our laboratory using a Cary 300 Conc UV-Visible Spectrophotometer coupled to a personal computer loaded with the Cary Win UV ADL Shell Application software.

The TOC of the μm -fractionated HA samples and the unfractionated HA solutions will be measured with a UIC, Inc., Model CM5014 CO_2 Coulometer, CM5130 Acidification Module and CM5120 Furnace Apparatus (following the procedure SP 12-2, Rev 0). The instrument calibration will be checked with standard solutions of sucrose ($\text{C}_{12}\text{H}_{22}\text{O}_{11}$). The samples to be measured will first be acidified to pH of about 4-5 and purged with N_2 to remove traces of inorganic carbon, which would alter the TOC measurements.

7.2.5. pH Control

The pH of the samples will be monitored, but there will be no experiments explicitly intended to study the effects of pH, for the reasons explained in paragraph 7.1.1.1.5.

7.3. Sample Handling, Storage, and Disposal

Standard procedures for sample identification, handling, storage, shipping, archiving and disposition have been described in Sandia National Laboratories Nuclear Waste

Management Program Procedure NP 13-1. Sample handling will be performed in accordance with NP 13-1.

Samples will be labeled with unique identification numbers and recorded in laboratory notebooks. Solutions will be handled and stored in accordance with documented procedures.

Samples will be stored in the SNL Carlsbad laboratory in various places depending on the experimental procedure.

Solutions will be disposed of in accordance with standard operating procedures in place at the SNL Carlsbad laboratory.

7.4. Equipment Testing

The equipment used for these experiments will be tested in accordance with the Sandia National Laboratories Nuclear Waste Management Program Procedure NP 12-1, Control of Measuring and Test Equipment, and the specific procedure of each instrument.

8. Data Handling

8.1. Data Processing and Mathematical Models

Data processing may be done by hand calculation with the aid of an electronic calculator, or with a standard spreadsheet program, such as Microsoft Excel, according to the Nuclear Waste Management Program Procedure NP 9-1 ("Analysis"). The experimental results and the calculations generated from these results will be reviewed by technical peers.

8.2. Data Identification and Use

Data amenable to written recording will be inscribed by hand in appropriate laboratory notebooks. Such information includes, but is not limited to:

- reagent and solution preparation procedures and results
- sample preparation procedures
- sample composition and conditions e.g. pH, reagent volume, reagent concentration, temperature
- sample handling
- sample analysis procedures and results

8.3. Data Transfer and Reduction Controls

Typical data transfer is from instrumental output to laboratory notebook and from laboratory notebook to a spreadsheet program, if applicable. Printed copies of instrumental output will be permanently attached to the laboratory notebook within the section dedicated to the pertinent experiment.

8.4. Identification, Segregation, Disposal of Erroneous Data

Data suspected to be erroneous will be tested by comparison to replicate samples or replicate experiments. Statistical justification for rejection of erroneous data will be provided within the laboratory notebook.

9. Training and Other Standard Procedures

All personnel participating in the work described in this Test Plan will be trained and qualified for the assigned tasks. This requirement will be implemented in accordance with NWMP procedure NP 2-1, "Qualification and Training." Evidence of qualification and training will be documented with Form NP 2-1-1, "Qualification and Training."

Additionally, the following NWMP Procedures and Project Specific Procedures are applicable:

SOP-C001: "Standard Operating Procedure for Activities in the SNL/Carlsbad Laboratory Facility."

SP 13-1, "Chain of Custody"

SP 12-3, "Calibration, Use, and Maintenance of the DELSA-440 Electrophoretic Mobility Analyzer"

SP 12-2, "Use and Maintenance of the UIC, Inc. Model CM5014 CO2 Coulometer, CM5130 Acidification Module and CM5120 Furnace Apparatus"

NP 6-1, "Document Review Process"

NP 9-1, "Analysis"

NP 13-1, "Sample Control"

NP 12-1, "Control of Measuring and Test Equipment"

NP 20-2, "Scientific Notebooks"

NP 2-1, "Qualification and Training"

NP 17-1, "Records"

10. Health & Safety

The health and safety requirements relevant to the tasks for work in this test plan are described in SOP-C001.

11. Permitting/Licensing

There are no special licenses or permitting requirements for the work described in this test plan.

12. References

- Benes, P., and J. Mizera, Application of Electrophoresis to the Study of the Complexation of Cadmium with Humic Substances using Cd109 as Radiotracer, in *Radiochimica Acta*, vol. 74, pp. 185-188, 1996.
- Bertha, E.L., and G.R. Choppin, Interaction of Humic and Fulvic Acids with Eu(III) and Am(III), in *Journal of Inorganic Chemistry*, vol. 40, pp. 655-658, 1978.
- Brush, L.H., *Test Plan for Laboratory and Modeling Studies of Repository and Radionuclide Chemistry for the Waste Isolation Pilot Plant*, SAND90-0266. Sandia National Laboratories. Albuquerque, NM, September 1990
- Bryan, C.R., and Y. Wang Y, *Experimental Work to Develop a Model for Cement Borehole Plug Degradation at the WIPP Site*. TP 00-06. Sandia National Laboratories. Carlsbad, NM, January 2001.
- Chen J-F., Y.-X. Xia, and G.R. Choppin, Derivative Analysis of Potentiometric Titration Data to Obtain Protonation Constants, in *Analytical Chemistry*, vol. 68, no. 22, pp. 3973-3978, 1996.
- Choppin G.R., Humic and Radionuclide Migration, in *Radiochimica Acta*, vol. 44/45, pp. 23-28, 1988.
- DOE (US Department of Energy). 1996. *Title 40 CFR Part 191 Compliance Certification Application for the Waste Isolation Pilot Plant*. DOE/CAO-1996-2184, Vol. 1-21. Carlsbad, NM: U.S. Department of Energy, Carlsbad Area Office.
- Erten, H.N., and Z. Gokmenoglu, Sorption Behavior of CO_2^+ , Zn^{2+} and Ba^{2+} Ions on Alumina Kaolinite and Magnesite, in *Journal of Radioanalytical and Nuclear Chemistry*, vol. 182, no. 2, pp. 375-384, 1994.
- Esteves Da Silva J., A. Machado, and M. Pinto, Study of the Complexation of Cu(II) by Fulvic Acids Extracted from a Sewage Sludge and its Compost, in *Fresenius Journal of Analytical Chemistry*, vol. 357, pp. 950-957, 1997.
- Fukushima M., K. Nakayasu, S. Tanaka, and H. Nakamura, Chromium(III) Binding Abilities of Humic Acids, in *Analytical Chimica Acta*, vol. 317, pp. 195-206, 1995.

- Gaffney J.S., N.A. Marley, S.B. Clark, in *Humic and Fulvic Acids. Isolation, Structure, and Environmental Role*, J.S. Gaffney, N.A. Marley, and S.B. Clark ed., pp. 2-16. Washington, DC: ACS, 1996
- Hamilton-Taylor, J., L. Giusti, and W. Davison, Sorption of Trace Metals (Cu, Pb, Zn) by Suspended Lake Particles in Artificial (0.005M NaNO₃) and Natural (Esthwaite Water) Freshwaters, in *Colloids and Surface A.*, vol. 120, pp. 205-219, 1997.
- Helton, J.C., J.E. Bean, K. Economy, J.W. Garner, R.J. MacKinnon, J. Miller, J.D. Schreiber, and P. Vaughn, Uncertainty and Sensitivity Analysis for two-Phase Flow in the Vicinity of the Repository in the 1996 Performance Assessment for the Waste Isolation Pilot Plant: Undisturbed Conditions, in *Preliability Engineering & System Safety*, vol. 69, no. 1-3, pp. 227-261, 2000.
- Hunter R.J., *Introduction to Modern Colloid Science*, Oxford Science Publications, 1993.
- Kienzler, B. Personal communication, ERMS No.523262, July 2001.
- Kim, J.I., H. Wimmer, R. Klenze, A Study of Curium(III) Humate Complexation by Time Resolved Laser Fluorescence Spectroscopy (TRLFS), in *Radiochimica Acta*, vol. 54, pp. 35-41, 1991.
- Kim, J.S., E.S.K. Chian, F.M. Saunders, E. M. Perdue, and M.F. Giabbai, in *Aquatic Humic Substances. Influence on Fate and Treatment of Polluants*. I.H. Suffert and P. MacCarthy, ed., pp. 473-497. Washington, DC: American Chemical Society, 1989
- Labonne-Wall, N., G.R. Choppin, C. Lopez, and J.-M. Monsallier, in *Actinide Speciation in High Ionic Strength Media*. D.T. Reed, S.B. Clark, and L. Rao, ed., pp. 199-211. New York, NY: Plenum Publish, 1999.
- Manciu, M., and E. Ruckensein, Role of the Hydration Force in the Stability of Colloids at High Ionic Strengths, in *Langmuir*, vol. 17, pp. 7061-7070, 2001.
- Nash, K.L., and G.R. Choppin, Interaction of Humic and Fulvic Acids with Th(IV), in *Journal of Inorganic and Nuclear Chemistry*, vol. 42, pp. 1045-1050, 1980.
- Novak, C.F., Calculation of Actinide Solubilities in WIPP SPC and ERDA6 Brines under MgO Backfill Scenarios Containing either Nesquehonite or Hydromagnesite as the Mg-CO₃ Solubility-Limiting Phase, Sandia National Laboratories memorandum to R. V. Bynum. WPO 46124, 1997
- Parks, G.A., The Isoelectric Points of Solid Oxides, Solid Hydroxides, and Aqueous Hydroxo Complex Systems, in *Chemical Reviews*, pp. 177-197, 1965.
- Samadfam, M., Y. Niitsu, S. Sato, and H. Ohashi, Complexaion Thermodynamics of Sr(II) and Humic acid, in *Radiochimica Acta*, vol. 73, pp. 211-216, 1996.

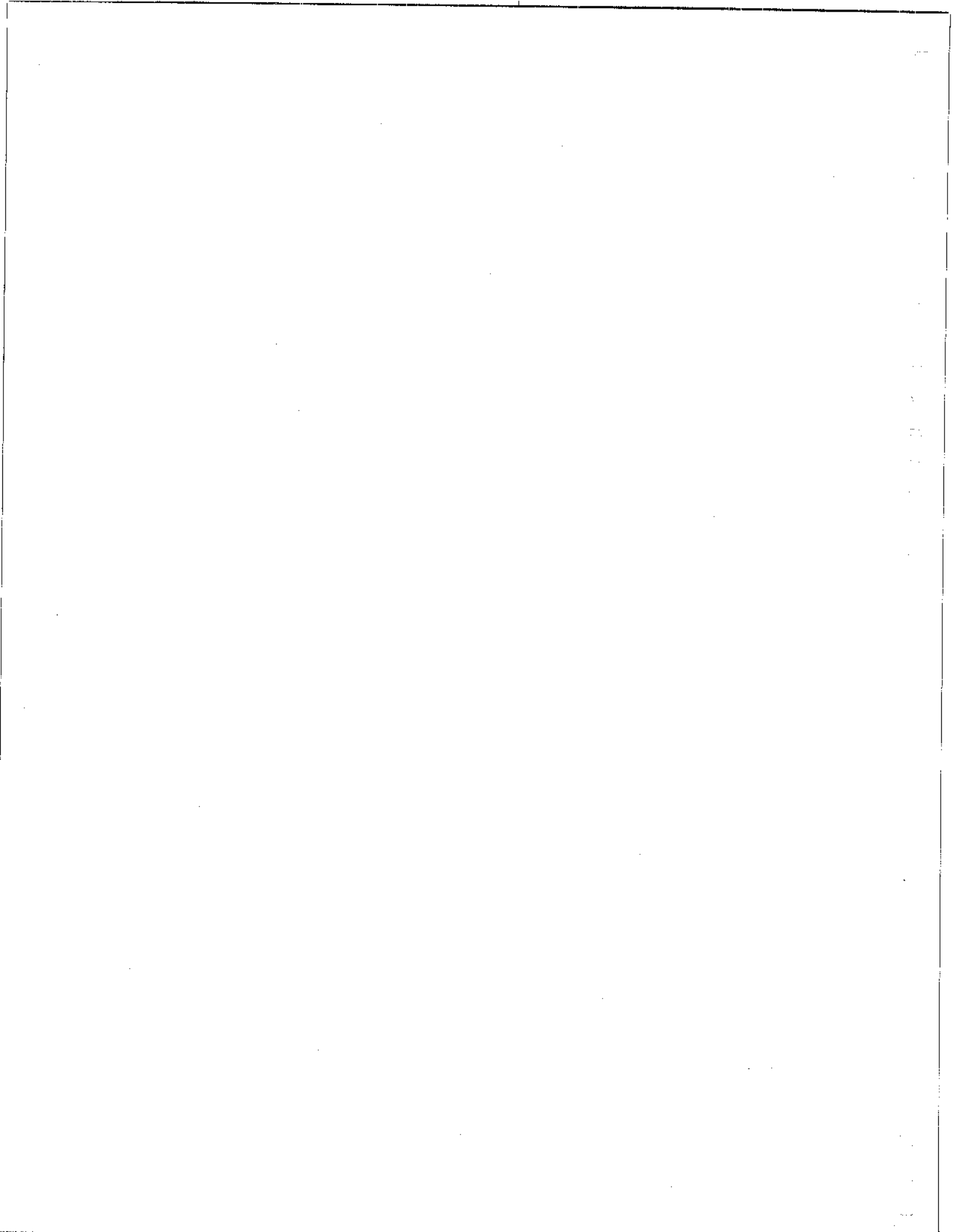
- Seibert, A., A. Mansel, C.M. Marquardt, E. Keller, J.V. Kratz, and N. Tratmann, Complexation Behaviour of Neptunium with Humic acid, in *Radiochimica Acta*, vol. 89, pp. 505-510, 2001.
- Shahwan, T., S. Suzer, and H.N. Erten, Sorption Studies of Cs⁺ and Ba²⁺ Cations on Magnesite, in *Applied Radiation and Isotopes*, vol. 49, no. 8, pp. 915-921, 1998.
- Smith, R. M., A.E. Martell, and R. Motekaitis, *NIST Critically Selected Stability Constants of Metals Complexes Database, Version 5.0. User's Guide*. Gaithersburg, MD. Technology Administration, National Institute of Standards and Technology, Standard Reference Data Program. U.S. Department of Commerce. 1998
- Stevenson, F.J., *Humus Chemistry*. Wiley and Sons, New York, NY, 1994.
- Tombacz, E., and E. Meleg, A Theoretical Explanation of the Aggregation of Humic Acids as a Function of pH and Electrolyte Concentration, in *Organic Geochemistry*, vol. 15, no. 4, pp. 375-381, 1990.
- U.S. Environmental Protection Agency, *Criteria for the Certification and Recertification of the Waste Isolation Pilot Plant's Compliance with 40 CFR Part 191 Disposal Regulations: Certification Decision*. Washington, D.C: US Environmental Protection Agency, 1998.
- Wall, N.A. and G.R. Choppin, Humic Acids Coagulation. Influence of Divalent Cations. Sandia National Laboratories report SAND2001-0036J (submitted to *Applied Geochemistry*), 2002.
- Wall, N.A., M. Borkowski, J.C. Chen, and G.R. Choppin, Complexation of Americium with Humic, Fulvic and Citric Acids at High Ionic Strength. Sandia National Laboratories report SAND2001-0519C (to be published in *Radiochimica Acta*), 2002.
- Wang, Y., C.R. Bryan, and N.A. Wall, *Experimental Study of WIPP MgO Backfill at Sandia National Laboratories Carlsbad Facility*. TP 00-07, Rev 1. Sandia National Laboratories. Carlsbad, NM: . June 2001.

NOTICE: This document was prepared as an account of work sponsored by an agency of the United States Government. Neither the United States Government nor any agency thereof, nor any of their employees, nor any of their contractors, subcontractors, or their employees, makes any warranty, express or implied, or assumes any legal liability or responsibility for the accuracy, completeness, or usefulness or any information, apparatus, product or process disclosed, or represents that its use would not infringe privately owned rights. Reference herein to any specific commercial product, process or service by trade name, trademark, manufacturer, or otherwise, does not necessarily constitute or imply its endorsement, recommendation, or favoring by the United States Government, any agency thereof or any of their contractors or subcontractors. The views and opinions expressed herein do not necessarily state or reflect those of the United States Government, any agency thereof or any of their contractors.

This document was authored by Sandia Corporation under Contract No. DE-AC04-94AL85000 with the United States Department of Energy. Parties are allowed to download copies at no cost for internal use within your organization only provided that any copies made are true and accurate. Copies must include a statement acknowledging Sandia Corporation's authorship of the subject matter.

3 GEOCHEMISTRY

3.4 Experimental Determination and Calculation...



3.4 Experimental Determination and Calculations of Metals/Ligand Interactions in the WIPP¹

Nathalie A. Wall¹, Donald E. Wall¹, Emily R. Giambalvo¹, and Gregory R. Choppin²

¹Sandia National Laboratories - Carlsbad Programs Group

²Florida State University

This material was presented at the 48th Bioassay, Analytical, and Environmental Radiochemistry Conference, October 28, 2002 – November 1, 2002, in Las Vegas, NV.

¹ This work covered by WBS #1.3.5.4.1.1

Shipments

Table 1. Transuranic Waste Shipments Received at WIPP as of September 23, 2002, WIPP.

Site	Shipments	Miles
Argonne National Laboratory	0	0
Hanford Site	11	19,888
Idaho National Engineering and Environmental Laboratory	483	684,864
Los Alamos National Laboratory	25	8,550
Lawrence Livermore National Laboratory	0	0
Mound Plant	0	0
Nevada Test Site	0	0
Oak Ridge National Laboratory	0	0
Rocky Flats Environmental Technology Site	677	536,744
Savannah River Site	22	33,880
Total received at WIPP	1,228	1,283,926

The Wastes

U.S. definition of TRU waste: waste with > 100 nCi of α -emitting TRU isotopes (with half life >20 y.) per g of waste.

WIPP Actinide Source Term Program

Important radioelements for the WIPP: Pu, Am > U, Th >> Np

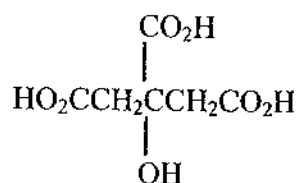
Predicted actinide oxidation states: Pu(III), Pu(IV), Am(III), U(IV), U(VI), Th(IV), Np(IV), Np(V)

Use of oxidation state analogs: Am(III) and Th(IV) used to predict upper bounds for solubilities of: Pu(III), and U(IV), Np(IV), and Pu(IV)

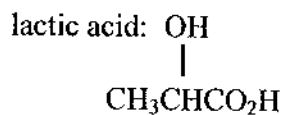
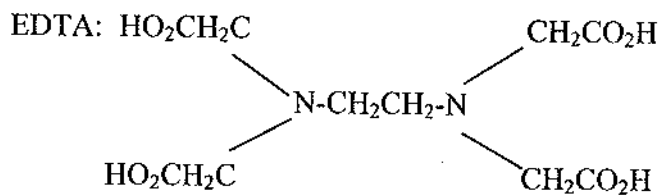
Metal complexing Ligands present in wastes

Acetic Acid: $\text{CH}_3\text{-CO}_2\text{H}$

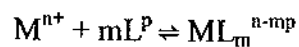
Citric acid:



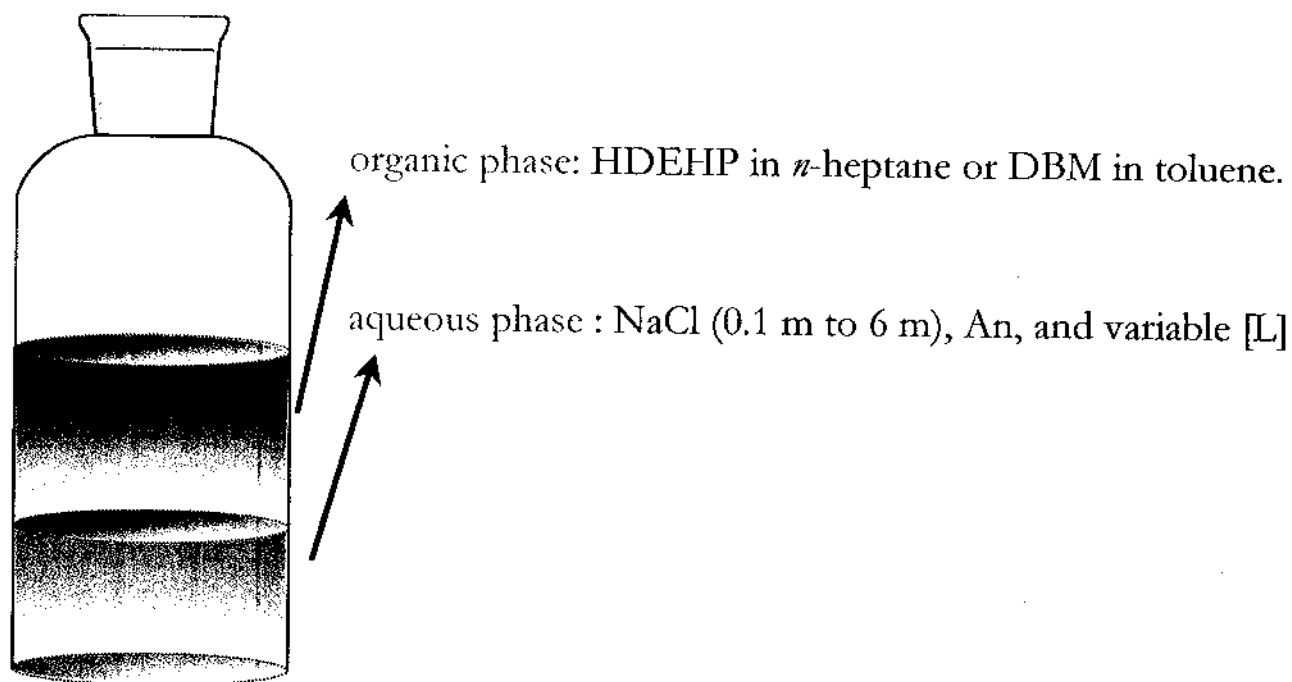
Oxalic acid: $\text{HO}_2\text{CCO}_2\text{H}$



Determination of Stability Constants



$$\beta_m = \frac{[\text{ML}_m^{n-mp}]}{[\text{M}^{n+}] [\text{L}^p]^m}$$

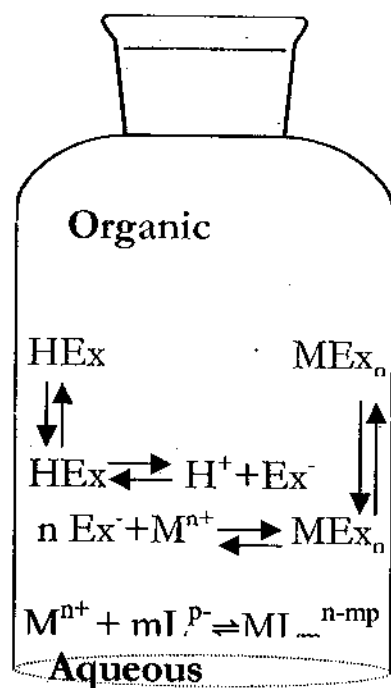


PHASE SEPARATION

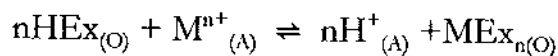
Measurements:

- ^{241}Am : automatic γ counter.
- ^{230}Th , ^{237}Np : LSC.
- pHr (i.e. pH-meter reading) with a Corning Semi-Micro Combination glass electrode, attached to Accumet 950 pH/ion Meter.
- pHr converted to pcH (i.e. $-\log[\text{H}^+]$):
 $\text{pcH} = \text{pHr} + 0.255 \times I$, (I is NaCl molality).

Figure 1. Experimental determination of stability constants: solvent extraction.



In absence of ligand



$$K_{\text{Ex}} = \frac{[\text{H}^{+}_{(\text{A})}]^n [\text{ME}_{x_n(\text{O})}]}{[\text{HE}_{x(\text{O})}]^n [\text{M}^{n+}_{(\text{A})}]} = \frac{[\text{H}^{+}_{(\text{A})}]^n}{[\text{HE}_{x(\text{O})}]^n} \times D_0$$

$$\log D_0 = \log K_{\text{Ex}} + \log [\text{HE}_{x(\text{O})}]^n + n \text{pH}$$

In presence of ligand

$$D = \frac{\sum [\text{M}]_{(\text{O})}}{\sum [\text{M}]_{(\text{A})}} \quad \text{and} \quad \frac{D_0}{D} - 1 = \beta' [\text{L}^-]$$

with

$$* \beta' = \frac{\beta}{\alpha}$$

$$* \alpha_M = 1 + \sum^{\text{OH}} \beta_i [\text{OH}^-]^i + \sum^{\text{B}} \beta [B^-]^k$$

Figure 2. Experimental determination of stability constants: solvent extraction.

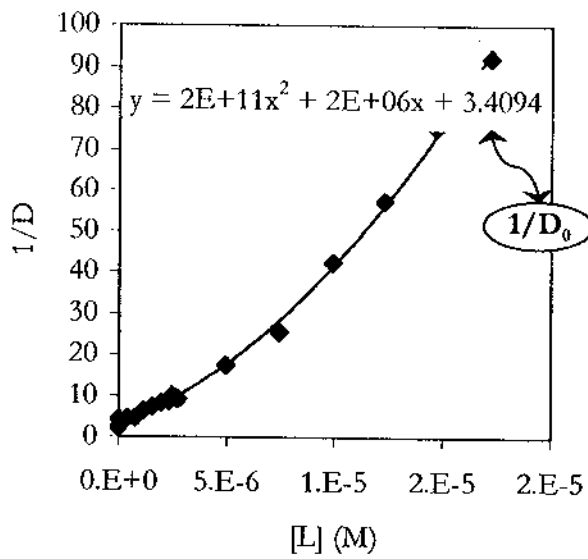


Figure 3. Graphs.

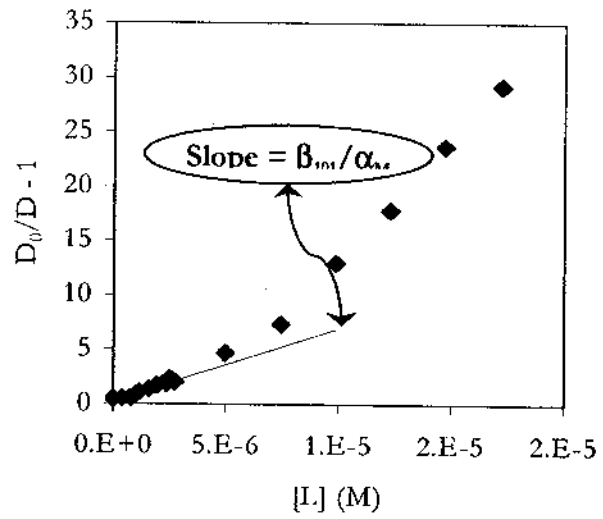


Figure 4. Graphs (cont.)

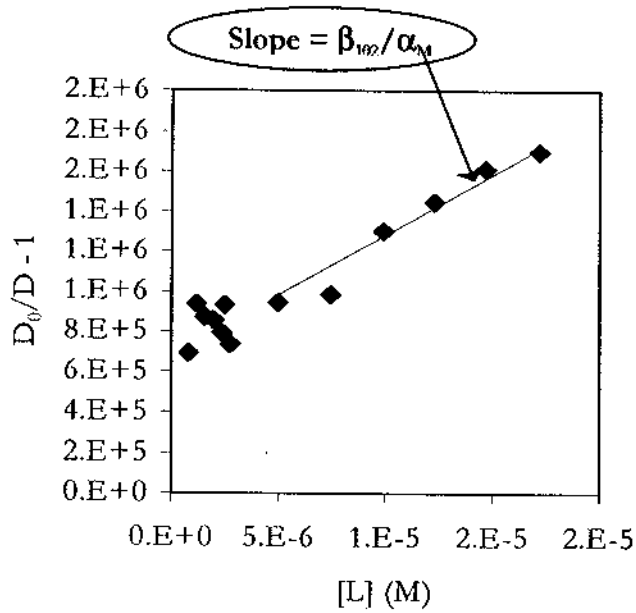


Figure 5. Graphs (cont.)

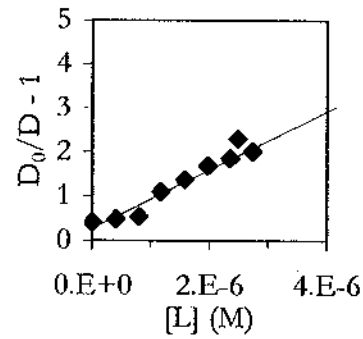


Figure 6. Graphs (cont.)

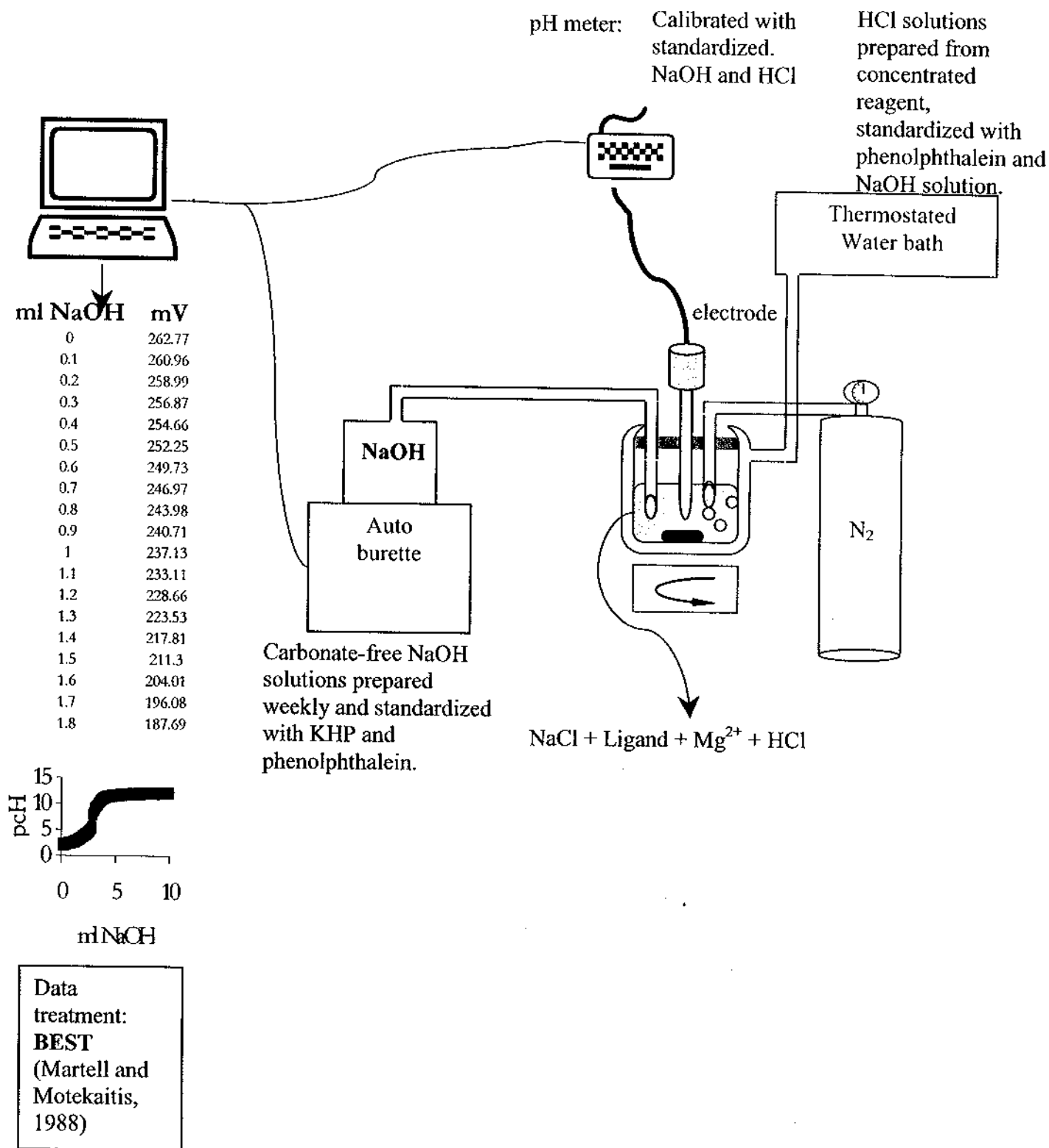


Figure 7. Experimental determination of stability constants: potentiometric titration (Mg²⁺).

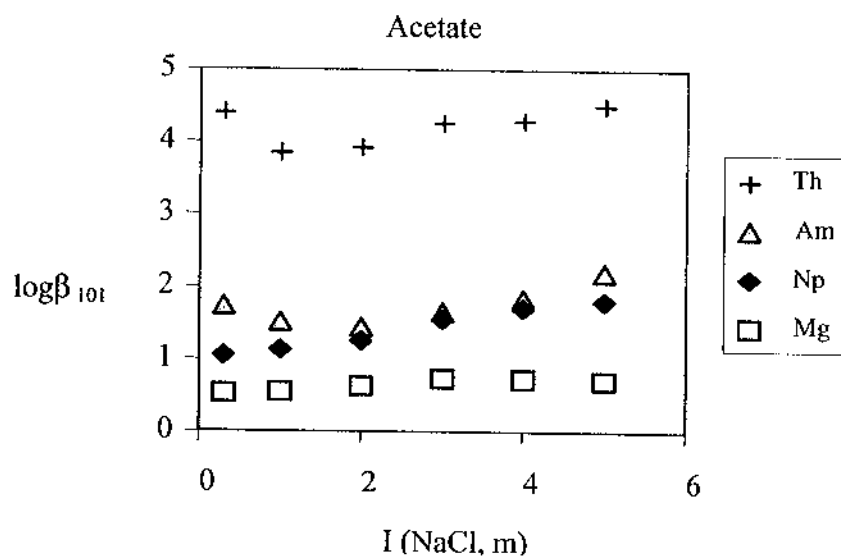


Figure 8. Experimental results.

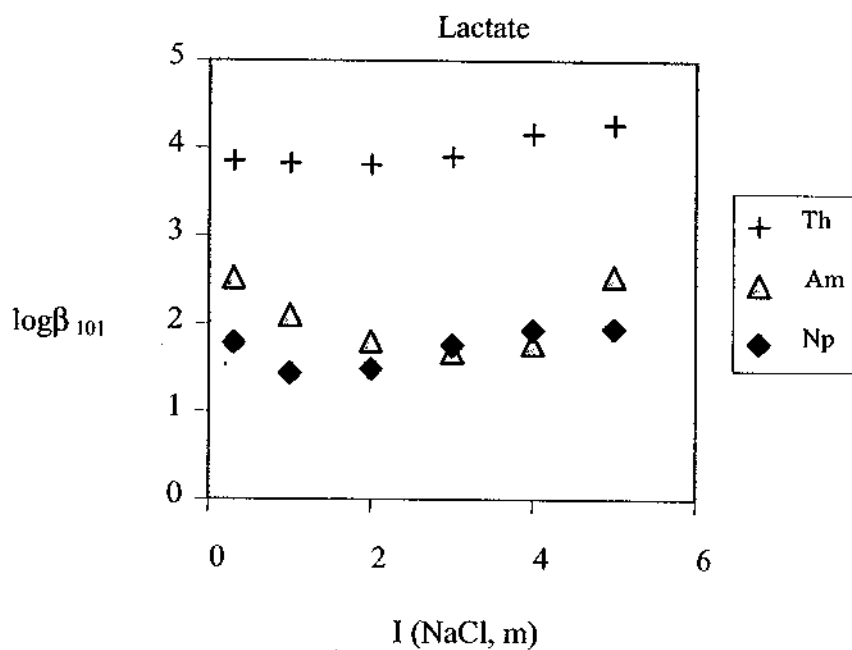


Figure 9. Experimental results (cont.)

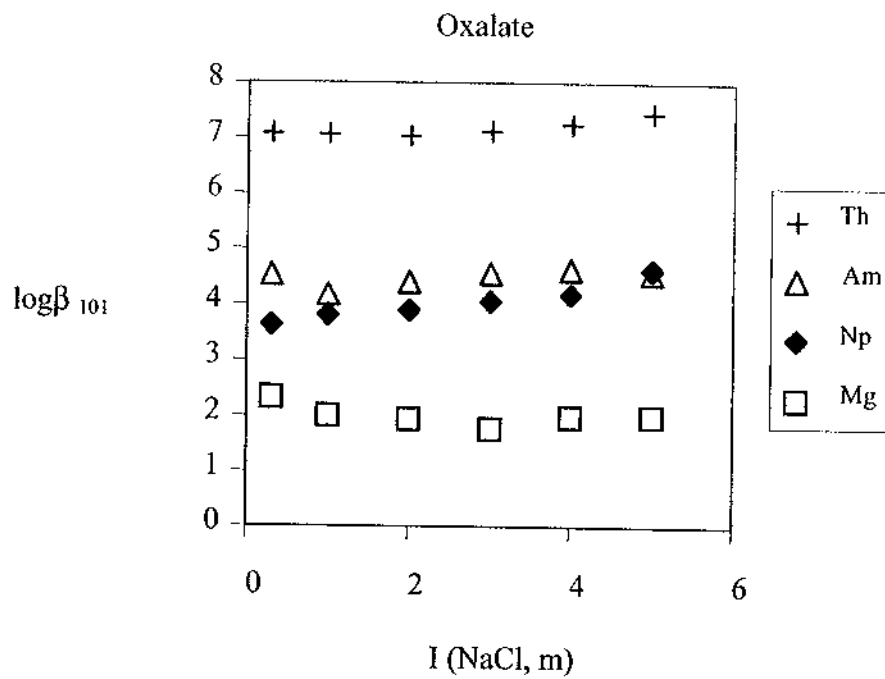


Figure 10. Experimental results (cont.)

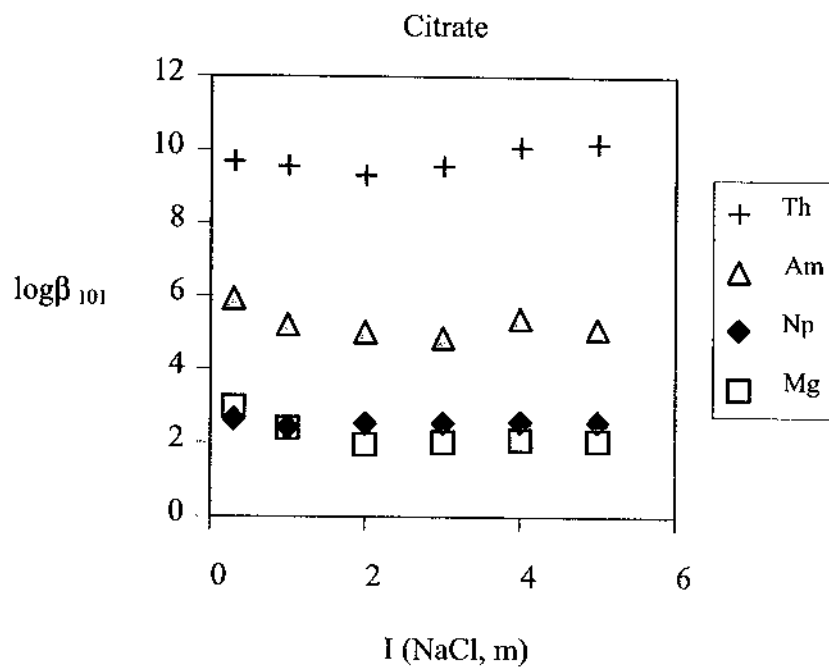


Figure 11. Experimental results (cont.)

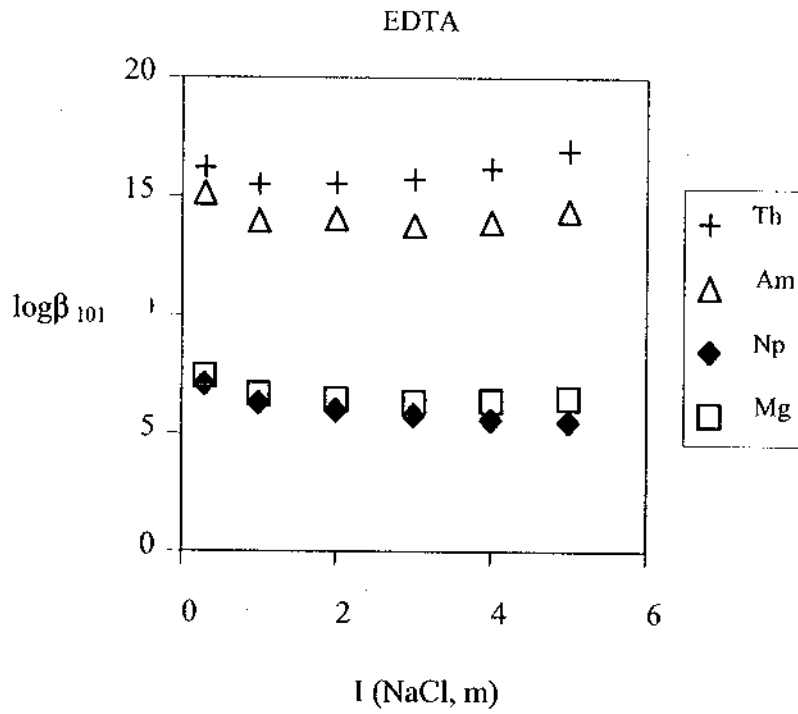


Figure 12. Experimental results (cont.)

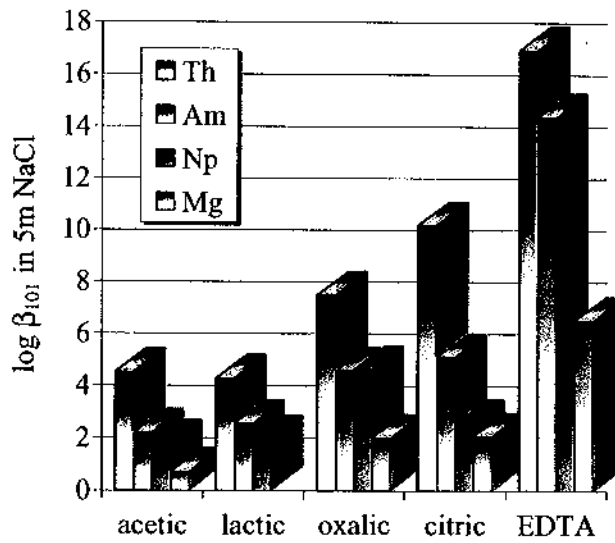


Figure 13. Data summary: log β_{101} in 5m NaCl.

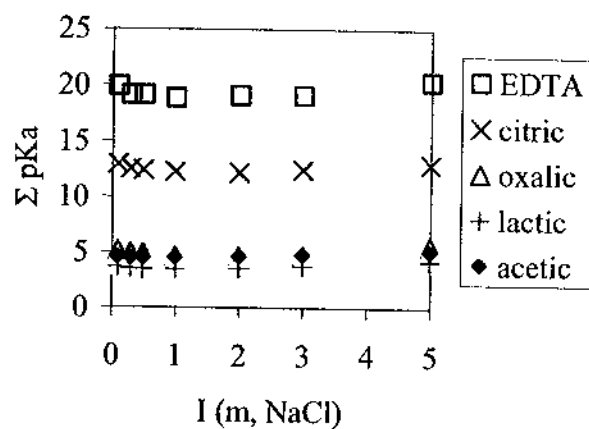


Figure 14. Data summary: $\log\beta_{101}$ in 5m NaCl (cont.)

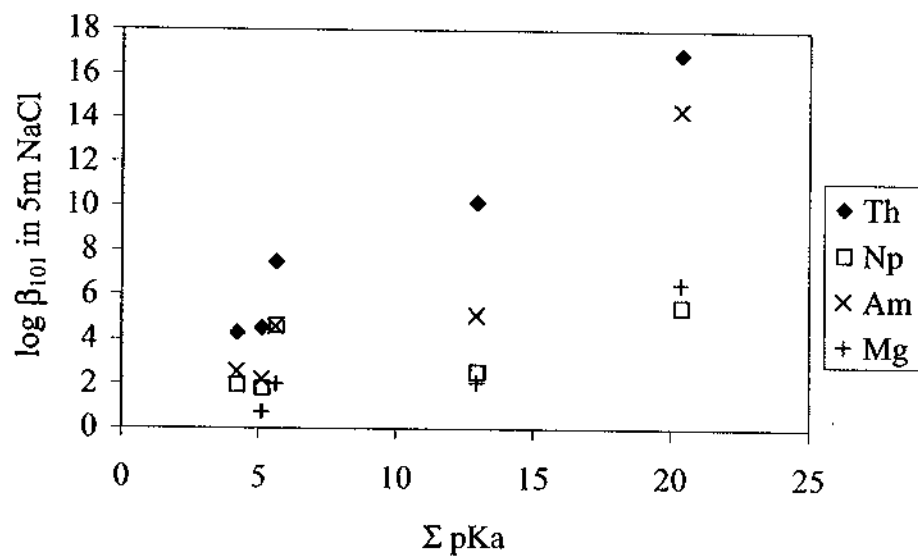


Figure 15. Data summary: $\log\beta_{101}$ in 5m NaCl (cont.)

Pitzer Ion-Interaction Model

Pitzer ion-interaction model (Pitzer, 1973, 1991):

- semi empirical model for calculating activity coefficients for high ionic strength solutions (2 m to 6 m).
- proven accurate for calculating solubilities in multicomponent electrolyte solutions (Harvie et al., 1984).

$$a_i = \gamma_i \cdot c_i$$

$$\mu_i = \mu_i^0 + RT \ln a_i$$

$$\frac{\partial G}{\partial n_i} = \mu_i = \mu_i^0 + RT \ln a_i$$

a_i : activity of i ,

γ_i : activity coefficient of i ,

μ_i : chemical potential of i ,

G : Gibbs free-energy function.

Pitzer Parameters

Pitzer model approach: $\ln \gamma_i = z_i^2 f^y + \sum_j D_{ij}(I) c_j + \sum_{j,k} E_{ijk} c_j c_k + \dots$

with $f^y = -0.392 \left[\frac{\sqrt{I}}{1+1.2\sqrt{I}} + \frac{2}{1.2} \ln(1+1.2\sqrt{I}) \right]$

Table 2. Normalized Chemical Potential μ^0/RT .

Chemical potential for solute species in aqueous phase:

$$\frac{\mu_i}{RT} = \frac{\mu_i^0}{RT} + \ln m_i + \ln \gamma_i$$

μ_i : Chemical potential of i,
 μ_i^0 : Standard chemical potential of i,
 m_i : molality of i,
 γ_i : activity coefficient of i.

Species	m^0/RT	Species	m^0/RT
HAc _(aq)	-158.300	H ₄ EDTA _(aq)	0.000
Ac ⁻	-147.347	H ₃ EDTA ⁻	5.761
		H ₂ EDTA ²⁻	12.870
H ₃ Cit _(aq)	0.000	HEDTA ³⁻	28.710
H ₂ Cit ⁻	7.476	EDTA ⁴⁻	53.050
HCit ²⁻	18.620		
Cit ³⁻	33.410	HLac _(aq)	0.000
		Lac ⁻	8.798
H ₂ Ox _(aq)	0.000		
HOx ⁻	3.209		
Ox ²⁻	13.017		

Table 3. Normalized Chemical Potentials (μ^0/RT) (cont.)

Species	m^0/RT	Species	m^0/RT
MgAc ⁺	-333.378	NpO ₂ Ac _(aq)	-526.061
MgCit ⁻	-162.261	NpO ₂ Cit ²⁻	-343.747
MgEDTA ²⁻	-153.734	NpO ₂ EDTA ³⁻	-335.708
MgOx _(aq)	-179.185	NpO ₂ Ox ⁻	-365.851
MgLac ⁺	999.999	NpO ₂ Lac _(aq)	-364.837
ThAc ³⁺	-448.525	AmAc ²⁺	-395.356
ThCit ⁺	-285.898	AmCit _(aq)	-228.543
ThEDTA _(aq)	-285.419	AmEDTA ⁻	-232.324
ThOx ²⁺	-297.428	AmOx ⁺	-242.853
ThLac ³⁺	-291.152	AmLac ²⁺	-241.436

ACTIVITY COEFFICIENTS

Pitzer expression for the activity coefficients of cation (C) and anions (A):

$$\ln \gamma_c = Z_c^2 f^y(I) + 2\beta_{CCl}^{(1)} \{2g(I) - Z_c^2 g(I)m\}m + 2(\beta_{CCl}^{(0)} + \Phi_{NaC})m + \left(3C_{CCl}^\Phi + \frac{3|Z_c|}{2} C_{NaCl}^\Phi + \Psi_{CNaCl} \right) m^2$$

$$\ln \gamma_A = Z_A^2 f^y(I) + 2\beta_{NaA}^{(1)} \{2g(I) - Z_A^2 g(I)m\}m + 2(\beta_{NaA}^{(0)} + \Phi_{ACl})m + \left(3C_{NaA}^\Phi + \frac{3|Z_A|}{2} C_{NaCl}^\Phi + \Psi_{ANaCl} \right) m^2$$

where $f^y = -0.392 \left[\frac{\sqrt{I}}{1+1.2\sqrt{I}} + \frac{2}{1.2} \ln(1+1.2\sqrt{I}) \right]$

and $g(I) = \frac{1 - (1+2\sqrt{I})\exp(-2\sqrt{I})}{2^2 I}$

Neutral species: $\ln \gamma_{H_2Ox} = 2m_{Na} \lambda_{Na, H_2Ox} + 2m_{Cl} \lambda_{Cl, H_2Ox}$

Table 4. Binary Pitzer Parameters ($\beta^{(0)}$, $\beta^{(1)}$, $\beta^{(2)}$, C^ϕ).

Cation	Anion	$\beta^{(0)}$	$\beta^{(1)}$	$\beta^{(2)}$	C^ϕ
Na ⁺	Ac ⁻	0.1426	0.22	0	-0.00629
Na ⁺	H ₂ Cit ⁻	-0.1296	0.29	0	0.013
Na ⁺	HCit ²⁻	-0.0989	1.74	0	0.027
Na ⁺	Cit ³⁻	0.0887	5.22	0	0.047
Na ⁺	H ₃ EDTA ⁻	-0.2345	0.29	0	0.059
Na ⁺	H ₂ EDTA ²⁻	-0.1262	1.74	0	0.054
Na ⁺	HEDTA ³⁻	0.5458	5.22	0	-0.048
Na ⁺	EDTA ⁴⁻	1.016	11.6	0	0.001
Na ⁺	HOx ⁻	-0.2448	0.29	0	0.068
Na ⁺	Ox ²⁻	-0.2176	1.74	0	0.122
Na ⁺	Lac ⁻	-0.0563	0.29	0	0.047
Na ⁺	AmEDTA ⁻	-0.2239	0.29	0	0.002
Na ⁺	NpO ₂ Cit ²⁻	-0.4226	1.75	0	0.142
Na ⁺	NpO ₂ EDTA ³⁻	0.683	5.911	0	0
Na ⁺	NpO ₂ Ox ⁻	-0.5418	0.29	0	0.095
Cation	Anion	$\beta^{(0)}$	$\beta^{(1)}$	$\beta^{(2)}$	C^ϕ
Na ⁺	MgCit ⁻	0.1742	0.29	0	-0.06923
Na ⁺	MgEDTA ²⁻	0.2134	1.74	0	0.00869
H ⁺	Ac ⁻	0	0	0	0
AmAc ²⁺	Cl ⁻	0.309	1.74	0	-0.132
AmOx ⁺	Cl ⁻	-0.9374	0.29	0	0.248
AmLac ²⁺	Cl ⁻	0.8397	1.74	0	-0.332
ThAc ³⁺	Cl ⁻	1.061	5.22	0	0.109
ThCit ⁺	Cl ⁻	-0.7467	0.29	0	0.319
ThOx ²⁺	Cl ⁻	-0.343	1.74	0	0.5
ThLac ³⁺	Cl ⁻	0.6677	5.22	0	0.341
MgAc ⁺	Cl ⁻	-0.0833	0.29	0	0.0987

Table 5. Ternary Pitzer Parameters (θ , Ψ).

Anion <i>i</i>	Anion <i>j</i>	Cation <i>k</i>	q_{ij}	$y_{ij,k}$
Ac ⁻	Cl ⁻	Na ⁺	-0.09	0.01029

Table 6. Neutral-Ion Interaction Parameters.

Neutral	Ion	l
HAc _(aq)	Cl ⁻	0
H ₃ Cit _(aq)	Cl ⁻	0
H ₄ EDTA _(aq)	Cl ⁻	0
H ₂ Ox _(aq)	Cl ⁻	0
H ₂ Ox _(aq)	HSO ₄ ⁻	0
HLac _(aq)	Cl ⁻	0
AmCit _(aq)	Cl ⁻	-0.406
ThEDTA _(aq)	Cl ⁻	0.1111
NpO ₂ Ac _(aq)	Cl ⁻	0
NpO ₂ Lac _(aq)	Cl ⁻	0.015
MgOx _(aq)	Cl ⁻	0.0189

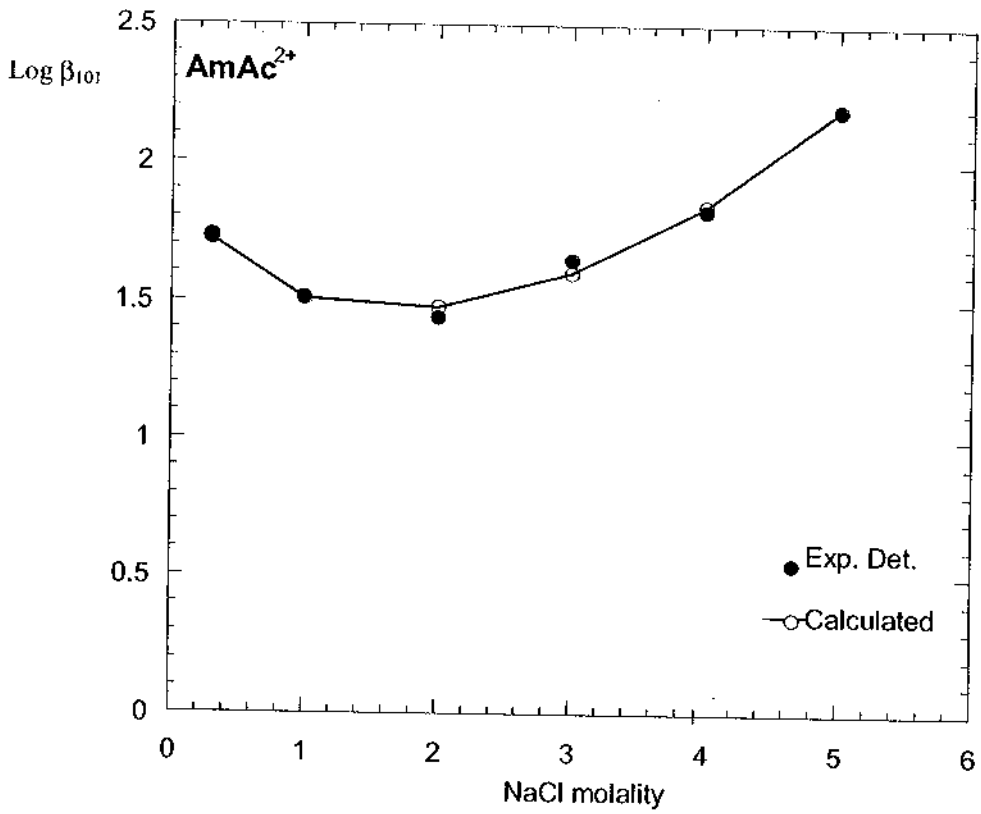


Figure 15. Examples of modeled data.

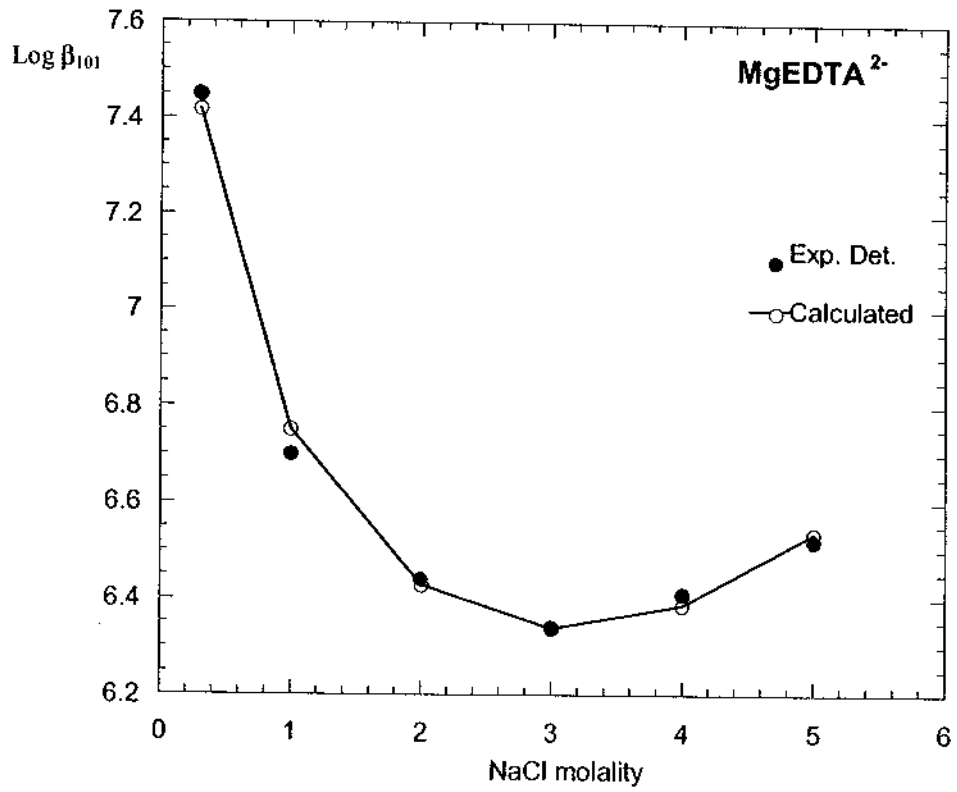


Figure 15. Examples of modeled data (cont.)

Acknowledgements

U.S. DOE CARLSBAD FIELD OFFICE

FLORIDA STATE UNIVERSITY

The experimental work was performed at FSU, supported at Sandia National Laboratories by the U.S. DOE, and at FSU under a Sandia-approved quality assurances program.

We thank Andrew H. Bond, Marian Borkowski, Micheal G. Bronikowski, Jian Feng Chen, Stefan Lis, Jiri Mizera, Oleg Pokrovsky, Yuan-Xian Xia.

SANDIA NATIONAL LABORATORIES

Thanks to Laurence H. (Larry) Brush, Robert C. Moore, Craig F. Novak.